UNIVERSITÀ DEGLI STUDI DI PADOVA

DIPARTIMENTO DI INGEGNERIA DELL'INFORMAZIONE

CORSO DI LAUREA MAGISTRALE IN BIOINGEGNERIA INDUSTRIALE

"New Paradigms in Patient-specific 3D Printing and Cartilage Computational Modeling"

Laureando: Damiano Coato

Relatore: Prof. Mattia Veronese

Correlatore: Prof. Paolo Gargiulo

*To my family
and friends*

SUMMARY

0 ABSTRACT

Osteoarthritis (OA) is a prevalent joint disorder that affects more than 500 million patients worldwide, with knee OA being the most prevalent form. It is a leading cause of disability, especially among older adults, and the trends of an ageing population and increasing obesity are likely to compound this. The loss of articular cartilage is a hallmark of the disease and a primary cause of joint degeneration, which results in pain, stiffness, and limited mobility. Chondral lesions constitute one of the major extrinsic risk factors for OA, leading to important societal and economic burden.

The present work was carried out at the Reykjavik University (Iceland), in the frame of the European project RESTORE, a multidisciplinary project with the objective of develop and validate innovative solutions for the treatment of chondral lesions and cartilage regeneration. The purpose of this thesis is to develop novel methodologies that enhance the understanding of cartilage behaviour and implement personalized solutions to prevent possible complications arising from diseases or injuries. Specifically, this study aims to use both computational and experimental techniques to characterize innovative PolyJet materials and establish a new test configuration that is customized for each patient. To achieve this, patient-specific medical data was processed to create a 3D model that serves as a starting point for computational analyses and advanced additive manufacturing. Two innovative materials were digitally created to simulate the mechanical properties of articular cartilage and printed with the morphologies of each patient's femoral cartilage, along with the femur and tibia bones. Following the 3D printing process, mechanical tests were performed on the printed models and various finite element analyses were conducted to compare and validate the results obtained.

1 INTRODUCTION

1.1 Anatomical Features of the Knee Joint

The knee joint is one of the most complex and important joints in the human body. It is a hinge joint that allows for flexion and extension, as well as some rotation. It is formed by the articulation of three bones: the femur, tibia, and patella. In this chapter, we will focus on the anatomy of the femur, tibia, and femoral cartilage.

The knee is not only the largest joint in the human body but also one of the most complex from a functional standpoint. It is susceptible to injuries due to its anatomical characteristics, the interrelation of its structural components, and the significant external forces that act on it. It is composed of three bones and an extensive network of ligaments and muscles. The knee joint is primarily a hinge joint, allowing movement along one axis in terms of flexion and extension of the knee in the sagittal plane. However, it also permits slight medial rotation during flexion and the final stage of extension, as well as lateral rotation when unlocking the knee. Despite being primarily a hinge joint, the knee is also classified as a bi-condylar type of synovial joint due to the presence of two condyles and other secondary movements [1].

The knee joint is formed by the articulation of three bones: the femur, tibia, and patella (Figure 1). These three bones articulate through tibiofemoral and patellofemoral joints and are covered in articular cartilage, which is an extremely hard, smooth substance designed to decrease friction forces. The medial and lateral condyles of the femur articulate with the tibia to form the tibiofemoral joint, the knee's weight-bearing joint. Similarly, the anterior and distal parts of the femur articulate with the patella to form the patellofemoral joint [2].

The femur, or thigh bone, is the longest and strongest bone in the human body. The distal aspect of the femur forms the proximal articulating surface for the knee, which is composed of two large condyles, the medial and the lateral. These condyles articulate with the tibial plateau, forming the knee joint. The medial condyle is larger than the lateral condyle and is responsible for bearing most of the weight that is transmitted through the knee joint. The femur also has the patella surface, which is the smooth, concave surface located at the anterior aspect of the distal end of the bone. This surface articulates with the patella, or kneecap, a sesamoid bone located within the quadriceps tendon [1]. The patella surface and the patella together form the patellofemoral joint. The intercondylar groove, also known as the intercondylar notch, is a deep groove located on the posterior aspect of the distal end of the femur, between the medial and lateral femoral condyles. This groove serves as a passageway for the anterior cruciate ligament

(ACL) and posterior cruciate ligament (PCL), which are two important ligaments in the knee joint (Figure 1).

The tibia, or shin bone, is the second largest bone in the human body. It articulates with the femur at the knee joint and with the fibula at the proximal and distal tibiofibular joints. The fibula provides a surface for important muscles and ligaments to attach to, although it is not directly involved in the knee joint. The proximal end of the tibia has two asymmetric, relatively flat, articular surfaces, the medial and lateral tibial plateaus, which articulate with the femoral condyles. The tibial plateau is covered with a layer of articular cartilage, which helps to reduce friction and absorb shock in the knee joint. The medial tibial plateau has a greater length than the lateral plateau in the anteroposterior direction, and the proximal tibia has a larger diameter than the posterior shaft, which is sloped at an angle of approximately 7° to 10° to facilitate the flexion of the femoral condyles on the tibia [2]. The tibial condyles are separated by the intercondylar tubercles, which are two roughened bony spines that play a crucial role in knee extension. When the knee is extended, these tubercles are lodged into the intercondylar notch of the femur, thereby increasing the stability of the joint. Overall, the tibiofemoral joint is a relatively unstable joint as the plateaus are slightly convex anteriorly and posteriorly. This emphasizes the importance of the other structures of the knee such as the menisci.

The articulating surfaces of the femur and tibia are covered with a layer of smooth, white, glistening articular cartilage. This cartilage helps to reduce friction and distribute weight evenly across the joint. The cartilage in the knee is thicker than in any other joint in the human body, which is necessary to withstand the high loads placed on the joint during weight-bearing activities. The knee joint is also surrounded by a joint capsule, which is composed of two layers: an outer fibrous layer and an inner synovial layer. The fibrous layer is thick and strong and helps to stabilize the joint. The synovial layer lines the inner surface of the joint capsule and produces synovial fluid, which lubricates the joint and nourishes the articular cartilage [1].

In conclusion, the anatomy of the knee joint is complex and involves the interaction of several bones and cartilage structures. Understanding the anatomy of the knee is essential for diagnosing and treating knee injuries and diseases.

Right knee in flexion: anterior view

- Anterior cruciate ligament
- Lateral condyle of femur (articular surface)
- Popliteus tendon
- Fibular collateral ligament
- Lateral meniscus
- Transverse ligament of knee
- Head of fibula
- Gerdy's tubercle
- Posterior cruciate ligament
- Medial condyle of femur (articular surface)
- Medial meniscus
- Tibial collateral ligament
- Medial condyle of femur
- Tuberosity of tibia

Right knee in extension: posterior view

- Adductor tubercle (medial epicondyle of femur)
- Medial condyle of femur (articular surface)
- Medial meniscus
- Tibial collateral ligament
- Medial condyle of femur
- Posterior cruciate ligament
- Anterior cruciate ligament
- Posterior meniscofemoral ligament
- Lateral condyle of femur (articular surface)
- Popliteus tendon
- Fibular collateral ligament
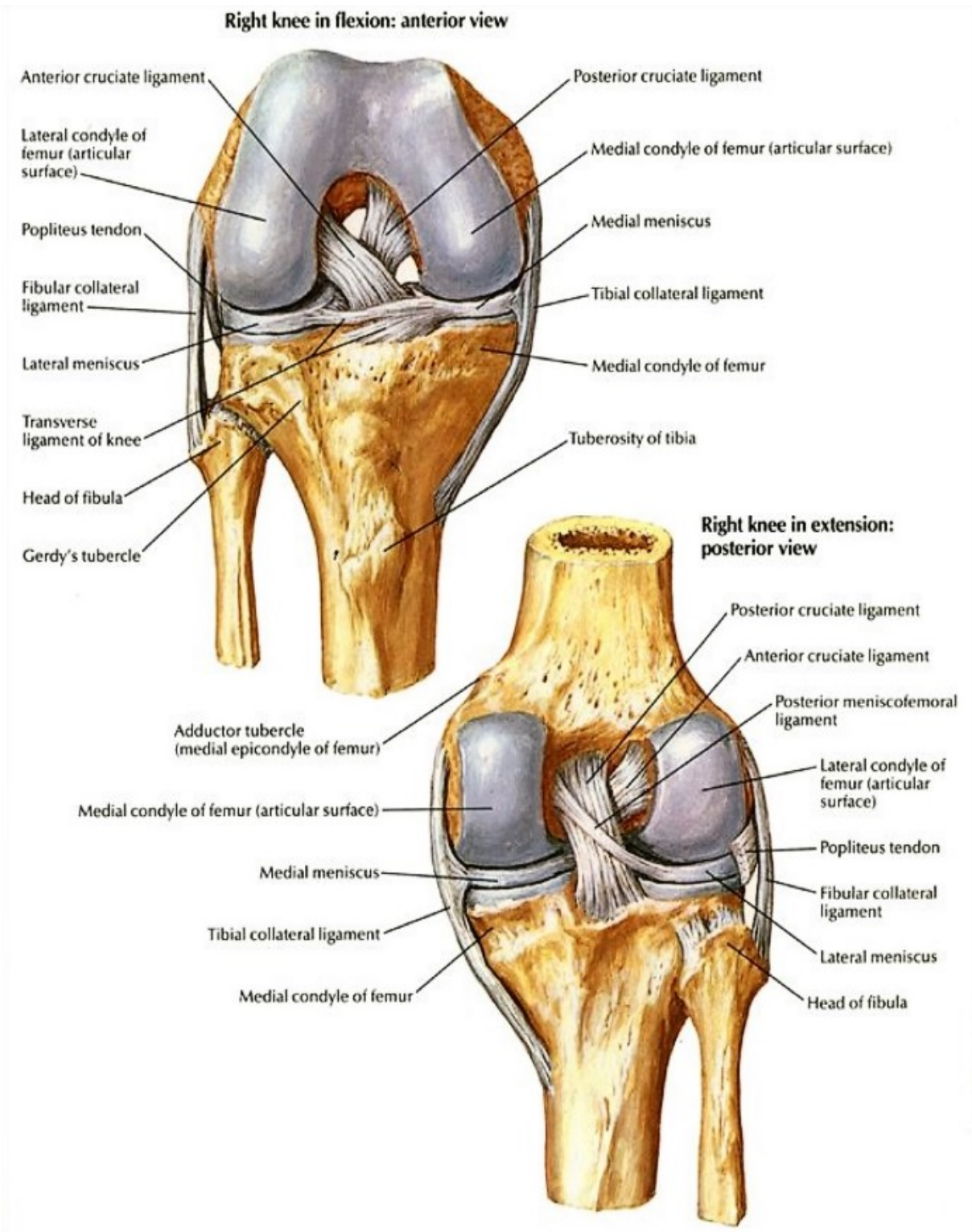- Lateral meniscus
- Head of fibula

Figure 1. Anatomy of the knee.

3

1.2 Cartilage Tissue

Articular cartilage is a specialized connective tissue that covers the surface of bones in synovial joints. It plays a critical role in joint function by providing a low-friction and wear-resistant surface for the bones to move against each other. The structure and composition of articular cartilage are specifically adapted to its mechanical functions. In this chapter, we will discuss the key components and organization of articular cartilage.

1.2.1 Role, Composition and Structure of Articular Cartilage

Role

There are three main types of human cartilage: hyaline, elastic, and fibrocartilage. These cartilages differ in their proportions of collagen, elastin, and proteoglycans. Hyaline cartilage is the most common type and is found in various parts of the body, but mostly in synovial joints where it is called articular cartilage. Articular cartilage is a specialized type of connective tissue that covers the surface of bones in joints. Its role is to provide a smooth, low-friction surface that allows bones to glide over each other with minimal wear and tear. Articular cartilage is also important for shock absorption, which helps to protect bones from damage during weight-bearing activities like walking, running, and jumping. It acts as a cushion between the bones, absorbing the impact of the forces that are transmitted through the joint. Another important function of articular cartilage is to distribute weight evenly across the joint surface. This helps to prevent excessive stress on any one area of the joint, which can lead to degeneration or injury over time. It is a porous solid, which allows the synovial fluid to permeate it. The synovial fluid serves multiple purposes: it nourishes the cartilage, which has no blood vessels; it lubricates the joint to allow for smooth articulation; and it carries a significant portion of the joint's load through exudation from the porous solid [3]. Due to the lack of blood vessels, nerves, and lymphatics, articular cartilage has a limited capacity for repair and regeneration [4]. Damage to the cartilage can lead to joint pain, stiffness, and loss of function, and in severe cases can lead to degenerative joint diseases such as osteoarthritis.

Composition

Articular cartilage consists of a solid phase and a fluid phase, the proportion of which can vary depending on factors such as age, gender, and location within the joint. Typically, the solid

phase makes up about 20-30% of the volume or 10-20% of the weight, while the fluid phase accounts for approximately 70-80% of the volume or 80-90% of the weight [5]. The solid phase contains type II collagen fibrils, proteoglycans, other glycoproteins, and chondrocytes. Meanwhile, the fluid phase is primarily composed of water with electrolytes.

Chondrocytes are the only cells found in articular cartilage and are responsible for producing and maintaining the extracellular matrix (ECM). The ECM is composed of a complex mixture of water, collagens, proteoglycans, and non-collagenous proteins that provide the cartilage with its unique mechanical properties. The water content of articular cartilage ranges from 60% to 80% and is crucial in maintaining the tissue's mechanical properties. Inorganic ions such as calcium, magnesium, and phosphate are also present and play a vital role in mineralization. Proteoglycans consist of a protein core with glycosaminoglycans attached to form a bottlebrush-like structure. Near the surface of the cartilage, proteoglycan concentration is relatively low, and water content is high, while in the deeper regions near the subchondral bone, the proteoglycan concentration is highest, and water content is lowest. Collagen makes up 60 to 70% of the dry weight of the tissue, with type II being the predominant collagen in articular cartilage. Collagen architecture varies through the depth of the tissue [6].

Structure

The structure of cartilage is not uniform, but instead can be divided into four zones along its depth: superficial, middle, deep, and calcified (Figure 1). Each zone has its own biochemical, structural, and cellular characteristics [6].

The superficial zone is the outermost layer of articular cartilage, accounting for 10-20% of its total thickness [4]. It is composed of tightly packed collagen fibres, mostly type II and IX, that run parallel to the joint surface. Flattened chondrocytes are abundant in this zone, along with low levels of proteoglycan and high levels of collagen fibrils, making the cartilage highly resistant to compression. The integrity of this layer is crucial for the protection and maintenance of the deeper layers. The fibre arrangement in this zone helps to resist shear forces generated by joint movement. Moreover, it is in contact with synovial fluid and is responsible for most of the tensile properties of cartilage, which allow it to resist the tensile, shear, and compressive forces that occur during joint articulation. The superficial zone also has relatively low permeability to fluid flow, which helps to retain fluid within the collagen matrix during compression, enabling it to support significant compressive loads. Over 90% of the load is supported by the pressurized fluid.

Beneath the superficial zone is the middle zone, which represents 40% to 60% of the total cartilage volume and provides an anatomic and functional bridge between the superficial and deep zones [6]. It is composed of round chondrocytes with low density and a mixture of collagen types II, IX, and XI. Compared to the superficial zone, it has a lower collagen and water content but a higher concentration of proteoglycans, especially aggrecan. In this layer, collagen fibrils are in a random, mostly oblique, arrangement. Functionally, the middle zone is the first line of resistance to compressive forces.

The deep zone comprises the next 20 to 30% of the articular cartilage volume and is responsible for withstanding the highest stresses and providing the greatest resistance to compressive forces [6]. Collagen fibrils are arranged perpendicular to the articular surface, with the largest diameter collagen fibrils in a radial disposition. The deep zone has the highest proteoglycan content and the lowest water concentration. Chondrocytes are typically arranged in columnar orientation, parallel to the collagen fibres and perpendicular to the joint line.

Finally, the calcified zone is the transition between the cartilage and the underlying subchondral bone, partly mineralized [4]. This layer plays an integral role in securing the cartilage to the bone, by anchoring the collagen fibrils of the deep zone to the subchondral bone. The collagen architecture is similar to that of the deep zone, but there is an increase in mineral content, and the chondrocytes are arranged in columns. In this zone, the cell population is scarce, and chondrocytes are hypertrophic.

The distinct four zones along the cartilage depth with different structures make cartilage an anisotropic material.
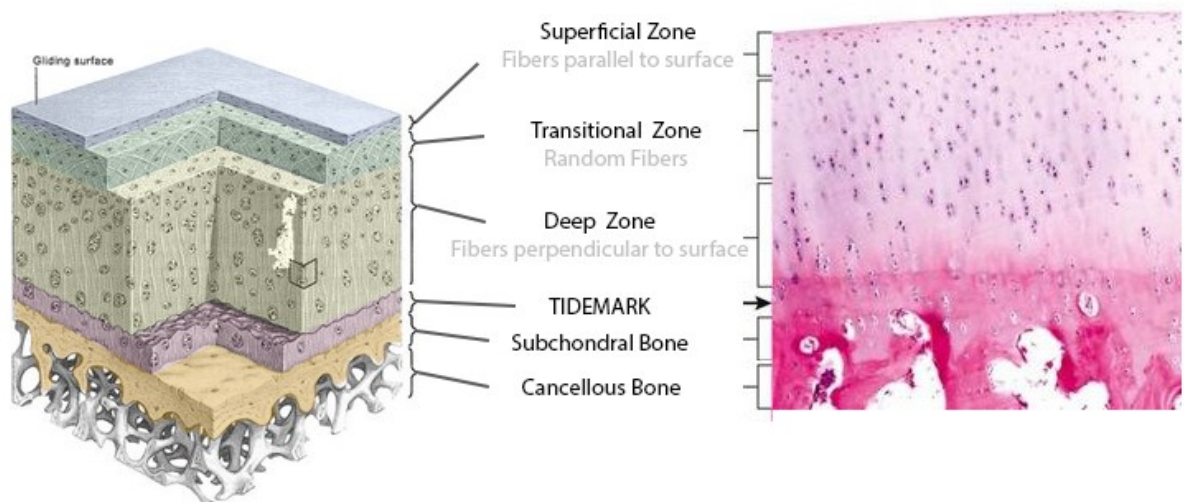

Figure 2. Structure of articular cartilage with the four different zones.

1.2.2 Mechanical Characterization and Behaviour of Articular Cartilage

The biomechanical properties of articular cartilage are crucial to its function and are affected by various factors, including composition, structure, and loading conditions. In this chapter, we will discuss the elastic, viscoelastic, compressive, and tensile behaviour of articular cartilage.

Elastic Behaviour

Linear elastic behaviour is the most straightforward mechanical behaviour for small deformations. It occurs when the material fully recovers its original shape after removing the applied load. Linear behaviour can be observed when stress and strain follow a linear relationship, meaning they are directly proportional. The constant of proportionality between stress and strain is called the longitudinal elastic modulus or Young's modulus. Young's modulus represents the slope of the stress-strain curve and describes the stiffness of the material. The higher the modulus, the stiffer the material and the less elastic deformation occurs. Poisson's ratio is another coefficient that indicates the ratio of transverse strain to axial strain in an axially loaded specimen. Poisson's ratio is 0.5 for incompressible materials and 0 for compressible ones. When a load is applied to any material, such as cartilage, it undergoes deformation. Strain is defined as the percentage change in the length of the material from its original length, while stress is defined as force per unit area. Articular cartilage is considered to be an elastic material, meaning that it is capable of returning to its original shape after being deformed by an external force. The elastic properties of cartilage are primarily determined by its extracellular matrix (ECM), which is composed of collagen fibres, proteoglycans, and water. Collagen fibres provide tensile strength, while proteoglycans and water contribute to the compressive stiffness of cartilage. The elastic modulus of articular cartilage ranges from 0.1 to 10.0 MPa, depending on the location, age, and health of the tissue [6].

Viscoelastic Behaviour

In addition to its elastic properties, articular cartilage exhibits viscoelastic behaviour, which means that it exhibits both elastic and viscous responses to applied loads. The viscous behaviour is due to the flow of interstitial fluid within the ECM, which dissipates energy and causes a time-dependent response. The viscoelastic properties of cartilage are important for understanding its behaviour under cyclic loadings, such as during walking or other repetitive activities. The viscoelastic behaviour of cartilage is characterized by a complex modulus that includes both elastic and viscous components [7].

Articular cartilage exhibits highly viscoelastic behaviour due to two mechanisms: flow-dependent viscoelasticity, which is caused by the drag forces of interstitial fluid through the solid porous matrix, and independent flow viscoelasticity, which is caused by the intrinsic viscoelasticity of collagen fibres and proteoglycans. This time-dependent behaviour is characterized by synovial fluid acting as a viscous fluid during slow joint flexing and as an elastic solid during fast movements, providing shock absorption and load transfer. However, in pathological conditions, the synovial fluid loses its viscoelastic properties, failing to protect joints from mechanical damage during fast movements [7].

Stress-relaxation and creep tests are used to investigate the time-dependent behaviour of cartilage. A creep test is a mechanical test used to study the time-dependent deformation of a material under a constant load that is applied instantaneously. In the case of articular cartilage, a creep test involves applying a constant load to the cartilage, which is initially deformed and then allowed to deform further over time as fluid flows out of the porous matrix. The elastic modulus of the solid matrix alone provides the value of deformation at equilibrium, while the history of deformation is related to fluid flow and permeability. In contrast, the stress-relaxation test is used to examine the time-dependent decrease in stress of a material under a constant deformation that is applied instantaneously. During the loading phase, fluid exudes from the cartilage, while during the relaxation phase, it redistributes within the extracellular matrix.

Compressive Behaviour

To understand the properties of articular cartilage, it is important to examine its compressive behaviour, as it is designed to resist and distribute compressive loads evenly across the joint surface. The compressive behaviour of cartilage is affected by factors such as the composition and structure of the ECM, the loading rate, and the hydration state of the tissue. When subjected to compressive loads, articular cartilage exhibits a nonlinear response, with a stiffer behaviour at low strains and a softer behaviour at high strains. This nonlinearity is due to the deformation of collagen fibres and the compression of interstitial fluid within the ECM. Proteoglycans are the primary contributors to the compressive stiffness of cartilage due to their ability to electrochemically bind water [8]. When cartilage is compressed, it undergoes volume changes due to fluid movement, resulting in increased osmotic pressure and chemical expansion. Osteoarthritis, a degenerative cartilage disease, is often associated with a decrease in proteoglycans, resulting in a reduction of the tissue's compressive stiffness.

Several test configurations can be used to measure the compressive properties of cartilage. The frequently employed include indentation, confined compression, and unconfined compression tests.

The indentation test is the most common method used to evaluate the biomechanical properties of articular cartilage. It allows for the quantification of tissue stiffness in terms of instantaneous modulus (E_0) or equilibrium modulus (E_{eq}). Various types of indenters can be used, depending on the thickness of the sample and desired stiffness properties. The indenter, which may have a flat or spherical tip, is smaller than the surface being tested and is lowered onto the specimen.

Another technique is confined compression. To perform the confined compression test, a cylindrical disk of the material is placed in a chamber with rigid walls. The chamber walls prevent the cartilage from expanding laterally, resulting in deformation only in the direction of loading. A constant compressive load is applied to the cartilage through a porous filter, allowing fluid to flow from the cartilage through the filter as it is compressed. The stress and strain are recorded once equilibrium is reached, and the ratio is defined as the aggregate equilibrium modulus (H_a). Similar to the tensile equilibrium modulus, the aggregate modulus represents the stiffness of the solid matrix and is independent of fluid flow. This test also allows the measurement of the material permeability (k).

In contrast, the unconfined compression test involves placing the cylindrical disk in a chamber with non-rigid walls, allowing for radial expansion. The piston used to apply load is highly waterproof, enabling liquid outflow only through the side walls. This test is performed to obtain elastic properties, including instantaneous elastic modulus (E_0) and equilibrium elastic modulus (E_{eq}), after imposing a constant displacement until equilibrium is reached.

Tensile Behaviour

Although articular cartilage is primarily subjected to compressive loads, it can also experience tensile stresses during joint movements. The tensile behaviour of cartilage is influenced by the orientation and density of collagen fibres and the interstitial fluid content. Articular cartilage is stiffer in tension than in compression due to the alignment of collagen fibres in the tangential direction.

Uniaxial tensile tests are conducted to investigate the tensile behaviour of articular cartilage. These tests are performed on rectangular-shaped cartilage samples, which are hydrated in a saline bath and can be in the shape of a dog bone. The ends of the sample are fixed to clamps and a displacement is imposed to measure the force. The purpose of these tests is to characterize

the cartilage's resistance to fracture. Stepped stress-relaxation tests are also conducted to determine the instantaneous and equilibrium parameters. In all literature studies on articular cartilage, regardless of the type of test used, saline solution is utilized to maintain the tissue's structural integrity and prevent dehydration of the sample [8].

In conclusion, the biomechanical behaviour of articular cartilage is complex and influenced by many factors. Understanding the elastic, viscoelastic, compressive, and tensile properties of cartilage is essential for developing accurate models of joint mechanics and designing effective treatments for joint diseases and injuries.

1.3 Knee Osteoarthritis

Osteoarthritis (OA) is a progressive musculoskeletal condition that can affect any joint in the body, but the knee is the most affected as the predominant weight-bearing joint. The development of knee OA has been linked to excessive joint load and injury. Knee OA is characterized by structural and functional modifications to primarily articular cartilage and subchondral bone, but also Hoffa's fat pad, synovia, ligaments, and muscles, leading to the concept of observing OA as a whole joint disease. This chapter discusses knee OA and the impact that this condition has on articular cartilage, thus highlighting the essential need to understand its mechanisms to develop effective treatments.

Osteoarthritis (OA) is one of the most common joint disorders, affecting more than 500 million patients worldwide, accounting for 7% of the global population [9]. Its prevalence has increased by 48% from 1990 to 2019, making it the 15th highest cause of years lived with disability (YLDs) in 2019 [10]. OA is a leading cause of disability in the elderly population and the trends of an ageing population and increasing obesity are likely to compound this. Knee OA is the most prevalent form of the disease, accounting for about 85% of the global burden of OA [9]. It is estimated that approximately 10% of men and 13% of women aged 60 or older have knee OA, increasing even more with age. 80% of patients with OA experience limited mobility. About 25% of these patients can no longer perform the most important basic activities of daily life and 50% of patients with knee OA must quit their jobs within ten years of the disease onset [10]. Added to this, the annual economic burden of osteoarthritis is at least USD 89.1 billion, with knee and hip joint replacements accounting for the majority of that cost. Knee joint replacements are one of the most common surgical procedures performed worldwide, and knee OA accounts for most of these surgeries [9].

Overall, OA is a significant burden on both the economy and society, impacting mental health and increasing the likelihood of suicidal thoughts. These data are concerning but probably underestimate the true size of the problem. Furthermore, the development of treatments for osteoarthritis has not made comparable progress with that for many other musculoskeletal and chronic non-communicable diseases.

1.3.1 The Role of Articular Cartilage in Knee OA

The biomechanical properties of articular cartilage play a crucial role in its function and ability to withstand mechanical loading. The cartilage that covers the ends of the bones in the knee joint acts as a cushion and helps to reduce friction during movement. Due to its avascularity, articular cartilage does not heal spontaneously after injury and often requires surgical intervention. Osteoarthritis (OA) of the knee is a polysymptomatic degenerative joint disease characterized by the progressive wearing down of the articular cartilage [10]. This breakdown can cause various symptoms, such as pain, stiffness, swelling and limited joint mobility. As the cartilage thins, the joint's load-bearing capacity decreases, making it more prone to mechanical damage, further exacerbating cartilage loss and joint degeneration. As the disease progresses, the cartilage may wear away entirely, resulting in the bones rubbing against each other. This can lead to severe pain and disability, making it difficult to perform even simple tasks like walking or standing. OA's impact on articular cartilage includes a reduction in proteoglycan content and changes in collagen structure and function, making it less elastic and more susceptible to damage. Knee OA is a complex process influenced by various factors, including mechanical stress, inflammation, and genetic predisposition. Recent evidence suggests that knee OA is not merely a mechanical degeneration of articular cartilage, but an inflammatory disease of the entire synovial joint, affecting the synovium, meniscus, periarticular ligament, and subchondral bone [11].

The loss of articular cartilage in knee OA is considered a hallmark of the disease and is believed to be the primary cause of joint degeneration. This disease can have severe consequences on a patient's quality of life, with chronic pain, reduced mobility, and decreased function. The pain can be so severe that it limits a patient's ability to perform simple daily activities, such as walking, climbing stairs, and even standing, bathing, and dressing. As a result, patients may become less active, leading to weight gain, muscle weakness, and reduced cardiovascular fitness [10].

The assessment of cartilage condition and thickness is therefore crucial for both the detection and monitoring of the progression of OA.

Several scales, based on the degree of joint space narrowing and on damages to cartilage and underlying bone, are used to describe the severity of OA in the knee compartment. The standard scale is the Kellgren–Lawrence (KL) grading (Figure). It establishes a specific OA grade based on the combination of several features such as joint space narrowing and the presence of osteophytes. The scale is from 0 to 4, where 0 indicates a healthy cartilage and 4 indicates a severe state of OA.

- Grade 0: Normal (no features of OA)
- Grade 1: Doubtful (minute osteophytes)
- Grade 2: Mild (definite osteophytes, normal joint space)
- Grade 3: Moderate (moderate joint space reduction)
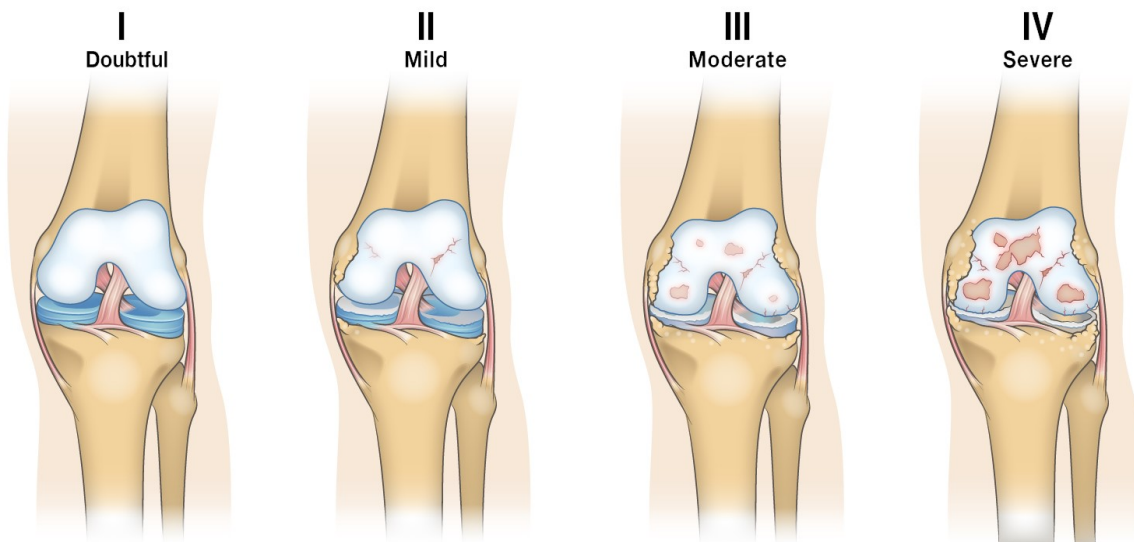- Grade 4: Severe (joint space greatly reduced, subchondral sclerosis)

Figure 3. Kellgren–Lawrence (KL) scale used to describe the severity of OA in the knee.

1.3.2 Risk Factors and Treatment

Risk Factors

Age, previous knee injuries, obesity, joint malalignment, and instability that result in increased mechanical stress are all strong risk factors for the development of knee OA [9]. Repetitive actions, like often kneeling and heavy lifting, together with professional sports activities, such as long-distance running, football, handball, and hockey, are associated with a higher risk of developing OA, due to more frequent injuries, causing cartilage defects, meniscal and anterior cruciate ligament (ACL) tears. Physical inactivity also contributes to the increasing prevalence of OA, leading to less stable and weaker joints. Women are more likely to develop OA due to differences in knee anatomy and kinematics compared to men. There is a connection between OA and an increased risk of developing cardiovascular and atherosclerosis-related diseases, as well as depressive symptoms due to chronic pain [9].

Treatment

There is no cure for OA, and current treatment options are often costly and inefficient. Hence, there is a pressing need to understand the causes and underlying mechanisms of this degenerative disease to develop new, more effective, and personalised therapies to both alleviate pain and slow down disease progression. Even more so since the severity of the condition varies significantly from patient to patient. While some only face minor limitations in their well-being and daily life, others are affected by severe pain resulting in the need for continuous care. Current OA therapy recommendations range from non-drug measures (exercise, weight loss, physical therapy etc.) to creams and pills or injections, depending on the severity of OA pain [12]. Surgery can be seen as the last treatment option in case all other regimens have failed, or in case the damage to the joint is so severe that no other therapy is possible. However, all of these measures can only slow the progression of degenerative arthritis. Plus, taking medications oftentimes shows only limited success, and at the same time can lead to gastric complications and other potential adverse side effects.

Nevertheless, there is no non-surgical intervention that can prevent, halt, or delay OA progression. Joint replacement surgery is the only option for end-stage disease to improve quality of life [12]. Assessment of cartilage condition and thickness is therefore crucial for both the detection and monitoring of the progression of OA. In recent years, computer-assisted techniques, including finite element method (FEM) analysis, have become increasingly popular

for the diagnosis, and planning of knee replacement surgeries. FEM analysis provides a detailed understanding of the biomechanics of the knee joint, allowing surgeons to optimize the implant design and placement for each patient. FEA can also help predict post-operative outcomes, potentially reducing the risk of implant failure and improving patient satisfaction.

In conclusion, knee OA is a prevalent and debilitating disease that affects millions of people worldwide. The incidence and prevalence of knee OA are expected to rise in the coming years, making it a significant public health concern. The loss of articular cartilage is a hallmark of knee OA, and it is believed to be the primary cause of joint degeneration. The biomechanical properties of articular cartilage play a crucial role in its function and ability to withstand mechanical loading. Understanding the role of articular cartilage in knee OA is essential for developing effective treatments for the disease.

1.4 Gold Standards for the Evaluation of Cartilage and Bones

The main diagnostic tools used for evaluating human joint cartilage are X-ray, computed tomography (CT), and magnetic resonance imaging (MRI). Among these, MRI is the state-of-the-art imaging modality for the assessment of hyaline cartilage and has seen rapid development in the last decade [13]. MRI provides a visual assessment of the cartilage and offers a way to quantitatively evaluate its volume and dimensions. This imaging technique accurately estimates its geometry, thickness, and chemical composition. Moreover, MRI is capable of assessing not only the cartilage, but also other tissues involved in osteoarthritis (OA), such as subchondral bone, meniscus, and soft tissue [14]. On the other hand, CT imaging provides an excellent 3D representation of cortical bone, osteophytes, and soft tissue calcification and has been used to investigate changes in the joint, including trabecular bone remodelling, subchondral cysts, and bone sclerosis, all of which can be OA-related changes in the joint [13, 14].

To obtain high-quality images of both bone and cartilage structures, the two acquisition methods can be combined to create a hybrid imaging modality. The resulting images from MRI and CT scans can then be overlaid, creating a so-called image registration. This approach is innovative because it combines the two imaging technologies to provide precise and accurate visualization of both bones and cartilage.

1.4.1 Image Registration

Image registration is the process of aligning two or more images of the same scene taken from different viewpoints or using different imaging modalities. Its goal is to create a single image that combines information from multiple images, thereby improving the accuracy and reliability of image analysis. The registration process typically involves several steps, including pre-processing the images, selecting corresponding points or landmarks, estimating the transformation, and evaluating the quality of the registration. To perform image registration, the CT scan and MRI images are collected from the same body part or region, ensuring that they have the same spatial orientation and are of similar size and resolution. Corresponding points or landmarks are then selected in both images to establish the transformation between the two images. These landmarks can be identified manually or automatically using software tools. The newly created image can be used for various applications, including segmentation and the creation of 3D anatomical models.

1.4.2 Medical Image Segmentation

Medical image segmentation, essentially the same as natural image segmentation, refers to the process of extracting the desired object from a medical image (2D or 3D), which can be done manually, semi-automatically or fully automatically [15]. This process involves importing the image data, selecting the region of interest, and converting that region into a part. This conversion will create a digital 3D model that accurately approximates the size and shape of the region of interest that was segmented. The imaging modality used to obtain medical images can vary, such as CT, MRI, US, PET, X-ray, or hybrid, depending on the organ to be imaged and the imaging purpose [16]. The most common modalities used for 3D printing and other 3D modelling applications are computed tomography (CT) and magnetic resonance imaging (MRI). The international standard format for these imaging files is Digital Imaging and Communications in Medicine (DICOM). These DICOM datasets are medical image files that contain additional header information such as patient details, image positioning, pixel spacing, etc.

In this context, Mimics (Materialise's Interactive Medical Image Control System, Materialise, Leuven, Belgium) is a high-performing medical imaging software used to process medical images and create 3D models. It uses 2D cross-sectional medical images such as from CT and MRI to construct 3D models, which can then be directly linked to rapid prototyping, CAD, surgical simulation, and advanced engineering analysis.

1.4.3 EU RESTORE Project

RESTORE is a European project which aims to implement patient-specific solutions for cartilage regeneration [17]. It involves ten partners from eight different countries (Portugal, Spain, Italy, Germany, Sweden, Norway, Iceland, and Finland), including Research and Technological Development institutes and two small-medium sized enterprises. Bringing together orthopaedic surgeons, tissue engineers, material scientists, cell biologists and businesses, the project plans to develop a new generation of smart nano enabled 3D matrices that can fit into complex lesion geometry, modulate undesirable biological events, and remotely control, stimulate, and monitor cartilage repair. RESTORE will address the shortfalls of current therapeutic solutions, helping prevent or delay the onset of osteoarthritis [17].

In the frame of the EU project RESTORE, the Institute of Biomedical and Neural Engineering of Reykjavik University created a database containing several characteristics

regarding knee cartilages. The objective is to obtain bones and cartilages features to study new paradigms for assessing cartilage conditions.

The RESTORE database [18] is a repository of patient-specific anatomical models of knee anatomies and different chondral lesions. The database includes more than one hundred different measurements from 47 individuals (25 females, 22 males). They are divided into three categories: 24 degenerative (D), presenting arthrosis or undergoing total knee prosthesis replacement; 15 traumatic (T), having acute injuries; 8 healthy acting as control group (C). The RESTORE database is a structured set of 3D reconstructions of knee joints taken from different patients and based on their X-ray, MRI, and CT data. Exhaustive measurements, regarding the thickness, the grading of the cartilage, as well as the presence of medical pathologies such as cysts, and bone attrition, were performed on those medical images, for each patient, based on a robust radiological approach. It provides a complete overview of the patient's condition from those 2D images. The RESTORE database is freely accessible and provides a unique set of morphological measurements on bone and cartilage tissues.

1.5 Finite Element Analysis

Finite Element Analysis (FEA) is a computational simulation technique used to analyse and predict the behaviour of structures and systems in various fields of engineering. In recent years, FEA has also found numerous applications in bioengineering.

This chapter discusses the many applications of FEA in the field of bioengineering, where it has proven to be an essential tool for modern engineering practices. By allowing researchers and clinicians to simulate and analyse the mechanical behaviour of organs, devices, and tissues under different loading conditions, it provides valuable insights into the underlying mechanisms of various diseases and conditions. Moreover, FEA is crucial in diagnosing, treating, and preventing diseases associated with abnormal mechanical stresses, wear, and fatigue fracture mechanics.

1.5.1 Finite Element Method

There are three primary methods for solving engineering problems: the analytical method, the numerical method, and the experimental method. One numerical procedure used for analysing structures is the Finite Element Method (FEM), which involves creating a computer model of a material or design to be analysed for specific results. FEM is particularly useful for solving complex problems that cannot be effectively solved using analytical or experimental methods alone [19].

Many physical phenomena in science and engineering can be described using partial differential equations (PDEs), which involve rates of change with respect to continuous variables. FEM provides a set of mathematical tools used to approximate and solve the PDEs that govern the mechanical phenomenon being analysed [20]. It subdivides a complex space or domain into a finite number of small, countable pieces called finite elements, each of which can be described using relatively simple linear algebraic equations. FEM uses a system of points and elements to create a mesh that represents the geometry of the model structure. These elements are bonded together at their vertices, called nodes, and the mesh is programmed to contain the material and structural properties that define how the structure will react to certain loading conditions. The basic idea is to make calculations at a limited number of points and then interpolate the results for the entire domain [21]. Since any continuous object has infinite degrees of freedom, FEM reduces the number of degrees of freedom from infinite to finite by using meshing.

By using these functions and the actual geometry of the element, the equilibrium equations between the external forces acting on the elements and the displacements occurring on its nodes can be determined. The accuracy of the final results is contingent upon the shape and size of the elements, where smaller elements produce more precise results but require longer analysis times. Enhanced accuracy can be achieved by increasing the number of calculation points, such as nodes and elements.

The forces that are applied to the FE model depend on the tested hypothesis and so can be either non-physiological or realistic. The model structure is then solved, and the outcome is a series of nodal displacements. The resulting strains and stresses are calculated and displayed. Their magnitudes reflect the mechanical behaviour of the structure and can be represented numerically or as a colour-coded projection onto the model geometry. Deformation can be quantified in a number of ways, including principal strains, shear stress, total displacement, and strain energy density, depending on the question [22].

Finite element analysis (FEA) has been used for many years by engineers to predict how structures or devices may behave under different circumstances. With the advancements in computer systems, FEA has been greatly improved and has been applied to various biomedical applications.

FEA Workflow

Finite Element Analysis (FEA) is a computational method that involves three main phases: pre-processing, processing, and post-processing [23]. In the pre-processing stage, the geometry, mesh, constitutive models, and boundary conditions are defined. This includes preparation of the geometric model, discretization of the entire volume into finite elements, assignment of mechanical properties to the materials, identification of loads and constraints, and choice of the type of solution. In the processing stage, the mathematical equations describing the model are solved numerically to complete the analysis without errors. In the post-processing stage, the results are extracted from the simulation software and analysed with appropriate programs for further calculations. The post-processing stage also involves analysis of the results, including mesh convergence analyses, verifications, and validations against experimental data, to achieve reliable FEA results.

Advantages of FEA

Finite Element Analysis (FEA) is a computational simulation technique that has proven to be an extremely valuable and powerful tool across a broad range of engineering disciplines, including bioengineering. The benefits of incorporating FEA in engineering are manifold. Firstly, FEA enables an accurate and reliable representation of real-world systems by incorporating geometries, material properties, behaviours, contacts, boundary conditions, loads, and other pertinent factors. Secondly, FEA facilitates the early detection of issues in systems, structures, or devices before their physical construction. This allows for prompt redesigns and optimizations of crucial elements such as materials, shape, weight, and size, resulting in significant cost and time savings, as well as a lowered risk of failure. All of this enables the study of intricate physical phenomena that would be arduous or unfeasible to investigate experimentally. Moreover, multiple results can be extracted from a single analysis, which would otherwise require multiple experiments. FEA also permits the analysis of various parameters such as stresses, strains, displacements, pressures, temperatures, magnetic or electric fields, and others, throughout the internal and external structure being investigated, providing a more comprehensive understanding compared to the limited information obtained by traditional methods. Additionally, FEA enables pinpointing information in specific locations of interest. FEA offers distinct benefits in the realm of bioengineering. It plays a pivotal role in understanding how organs and tissues react to stress, evaluating the effectiveness of joint replacement components, and forecasting how both musculoskeletal tissues and biomaterials will evolve over time. It also facilitates meticulous simulations of surgical procedures, prosthetic implants, and other medical devices, leading to refined designs and better outcomes. Furthermore, FEA promotes a more profound comprehension of various medical conditions, enabling the anticipation and diagnosis of diseases, injuries, and other health complications. However, the FEM is also known to require considerable amounts of computational resources, which have been supported by the current advances in hardware and software design.

In conclusion, FEA is a powerful tool that allows for the accurate and reliable study of complex systems across various fields, including bioengineering. Its numerous advantages, including design optimization, identification of problems, and detailed simulations, make it an essential part of modern engineering practices.

1.5.2 FEM Applications in Bioengineering

Mechanical forces play a significant role in the functioning of the human body, and disturbances in the mechanical state of organs can lead to the development of various diseases [20]. For instance, cardiovascular diseases such as atherosclerosis, which is the accumulation of plaque in arteries, and hypertension, which is high blood pressure, are associated with mechanical stresses and strains that affect the arterial walls. Similarly, osteoarthritis, which is a degenerative joint disease, is linked to abnormal mechanical stresses on the joint cartilage. Falls can lead to bone fractures, while long-term loading can result in lumbar disc degeneration. Therefore, understanding the mechanical state of organs is crucial in the diagnosis, treatment, and prevention of many diseases. Implants are becoming increasingly common, but they require better mechanical designs and more reliable materials. Implant surgeries, such as stent implantation for atherosclerosis and total knee replacement, may be required when organs lose function. However, implants can raise issues, like medial tilting in ankle replacements and fatigue and wear of the liner in hip implants. To improve medical designs, it is also crucial to study the mechanical behaviour of implants [20]. In this context, Finite Element Analysis (FEA) is playing an increasingly important role. In particular, FEA is becoming prevalent in bioengineering to study the mechanical state of organs, tissues, and devices. Some of the possible applications in various bioengineering fields are briefly illustrated below, from the study of soft and hard tissues to surgical planning, passing through tissue engineering and drug delivery.

Hard and Soft Tissues

Finite Element Analysis (FEA) is commonly used to study the mechanical behaviour of both hard and soft tissues, including bones, teeth, cartilage, skin, muscles, ligaments, and intervertebral discs [20]. FEA is useful for understanding tissues' responses to mechanical loads and fracture risks, designing orthopaedic implants, predicting pressure sores and blister risks, and developing better surgical procedures for tendons and ligaments. Additionally, FEA can simulate tissue deformation, displacement, and stress distribution to predict tissue damage under specific loading conditions, which is crucial for identifying potential injuries.

Devices and Implants

FEA is also a powerful tool for designing and optimizing medical devices, including orthopaedic and prosthetic devices [21]. It can be used to evaluate the performance of implants

under different loading conditions and aid in the design and optimization of prosthetic devices such as artificial heart valves and cochlear implants. Through FEA, researchers can optimize the placement, design, and material properties of these devices, reduce failure rates, and improve their longevity. This can lead to the development of better implants and assist in predicting their long-term durability.

Tissue Engineering

FEA has been applied in tissue engineering to design and optimize scaffolds for tissue regeneration, predicting their response to various loading conditions. It helps in simulating cell behaviour like attachment, proliferation, and differentiation to develop tissue-engineered constructs that mimic the mechanical properties of natural tissues.

Drug Delivery

FEA has many applications beyond tissue engineering, including predicting the behaviour of drug delivery systems like drug-eluting stents. By simulating these systems, FEA can predict drug release rates and distribution of drugs, as well as the mechanical stresses and strains under different loading conditions. This allows for optimizing drug release profiles, understanding drug transport mechanisms, and developing new systems to treat various conditions.

Surgical Planning

FEA can also be used for surgical planning to improve outcomes by optimizing the surgical plan. It can provide information on the effects of different surgical techniques by simulating surgical scenarios. FEA can identify the best location for incisions, estimate bone strength post-surgery, and provide feedback on the feasibility of interventions.

Cardiovascular Modeling

FEA is widely used in simulating the mechanical behaviour of the cardiovascular system, allowing researchers to study blood flow and vessel wall mechanics. FEA can assist in studying the development and progression of atherosclerosis, as well as the effects of stents on blood flow in coronary arteries. Moreover, it can assist in the design of heart valves, assist devices, and artificial blood vessels. FEA is extensively employed in cardiovascular biomechanics to

study the mechanics of arterial walls and their response to different mechanical stimuli. Additionally, it can simulate hemodynamic conditions in the heart, helping determine the optimal positioning and sizing of stents to improve blood flow in occluded arteries. Furthermore, FEA can be used to simulate blood flow in patient-specific cardiovascular models, which can aid in the diagnosis and treatment of cardiovascular diseases.

Joints

One of the most important applications of FEA is the study of joints' biomechanics. FEA is applied in joint biomechanics for several purposes, such as evaluating joint mechanics, designing implants, predicting joint failure, and assessing surgical procedures [24]. It enables the examination of joint mechanics under different loading conditions like compression, tension, bending, and shear, allowing for the analysis of stress and strain distribution in joint structures. This data is valuable for developing prevention and treatment strategies for joint injuries and diseases, as well as optimizing joint implant designs. FEA is also used to optimize the design of joint implants, such as total joint replacements, to enhance their longevity and functionality. By simulating joint implant performance under different loading conditions, it can identify potential failure modes and recommend modifications to the implant design to reduce the risk of failure. Additionally, FEA is used to evaluate the effectiveness of surgical procedures for joint injuries and diseases. For example, it can simulate the effects of ligament reconstruction surgery on the knee joint and predict the functional outcome of the surgery. FEA provides a virtual testing ground to optimize surgical techniques and develop personalized rehabilitation programs.

Finally, FEA predicts joint structure failure, such as cartilage, ligaments, and bones, under various loading conditions. It identifies factors that contribute to joint failure and recommends interventions to prevent or delay joint degeneration and osteoarthritis.

In summary, FEA is an extremely powerful tool with a broad range of applications in bioengineering, including the analysis of mechanical stresses and strains in biological tissues and structures. By allowing researchers and clinicians to simulate and analyse the mechanical behaviour of organs, devices, implants, and tissues under different loading conditions, it provides valuable insights into the underlying mechanisms of various diseases and conditions. Moreover, FEA is crucial in diagnosing, treating, and preventing diseases associated with abnormal mechanical stresses, wear, and fatigue fracture mechanics.

1.5.3 FEM Analysis of the Knee Joint

The knee joint is one of the most intricate and weight-bearing joints in the human body, experiencing significant forces during movement. Due to its complexity, understanding the biomechanics of the knee joint has been a topic of interest for many researchers. In recent years, Finite Element Analysis (FEA) has emerged as a powerful tool for this purpose. This chapter aims to discuss the applications of FEA in the study of the knee joint, also making a brief literature review on the constitutive models and finite elements used to simulate the behaviour of articular cartilage.

FEA Applications in the Study of the Knee Joint

Finite element analysis (FEA) has proven to be a valuable tool in comprehending the specific contributions of various tissue components in knee mechanics for the knee joint. From a clinical perspective, the simulations have been utilized to explore normal knee joint contacts, injury mechanisms, evaluate the mechanical impact of pathological conditions such as osteoarthritis, assess the performance and secondary effects of surgical interventions, and design and evaluate implants. A contemporary summary of the utility of finite element analysis in knee biomechanics can be found in [25].

FEA has been used extensively to study the normal contact mechanisms that occur within the knee joint, providing a more in-depth understanding of the behaviours of the various anatomical components under different loading conditions and during various activities such as walking, running, and jumping. FEA allows for a more detailed understanding of the distribution of loads, stresses, and deformations in the various anatomical structures involved in knee joint articulation.

Traumatic injuries to the knee joint can result from various causes, such as sports injuries, falls, or accidents, and can lead to significant damage to the knee joint and surrounding tissues. This result in complex and often unpredictable patterns of damage, making it difficult to accurately forecast the long-term effects of such injuries. FEA can be useful in studying the effects of such injuries and their impact on the knee joint, allowing clinicians and researchers to pinpoint risk factors and improve treatments and rehabilitation strategies.

Pathological conditions such as osteoarthritis, rheumatoid arthritis, and other degenerative diseases can have a significant impact on the knee joint. FEA can be used to understand the changes in load distributions, stresses, and strains that occur in the knee joint during these pathological conditions and identify the areas that are most affected by the disease. This

information can be used to develop treatment plans and surgical interventions to alleviate pain and improve joint function.

Surgical interventions are often used to treat knee joint conditions such as ligament injuries, meniscal tears, and other structural defects. Finite element analysis can be used to evaluate the performance of surgical interventions and identify any secondary effects that may occur as a result of the procedure. This can help to optimize the surgical approach and reduce the risk of complications such as implant failure or infection. The analysis can also be used to assess the long-term effects of surgical interventions and monitor the patient's recovery.

Implant surgeries, such as total knee replacement, may become necessary when organs lose function. While the use of implants is increasing, their efficacy heavily depends on the quality of their mechanical design and the reliability of the materials used. Additionally, implants can also encounter issues such as adverse effects, tilting, fatigue, and wear that can affect their long-term viability.

FEA is a powerful tool for designing and optimizing medical implants, particularly orthopaedic and prosthetic devices. It enables researchers to simulate the interactions between implants and biological tissues, thereby identifying potential complications and adverse effects on surrounding tissues. FEA can be used to evaluate the performance of implants, such as total knee replacement devices and patellar prostheses, under different loading conditions. This allows researchers to optimize the placement, design, and material properties of these devices, reducing failure rates and improving their long-term durability. FEA can lead to the development of better, more reliable, and more effective implants, ultimately improving the lives of patients.

Evaluation of Cartilage Condition using FEA

It is fundamental to have an appropriate understanding and assessment of knee joint biomechanics in order to improve the anticipation, diagnostics and treatment of related issues and injuries. Given that osteoarthritis (OA) is a progressive condition, it is crucial to identify early signs of OA. However, studying real human knees is limited because cadaveric knees are not easily available, human subjects cannot be deliberately injured, and obtaining data from inside an intact knee can be difficult and inaccurate. Diagnosing knee OA can also be challenging due to variations in symptoms among patients.

FEA is particularly useful in studying the behaviour of articular cartilage and identifying the factors that contribute to joint diseases such as osteoarthritis. These factors may include abnormal loading, altered joint kinematics, and changes in bone morphology. FEA can simulate

personalized risks for the onset and progression of OA and evaluate the effects of conservative preventative actions. It has shown great promise in managing knee OA by predicting the knee joint's response to various loads, identifying cartilage damage location and severity, and guiding treatment planning. FEA can also predict the effects of various parameters involved in knee pain and joint degradation, providing valuable information that is difficult to obtain from traditional analysis.

By providing valuable insights into joint and cartilage mechanics, FEA can aid in the development of new treatments and interventions for joint diseases, potentially slowing down or even reversing their progression and leading to an improved quality of life for patients.

Literature Review

Various FEA models of the knee joint have been developed in the literature for different purposes. These models can be classified into three categories: simplified models, detailed models, and subject-specific models. Simplified models use simple geometries and assumptions to study the biomechanics of the knee joint. Detailed models use complex geometries and material properties to provide more accurate results. Subject-specific models are developed based on the imaging data of individual patients, providing personalized information on the biomechanics of the knee joint.

The accuracy and reliability of FEA results depend on the precision and integrity of the 3D knee model. The development of sophisticated 3D models through imaging techniques enables to precisely capture the patient-specific geometries of both hard and soft tissues in the region of interest, in order to simulate complicated tissue responses more precisely, thereby reflecting more realistic biomechanical behaviours.

In literature, there are numerous studies that have used finite element analysis to study the knee joint for various applications. These include analysis of contacts within the knee joint, study of ligaments- and menisci-related injuries, study of cartilage diseases, and simulations of implants and prostheses. Reporting all of these studies would be an enormous and ultimately inconclusive task, given that the focus of the study is on articular cartilage. However, these studies differ not only in the choice of geometries to use but also in the particular assumptions made regarding the assigned material properties and finite elements used. The following paragraphs aim to provide a comprehensive overview of the constitutive models found literature for cartilage modeling and the finite elements that are best suited to simulate its behaviour, along with a brief section on bones.

1.5.3.1 Material Properties of Hard and Soft Tissues

Selecting appropriate material characteristics for finite element (FE) models to accurately reflect tissue behaviour is a crucial yet challenging step in biomechanical FEA studies. Material properties of hard and soft tissues remain controversial and can vary between in vivo and in vitro conditions, making it difficult to test the properties of tissues in vivo and assign appropriate material properties in FEA. Several studies have investigated the mechanical properties of bones and articular cartilage for different applications, particularly in the knee joint. Here follows a brief literature review of the mechanical properties used in FEA for cartilage and bones.

Material Properties of Articular Cartilage

In the field of knee joint modeling, various approaches have been employed to study the behaviour of articular cartilage. In their study, Wilson et al. developed an axi-symmetric biphasic FE model of the knee joint to study the maximum shear stress. The model consisted of the femoral condyle, tibial plateau, articular cartilage, menisci, and a zone of calcified cartilage. The authors assigned transversely isotropic poroelastic material properties to the menisci and cartilage, while bones were modelled as being much more stiffly elastic isotropic [24]. Un et al. have also contributed to the field with their earlier works. They developed an approximate method for modelling the 3D contact of soft biphasic tissues in a diarthrodial joint under physiological loading. Their model consisted of a cartilage layer on top of rigid bones. A biphasic constitutive relation was used to define the material properties of the articular cartilage [24]. Donzelli et al. developed a transversely isotropic, biphasic cartilage model to predict areas of cartilage failure and high levels of stress. They found that transversely isotropic models predicted peak stresses at the cartilage surface and at the cartilage-bone interface in agreement with results from impact loading. Other previous studies addressed articular cartilage as a composite material with highly anisotropic material properties [25].

However, under dynamic loading, the mechanical response of cartilage can be modelled as an isotropic material [24, 26, 27]. In previous studies, cartilage has been primarily modeled as a linear elastic isotropic material because the loading time of interest, corresponding to a fully extended leg touching the ground, is much shorter than the viscoelastic time constant of cartilage (1500 s). Moreover, this approach is considered appropriate due to the elastic response of cartilage during activities, such as walking or stair climbing, which involve loading frequencies greater than 1 Hz. Donzelli et al. demonstrated that this modeling technique is

accurate enough to predict instantaneous cartilage response, as they found no significant changes in the cartilage contact responses shortly after loading [24].

Blankenvoort et al. modeled cartilage as an elastic isotropic material with a Young's modulus of 5 MPa and Poisson's ratio of 0.45. This choice was based on the instantaneous response of cartilage to loading, which corresponds to a Young's modulus of 5-15 MPa and a Poisson's ratio of 0.5, and the response to long-term loading, which corresponds to a Young's modulus close to 1 MPa and a Poisson's ratio ranging from 0 to 0.4. Subsequently, many 3D FEA knee investigations have used the properties from the studies of Blankevoort et al. [24, 25].

Nevertheless, using a linear elastic behaviour law has limitations, especially during large deformations where the elastic material behaviour is not linear. This is the reason why it is more appropriate to consider cartilage as a hyperelastic material. There are several hyperelasticity models with varying complexities, but the Mooney-Rivlin model is widely used to model cartilage behaviour in the field of large deformations. The Neo-Hookean hyperelastic model, which is a simpler version of the Mooney-Rivlin model, is commonly used in the literature to describe the mechanical behaviour of cartilage, defined by a shear modulus (G) and a bulk modulus (K) that depend on the Young's modulus (E) and Poisson's ratio (υ).

Finally, in recent studies in the literature, cartilage has also been modeled as a poroelastic material, with isotropic poroelastic properties and specific coefficients, while other studies used a depth-dependent isotropic hyperelastic material (Ogden-compressible) or a fibril-reinforced poroviscoelastic material to investigate different aspects of cartilage behaviour under various loading conditions [24]. In summary, the material properties of the articular cartilages evoked in the literature are shown in Tables 1 and Table 2.

References	Behavioral laws	Material properties	
		E	υ
Cohen et al. (2003), Bei et al. (2004), Bei and Fregly (2004), Blankevoort et al. (1991)	Linear elastic isotropic	4	0.45
Blankevoort and Huiskes (1996), Blankevoort et al. (1991), Kempson (1980), Li et al. (2001a, b, 2002), Mommersteeg et al. (1996), Mow et al. (1982)	Linear elastic isotropic	5	0.45
Agneskirchner et al. (2004), Athanasiou et al. (1995), Carter and Wong (2003), Fernandes (2014), FuJISAwA et al. (1979), Peña et al. (2005a, 2006b, 2007), Yao et al. (2006a), Wan et al. (2013), Zheng et al. (2014), Trad et al. (2017)	Linear elastic isotropic	5	0.46
Peña et al. (2006b, 2008), Li et al. (1999b), Donzelli et al. (1999)	Linear elastic isotropic	9	0.46
Li et al. (2001a, b), Setton et al. (1993), Wang et al. (2014), Shriram et al. (2017), Richard et al. (2013), Luczkiewicz et al. (2016)	Linear elastic isotropic	10	0.4
Kempson (1979), Brown and DiGioia (1984)	Linear elastic isotropic	10.35	0.4
Russell et al. (2006), von Eisenhart-Rothe et al. (1997), Mavčič et al. (2000), Hodge et al. (1986)	Linear elastic isotropic	12	0.42
Bendjaballah et al. (1995), Brown et al. (1983), Hayes et al. (1972), Hayes and Mockros (1971), Moglo and Shirazi-Adl (2003), Ramaniraka et al. (2005a, b, 2007)	Linear elastic isotropic	12	0.45
Anderson et al. (1993), Rapperport et al. (1985), Wei et al. (2005), Yang and Radin (1990), Zaki et al. (2002), Goto et al. (2002), Nakajima et al. (1994)	Linear elastic isotropic	15	0.45
Oloyede et al. (1992), Repo and Finlay (1977), Beillas et al. (2004)	Linear elastic isotropic	20	0.45
Bachtar et al. (2006), Dalstra et al. (1995)	Linear elastic isotropic	25	0.3

(continued)

References	Behavioral laws	Material properties	
		E	υ
Zhang et al. (1999a, b)	Poroelastic isotropic	0.7 (k = 2.17*10^{-15} m^4/Ns)	0.1
Shirazi and Shirazi-Adl (2009a, b), Shirazi et al. (2008), Adouni et al. (2012)	Hyperelastic isotropic	10–18	0.49
Anderson et al. (2008), Harris et al. (2012)	Isotropic, nearly incompressible, hyperelastic Neo-Hookean	G = 13.6 k = 1359	0.495
Zahnert et al. (2000), Ghadially et al. (1978)	Hyperelastic Neo-Hookean	E = 3.4	0.49
Benvenuti (1998), Büchler et al. (2002), Kempson (1979), Kempson et al. (1976)	Hyperelastic Neo-Hookean	E = 10	0.4
Anderson et al. (2005)	Hyperelastic Mooney-Rivlin	$C_1 = 4.1$ $C_2 = 0.41$	0.4
Namani et al. (2003)	Hyperelastic Mooney-Rivlin	$0.2 \leq C_1 + C_2 \leq 2$	0.125

E: Young's modulus (MPa), υ: Poisson's ratio

Table 1.2 Poroviscoelastic material properties implemented for articular cartilages

Material properties	Femoral cartilage	Tibial cartilage	References
E_0 (MPa)	0.92	0.18	Halonen et al. (2014), Julkunen et al. (2007)
E_e (MPa)	150	23.6	Halonen et al. (2014), Julkunen et al. (2007)
E_m (MPa)	0.215	0.106	Halonen et al. (2014), Julkunen et al. (2007)
η (MPa s)	1062	1062	Julkunen et al. (2007), Halonen et al. (2014)
K_0 (10^{-15} m^4/Ns)	6	18	Julkunen et al. (2007), Halonen et al. (2014)
υ_m	0.15	0.15	Halonen et al. (2014), Wilson et al. (2003)
M	5.09	15.64	Julkunen et al. (2007), Halonen et al. (2014)
n_f	0.8–0.15z	0.8–0.15z	Halonen et al. (2014), Mow and Guo (2002)

E_0: initial fibril network modulus, E_e: strain-dependent fibril network modulus, η: damping coefficient, E_m: nonfibrillar matrix modulus, k_0: initial permeability, υ_m: Poisson's ratio, M: exponential term for the strain dependent permeability, n_f: fluid fraction, and z: normalized depth

Table 1 and Table 2. Synthesis of the behavioural laws in the literature to model the behaviour of cartilage tissue.

Material Properties of Bones

Despite the known heterogeneous and biphasic nature of bone tissue, different authors have modeled it as a homogeneous and solid elastic material. Since the stiffness of bone is much higher than that of the relevant soft tissues, its influence in many studies available in the literature was minimal [24]. Due to the relatively high density and Young's modulus of the femur, tibia, patella, and fibula compared to the cartilage and menisci in the knee joint, previous 3D finite element analysis (FEA) studies assumed that these bony structures were rigid bodies, in order to avoid unnecessary computational costs. On the other hand, several articles in the literature considered bones to be deformable bodies. In the study presented by Donahue et al., a 3D FE knee joint model was generated based on CT images to determine whether the assumption of bone as a rigid body could affect contact behaviour [24]. The results revealed that the contact responses within the knee joint have no significant difference whether the bone is assumed to be a rigid body or a deformable body. This explains why bones are considered either as a rigid body or as a linearly elastic isotropic material in the literature. Additionally, when the interest is focused on cartilage only, the difference between cortical and trabecular

bone is also negligible. In summary, the material properties of the bones evoked in the literature are shown in Table 3.

References	Behavior law	Material properties			
		Cortical bone		Cancellous bone	
		E	υ	E	υ
Dabiri and Li (2013), Gu and Li (2011)	Linear elastic isotropic	5000	0.3	–	–
Donahue et al. (2002, 2003), Zheng et al. (2014), Zheng (2014)	Linear elastic isotropic	8000	0.3	–	–
Anderson et al. (2008), Harris et al. (2012)	Linear elastic isotropic	17,000	0.29	–	–
Adams et al. (2007), Terrier et al. (2007)	Linear elastic isotropic	17,000	0.3	–	–
Katsamanis and Raftopoulos (1990)	Linear elastic isotropic	19,900	0.36	–	–
Benli et al. (2008), Izaham et al. (2012)	Linear elastic isotropic	20,000	0.3	–	–
Guess et al. (2010)	Linear elastic isotropic	20,000	0.2	–	–
Russell et al. (2006)	Linear elastic homogenous	2000	0.3	120	0.3
Brown and Ferguson (1980), Reilly et al. (1974), Brown et al. (1983)	Linear elastic isotropic	6900	0.26	690	0.3
Miyoshi et al. (2002a, b)	Linear elastic isotropic	8000	0.3	1500	0.2
Lengsfeld et al. (1998)	Linear elastic homogenous	15,000	–	1100	-
Bachtar et al. (2006)	Linear elastic isotropic	17,000	0.3	2000	0.2
Dalstra et al. (1993, 1995), Dalstra and Huiskes (1995)	Linear elastic isotropic	17,000	0.3	800	0.2
Duda et al. (1998)	Linear elastic homogenous	17,000	0.33	15,000	0.3
Büchler et al. (2002), Hayes and Bouxsein (1991), Rice et al. (1988)	Linear elastic non-homogenous	15,000	0.3	–	–

Table 3. A summary of the material properties assigned to the bony structure in literature.

1.5.3.2 Types of Finite Elements in Knee Joint FEA

Despite the progress that has been made in modelling subject-specific joint contact mechanics, many challenges still remain. In order to accurately model the knee joint, it is necessary to use finite elements that are appropriate for each tissue type. The articular cartilage of most joints in the human body has a complex geometry, undergoes large deformations, is subjected to large compressive loads, and is often thin compared to the surrounding anatomical support. These challenges make it difficult to obtain accurate, validated computational models of articular contact mechanics. The element type used to discretize the articular geometry is one of the most important choices that affect accuracy and robustness in simulations of articular contact. There are many different types of finite elements that can be used in finite element analysis, each with its own strengths and weaknesses. Some of the most commonly used finite elements in knee joint modeling include linear tetrahedral elements (TET4), quadratic

tetrahedral elements (TET10), linear hexahedral elements (HEX8), and quadratic hexahedral elements (HEX20) [27].

Linear tetrahedral elements (TET4) are the simplest and most computationally efficient type of finite element. They are frequently used due to the ease and robustness of performing automatic meshing, local and adaptive refinement, and the ability to accurately represent the geometry of complex structures, such as the menisci and ligaments. However, they overestimate stiffness at large deformations and require many elements to ensure solution convergence. Linear tetrahedral elements have limited accuracy when it comes to simulating the mechanical behaviour of articular cartilage. There are several examples in the recent literature that have used TET4 elements to discretize articular cartilage. Nevertheless, the TET4 element has several well-known numerical issues. First, TET4 elements can only represent a constant strain state, which necessitates a very fine discretization, often requiring long solution times. Second, TET4 elements lock for nearly incompressible materials as well as under bending deformations, which further reduces their accuracy.

Because of these issues, trilinear hexahedral elements (HEX8) have seen much wider use in joint contact analyses due to their ability to better simulate structures with a regular, box-like shape, such as bone. They are considered the gold standard for modeling articular cartilage due to their accuracy and computational efficiency. However, creating hexahedral meshes for complex geometries such as articular cartilage can be challenging and time-consuming.

The scenario changes when using more advanced high-order elements like quadratic hexahedral elements (HEX20). These advanced elements boast the addition of nodes not only at the vertices but also halfway along the edges, guaranteeing an accurate representation of complex curved geometries. In general, high-order elements (TET10, HEX20) are recommended to better track deformations and stresses in soft tissues such as cartilage, muscle, or ligament as they produce smoother strain and stress estimates with fewer elements compared to linear approximations (TET4, HEX8). Nevertheless, the issue with HEX20 elements still remains their high computational cost.

Quadratic tetrahedral elements (TET10) are an attractive alternative to TET4 elements. They maintain the advantages of tetrahedral mesh generation while offering a more accurate representation of curved boundaries compared to HEX8 elements, as their edges and faces can deform. Additionally, quadratic tetrahedral elements have a higher order of interpolation and can represent curvature and strain gradients more accurately. This makes them well-suited to better represent of the mechanical behaviour of articular cartilage. Maas et al. have demonstrated that quadratic tetrahedral elements are comparable both in computational cost and accuracy to the "gold standard" HEX8 elements for articular contact analysis.

In conclusion, even though the hexahedral elements have good accuracy, simulating complex geometries with these types of elements brings to higher labour costs for meshing and usually requires manual intervention. Tetrahedral elements, especially quadratic ones, are best suited for complex geometry. The accuracy of the model can also be balanced by decreasing the size of the elements and thus increasing their number. Figure 4 shows the finite elements mentioned up to now.
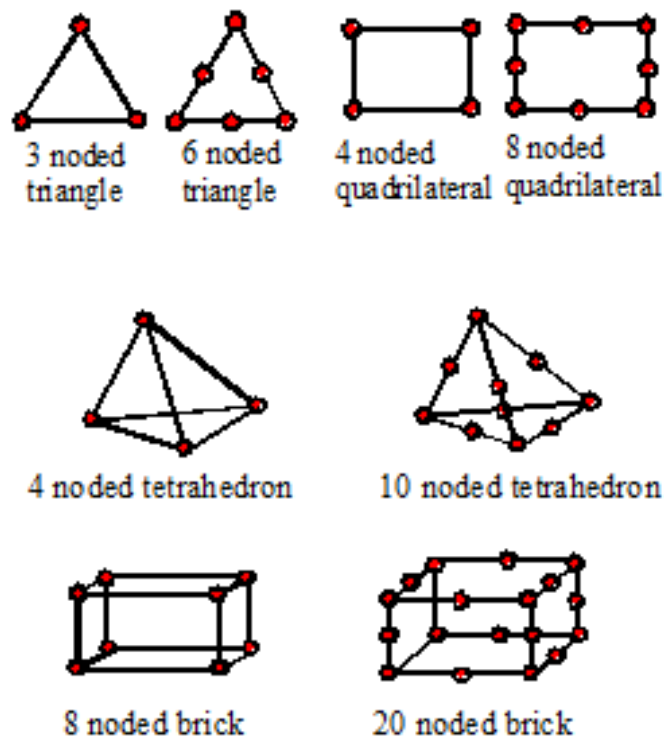

Figure 4. Types of finite elements

1.6 Additive Manufacturing in Healthcare

Additive manufacturing (AM), also known as 3D printing, is a revolutionary technology that has found extensive applications in medicine and bioengineering. By enabling the production of patient-specific medical devices, implants, tissues, and anatomical models for surgical planning and training, AM has the potential to transform the way healthcare is delivered. In this chapter, we will explore the various applications of AM in healthcare.

1.6.1 Additive Manufacturing

Additive manufacturing (AM) is defined by the ASTM society as "a process of joining materials to make objects from 3D model data, usually layer upon layer, as opposed to subtractive manufacturing methodologies" [30].

Additive manufacturing, also known as 3D printing or rapid prototyping, is a process of creating three-dimensional objects by adding material layer upon layer. This is in contrast to traditional manufacturing methods that involve subtractive processes to create a final product. A Computer-Aided Design (CAD) is used to create a digital design of the object, which is then translated into instructions for the 3D printer. The printer then uses a variety of materials, including plastics, metals, and even biological materials, to create the object layer by layer until the final product is complete. AM's main advantage is that it allows for the creation of highly complex and customized objects with precision and accuracy, revolutionizing the way many industries approach design and production.

Currently, additive manufacturing is utilized and being investigated for use in areas such as the medical, automotive, aerospace, and marine industries, as well as industrial spare parts. In the medical field, every patient is unique and, therefore, AM has significant potential in personalized and customized solutions.

1.6.2 AM Applications in the Medical Field

Additive manufacturing (AM), also known as 3D printing, is a revolutionary technology that has found extensive applications in healthcare. In medicine and bioengineering, AM has the potential to revolutionize the way healthcare is delivered by enabling the production of patient-specific medical devices, implants, and anatomical models for surgical planning and training. Using the classes-based classification, AM applications can be distinguished into the following categories: "models for preoperative planning, education and training", "inert implants", "tools,

instruments and parts for medical devices", "medical aids, supportive guides, splints and prostheses" and "biomanufacturing" [31]. For a more general classification, this can be modified so that implants do not need to be inert, and models for preoperative planning, education and training could also include postoperative and operative models using the term "medical models". So, the classification of medical applications of additive manufacturing is the following: 1. Implants; 2. Tools, instruments, and parts for medical devices; 3. Medical aids, supportive guides, splints and prostheses; 4. Biomanufacturing; 5. Medical models.

1. Implants

AM has revolutionized the way implants are created. An implant is a medical device that is surgically placed inside the body. They are typically used to replace or augment a missing or damaged body part, such as a tooth, a joint, or a pacemaker for the heart. Implants are designed to integrate with the body and become a permanent part of the patient's anatomy. Traditionally, implants were mass-produced, which often led to poor fit and discomfort for the patient. Now, 3D printing can create customized implants that are tailored to fit the unique anatomy of each patient. Implants are directly or indirectly additively manufactured to replace defective or missing tissue. The process involves creating a digital model of the patient's anatomy using medical imaging, such as CT or MRI scans. The model is then used to 3D print a customized implant that fits perfectly and is more comfortable for the patient. Before clinical operation, implants need to be sterilized. The implant material must be compatible with the surrounding tissue, and the surface characteristics can impact cell adhesion [31].

This approach has been used for a wide range of applications, including orthopaedic and dental implants, as well as craniofacial implants used in reconstructive surgery. Some of the latest studies have explored how to embed materials inside implants, for example, as a type of drug delivery system. However, the demanding and time-consuming requirements for tissue compatibility and approval processes can hinder the production of these implants.

2. Tools, Instruments, and Parts for Medical Devices

Tools, surgical instruments, and parts for medical devices are used to improve clinical operations and may require sterilization due to contact with body fluids, tissues, and organs. AM can create these components using biocompatible materials that can withstand the harsh conditions of the operating room. They can be tailored to meet the unique needs of individual patients, such as personalized drilling guides. The manufacturing process for medical device

parts and tools is similar to that of implants or preoperative models developed from medical imaging [32].

3. Medical Aids, Supportive Guides, Splints, and Prostheses

This class refers to external parts that are created using AM and can be combined with standard appliances to enable customization. Examples of such parts include hearing aids, custom orthotics, splints, braces, and prosthetic sockets. These devices can be customized to fit the specific needs of individual patients and can be made from materials that are both lightweight and strong.

Medical aids such as hearing aids and custom orthotics are now commonly produced using 3D printing technology. 3D printing allows for the creation of highly customized devices that are tailored to the specific needs of each patient. This can result in greater comfort and better performance of the medical aid. Furthermore, AM has been utilized to produce surgical guides that aid surgeons during complex surgeries. These guides are created through 3D printing and are based on a digital model of the patient's anatomy. They assist the surgeon during the procedure, ensuring greater precision and reducing the risk of complications. Splints are another medical device that can be produced using 3D printing. Traditionally, splints have been made from plaster or fiberglass, which can be uncomfortable and time-consuming to produce. With 3D printing, splints can be quickly and easily produced from digital models, reducing the time and cost associated with traditional methods [31].

Prostheses are perhaps one of the most exciting applications of 3D printing in the medical field. A prosthesis is an external device that is designed to replace a missing or damaged body part, such as a limb, an eye, or a breast. Prostheses are typically attached to the body and can be removed or adjusted as needed. 3D printing allows for the creation of highly customized prostheses that are tailored to the individual patient's needs. Using advanced imaging techniques, a 3D model of the patient's anatomy can be created, and a prosthesis can be designed to fit that specific model. This results in greater comfort, better function, and improved outcomes for the patient [33].

4. Biomanufacturing

Additive manufacturing has also played a crucial role in tissue engineering, a rapidly growing field that aims to create functional tissues and organs for transplantation. Biomanufacturing combines additive manufacturing and tissue engineering to produce biologically compatible materials that can interact with the body's natural systems. By layering

these materials in a precise pattern, 3D printers can create scaffolds that mimic the complex architecture of human tissues and organs, which can then be seeded with cells to promote tissue growth and regeneration. Various types of polymers, ceramics, and composite materials can be utilized, and porous structures are favoured to enhance cell viability and differentiation. The shapes of the scaffolds can be personalized to address defects or to replicate the geometry of the tissues, and this necessitates the capture of specific geometries through medical imaging or 3D scanning. The process typically requires sterility, and in vitro or in vivo cell growth may be necessary before final application.

This approach has been used to create a wide range of tissues, including skin, cartilage, and bone, and can also be used to test new drugs and treatments or to create replacement tissues and organs for transplantation [31].

5. Medical Models

One of the most significant applications of additive manufacturing in medicine is the creation of anatomical models. For clinical treatment, pre- or post-operative planning and implant planning, high-fidelity physical organ models are of significant importance. Moreover, they can be used for medical education in colleges and universities, providing students with more intuitive stereoscopic vision and tactile sensation [31,34].

The patient's condition can only be understood from the 2D plane by means of medical imaging technologies such as MRI or CT scans, which provide a two-dimensional representation of the patient's anatomy. However, these technologies may not provide the most accurate pre-operative guidance for surgery. Additionally, the traditional model production procedure is not suitable for rapid prototype modelling due to its difficulty and time-consuming nature. The advent of 3D printing has revolutionized medical modelling as clinicians are now able to conduct surgery preparation, simulation, and diagnosis using 3D printed models, which improves the operation's success rate by providing precise preoperative guidance for surgery. These 3D models enhance procedure repeatability, automate steps, and make the entire operation phase more precise, reducing the operation's anaesthesia time and infection risk. Moreover, 3D models can be used to explain dangerous and complex surgical procedures to patients and their family members, making them applicable for education purposes.

Chen et al. [34] used photographs collected from magnetic resonance scanning to print a knee joint disease model to provide orthopaedic postgraduates with a more vivid and understandable anatomical type of knee joint events. This allowed students to learn more about the causes, diagnosis, and treatment of the disease and better understand the anatomical parts

and spatial arrangement. Additionally, they could follow surgical criteria and execute simulation surgery experiments, which helped them discover information that is not technically accessible and improve their knowledge of the disease and anatomy.

AM Workflow in Medical Field

The process of creating personalized medical devices or patient-specific anatomical models typically starts with capturing the patient's geometry through Computed Tomography (CT), Magnetic Resonance Imaging (MRI), 3D scanning, or any design software [31]. The next step is converting the Digital Imaging and Communications in Medicine (DICOM) file or 3D CAD model generated from these scanning technologies into STL format. These data are then manipulated and optimized to obtain a 3D model of the patient's anatomy or to design patient-specific implants. AM technologies are used to print patient-specific anatomies or implants, which may require post-processing. The final step involves the validation and testing of models and, when the medical device or anatomical model is ready, the final step is the clinical application and follow-up.

1.6.3 Digital Anatomy Printers and PolyJet Technology

Digital Anatomy Printers (DAP) are a type of 3D printer specialized in creating models of human anatomy for medical education and training purposes. These printers use data from medical imaging technologies, such as CT or MRI scans, to create highly accurate and detailed 3D models of human organs and tissues. They can use different printing technologies, but the most commonly used recently, due to its various advantages, is the PolyJet technology.

PolyJet Technology

PolyJet is a 3D printing technology that builds parts by jetting thousands of photopolymer droplets onto a build platform and solidifying them with a UV light. It's one of the fastest and most accurate 3D printing technologies currently available. This technology allows manufacturers to create models using high-performance composites of materials with variations in rigidity and elasticity, blended transitions, multiple colours, textures, and transparencies. By using these different stiffness values and textures, biomedical models can mimic the mechanical properties of their pathologies without compromising the complexity of the geometric design.

In particular, PolyJet technology uses several heads to accurately deposit acrylic-based photopolymer droplets. These heads are placed on a jetting head that slides back and forth along

the x-axis, jetting tiny droplets of ultraviolet (UV) curable resin onto the build tray. Depending on the size of the object, the jetting head also moves along the y-axis until the layer is completed. After building each layer, UV bulbs alongside the jetting head harden the layer, and the tray moves down in the z direction a certain distance so the next layer can be printed. Where hollow parts or overhangs are required, the print head deposits a layer of removable gel-like support material that does not crosslink with the main build material. Half of the heads are dedicated to the support material, and the remaining heads are for the model material. PolyJet technology is among the few methods of 3D printing capable of printing multiple materials in a single build. Using this technology, single parts can be produced with a combination of alternative materials including combinations of thermoset and elastomeric materials. Further, fully cured models can be handled and used immediately, without additional post-curing.

Stratasys J850 Digital Anatomy Printer

The Stratasys J850 Digital Anatomy Printer is a cutting-edge 3D printer specifically designed for medical use. It uses advanced multi-material PolyJet technology to produce anatomical models with unparalleled accuracy and realism, enabling medical professionals to create lifelike models of organs, bones, and other body structures for surgical planning, medical education, and device testing. The J850 is unique in its ability to print models using materials that accurately mimic real human tissue and bone. This is achieved through precise control of material properties such as colour, transparency, and softness. This feature is extremely valuable in a medical context, allowing for more accurate surgical planning, enhanced medical education and research, and improved patient outcomes. The J850 also allows for the production of multi-material models, enabling the creation of complex structures with varying properties. The printer has the ability to create models with a range of materials, including rigid and flexible plastics, and boasts an extremely high level of colour accuracy. It also has a large build area of 490 x 390 x 200 mm.

The J850 Digital Anatomy Printer enables medical professionals to create anatomical models that accurately replicate a wide range of human tissues, from the pliable textures of organs and muscles to the rigid structures of bone and cartilage. Its high accuracy and detail make it a valuable tool for simulating complex surgical procedures, studying diseases and injuries, and improving patient outcomes.

The Digital Anatomy Creator, which is associated with the printer, allows to create new customized materials with the desired mechanical properties and geometry in each print slice by combining different materials together.

Overall, the Stratasys J850 Digital Anatomy Printer is a game-changing tool for medical professionals. Its unique digital materials and extensive library of anatomical pre-sets allow for the creation of biomechanical models that look, feel, and respond like the real thing. This advanced printer has the potential to revolutionize the medical field by providing medical professionals with a powerful tool to improve patient outcomes and advance medical research.

Stratasys Objet260 Connex3

The Stratasys Objet260 Connex3 3D printer is a versatile and high-quality 3D printing solution designed for a variety of applications, from rapid prototyping to full-colour product design. The printer uses PolyJet technology to create highly detailed and precise models with multiple materials and colours, allowing the production of complex and multi-functional parts. The printer can use a wide range of materials, including rigid and flexible plastics, transparent materials, and rubber-like materials. Additionally, it can produce parts in over 1,000 colours, enabling the creation of highly realistic models with fine details and smooth surfaces, also enabling to blend colours to create new shades. The printer has a build area of 255 x 252 x 200 mm and can produce high-resolution parts with a layer thickness as small as 16 microns. The Connex3 can print with multiple materials simultaneously, allowing the creation of parts with varying levels of rigidity, flexibility, and transparency. It is suitable for designers, engineers, and manufacturers looking to create high-quality and aesthetically pleasing models for product development in industries such as automotive, aerospace, and consumer goods.

In addition, the Objet260 Connex3 is also used for creating anatomical models. It can produce highly detailed models with a range of materials that accurately replicate the properties of human tissue. This makes it useful for medical professionals in fields such as surgery and education, as they can use these models to plan and practice procedures, as well as to teach students. The user-friendly interface and software also make it easy to customize prints to specific needs.

In summary, AM has unlocked numerous opportunities in the field of biomedical engineering. Patient-specific anatomical models, implants, and prosthetics can be produced using 3D printing technology. Additionally, 3D printing has the potential to transform tissue engineering and drug delivery systems. With the continuous development of 3D printing technology, its potential applications in healthcare are expected to grow even further.

2 AIM OF THE STUDY

The present work aims to combine Finite Element Analysis (FEA) and 3D printing technologies in order to develop new innovative methodologies that improve the understanding of cartilage behaviour and implement personalized solutions to mitigate potential complications caused by diseases or injuries. Overall, the objective of this thesis is to use both computational and experimental methods to characterize innovative PolyJet materials capable of mimicking cartilage behaviour and use 3D printing to establish new mechanical test configurations that are specific to each patient.

The specific aims of my research project were:

- To create two digital materials capable of simulating the mechanical behaviour of articular cartilage and compensating for differences in its composition resulting from age, health, and lifestyle. Subsequently, to print standardized samples using these materials and subject them to compression and tensile tests to characterize their properties. Finally, to use the results of these tests to extract the mechanical parameters needed for computational analyses.

- To create 3D models of the knee joint starting from MRI and CT images of patients with or without femoral cartilage damage. Then, subject these models to a finite element analysis, using both experimentally-derived material properties and those found in literature, to compare their behaviour.

- To print the 3D models created using digital materials and PolyJet technology with the goal of establishing a new personalized mechanical test configuration for each patient. Specifically, using the patients' anatomies, design and print special supports to use in a cartilage compression test that simulates the real loading conditions occurring in the patients' knees. In addition, perform a computational analysis of the models with supports to validate the results obtained from the tests.

3 MATERIALS AND METHODS

3.1 Segmentation and Image Registration

Using high performing medical imaging software (Materialise, Mimics), the MRI and CT scan images of the knee joint were processed to segment the different parts of the knee: femur, tibia, and femoral cartilage were considered. Different segmentation techniques such as thresholding, region growing, manual editing and Booleans were employed to isolate the anatomical parts. Once the segmentation process was completed, 2D masks were converted in highly accurate 3D objects. Finally, the 3D models were saved in .stl file format for further analysis. Below is the step-by-step explanation of the process.

MRI is considered the gold standard for imaging soft tissues, including cartilage, while CT scans are better suited for displaying hard tissues such as bone. To provide a more accurate visualization of both bones and cartilage, a novel approach was developed that combines CT scan and MRI images.

EU Restore Project

The preliminary data from which this work started come from the database of the European project RESTORE (https://restoreproject.eu/).

Participants

Participants were recruited as part of the European project RESTORE, (https://restoreproject.eu/, CORDIS grant agreement ID: 814558). The aim of RESTORE is to implement patient-specific solutions for cartilage regeneration. This study has been approved by the Icelandic Bioethics Commission (approval number: VSN-19-050).

Recruitment

After completing an informed consent, 47 subjects (24 females, 23 males, mean age = 50 years, std age = 19 years, min age = 20 years, max age = 81 years) underwent X-ray, CT scan and MRI of one knee at Landspitali University Hospital in Reykjavik, Iceland, using standardized acquisition protocols and patient positioning. From the total number of patients,

24 subjects (12 females, 12 males, mean age = 64 years, std age = 12 years, min age = 35 years, max age = 81 years) were suffering from degenerative (D) cartilage. They were on a waiting list for prosthetic replacement. Fifteen subjects (9 females, 6 males, mean age = 35 years, std age = 11 years, min age = 20 years, max age = 50 years) suffered from a knee trauma (T) with possible cartilage injury, and 8 participants (3 females, 5 males, mean age = 34 years, std age = 14 years, min age = 24 years, max age = 67 years) were involved in the study as control (C) subjects (no knee symptoms or history of trauma).

Scanning Process

Both protocols were performed with the knee in the same fixated position, evaluated by two radiological technicians, and under the supervision of a radiologist.

The CT scanner was a Toshiba Aquillion One, 320 slice, that covered a 16 cm area of interest in a single gantry rotation. Slice thickness was 0.5 mm with an increment of 0.25 mm. Tube voltage was 120 kV, tube current was 250 mA and effective mAs was 125. The protocol covered about 15 cm of area (axial plane) centred at the knee joint with small variations according to patient size. No intravenous contrast was administered. The initial CT dose index was set to 12.1 mGy. The preliminary dose-length product was 193.2 mGy*cm. These values were individually recalculated by the CT scanner for each patient according to size/thickness of the examined area.

The MRI scanner was a 3T Siemens Healthcare Prisma scanner. Volumetric 3D sequences with isotropic voxels of 0.6 mm were acquired in the axial plane with a surface coil without intravenous contrast. This allowed for reconstructions in various planes along regions of interest. A 3D fast spin echo, intermediate weighted and fat-suppressed sequence which allowed for morphologic evaluation of cartilage and for better assessment of subchondral bone marrow was used. The maximum field of view was 16 cm, with a minimum matrix size of 256 × 256. The area of interest was cartilage-covered areas around the knee. The protocol covered 14 cm centred at the knee joint.

Based on the quality and precision of the MRI and CT scan images obtained, two patients were selected for the purpose of this project, one from the control group (C), i.e. no symptoms from knee of history of trauma, and one from the degenerative group (D), i.e. patients who were suffering from degenerative cartilage and were on a waiting list for prosthetic replacement.

Data Processing and Analysis

The MRI and CT scan images of the left knee of a healthy 27-year-old subject with no history of osteoarthritis and of a 70-year-old subject suffering of degenerative cartilage were obtained. The scans were performed at the exact same position, i.e. with the knee joint in full extension.

All DICOM files from the scans were processed using a medical imaging software, Mimics. Mimics (Materialise Interactive Medical Image Control System) is a high-performing software for processing medical images and creating 3D models. A stack of images can be loaded into the software. If images in the XY plane (axial plane) are loaded, Mimics is able to calculate and create images in the XZ (coronal) and YZ (sagittal) direction. This allows to have a three-dimensional sensing of the 2D data. The segmentation process was carried out following the same protocol for bones and cartilages, respectively taken from CT scan and MRI. Knee bones of the femur, tibia and femoral cartilage were considered.

Image Registration

MRI is the state-of-the-art imaging modality for the assessment of cartilage, enabling a proper and accurate visualization of soft tissues in general. On the other hand, CT scan excel in displaying hard tissues, making it well-suited for bone representation. For this reason, cartilages were segmented from MRI images while bones from CT images. To provide a more accurate visualization of both bones and cartilage, a novel approach was developed that combines CT scan and MRI images.

The process involved several steps. For each patient, the bones of femur and tibia and femoral cartilage were segmented from the respective CT and MRI images. This involved creating a mask for each entity using a density threshold interval and refining the masks as needed for improved accuracy. The masks were then converted into highly accurate 3D objects. Starting from the individual images with segmentations and 3D objects, a new image was created with image registration. MRI and CT images were registered, and bones and cartilage objects were combined. During CT and MRI scans, patients were positioned in the same way for both scans to enable accurate superimposition of the images on corresponding anatomical parts. This alignment was achieved by selecting specific landmarks on the anatomy, with at least four points chosen for the most precise overlay possible. The most suitable landmarks included the highest and lowest points on the patella bone in the sagittal view, the upper point of the tibial tubercles, and the lateral side of the tibia in the coronal view. Other points could also be selected as landmarks as needed. The new image was then created, and the 3D objects were combined together. The result is basically a CT image with both the segmentation of bones

and cartilage segmentations taken from the MRI. On the newly created image, a realignment process was manually carried out to ensure proper alignment of the cartilage around the corresponding bone while avoiding overlapping. Once this operation was completed, bone and cartilage masks were created from 3D objects. Further editing operations were performed where needed. The anatomical correctness of the models was ensured by referring to the literature and verified with the help of a radiologist. Finally, a new image is created using the aligned CT scan and MRI images.

Since the segmentation process was carried out following the same protocols for bones and cartilages, below is a brief explanation of the step-by-step process.

Segmentation Process

The initial step in creating a 3D model of the knee joint from 2D data is segmentation. The segmentation process was carried out following the same protocol for bones and cartilages, respectively taken from CT scan and MRI. Knee bones of the femur, tibia and femoral cartilage were considered. Several tools to segment the regions of interest were used.

Firstly, a mask for each entity was created by setting a density threshold, one for the cartilages and one for the bones. The medical images generated from CT or MRI scanners are composed of grayscale information. Mimics allows the user to create models based on the grayvalues (converted in Hounsfield Units in CT images) within these images. A grayvalue is a number associated with an image pixel defining the shade of the pixel, in a scale from white to black. There is a direct relation between material density of the scanned object and the grayvalue assigned to each pixel in the image data. For this reason, Mimics allows calculation of the radio density in Hounsfield Units directly from a region of interest on CT scans.

The Hounsfield Unit (HU) is a relative quantitative measurement of radio density used by radiologists in the interpretation of computed tomography (CT) images [37]. Human tissues absorb or attenuate X-ray beams according to their density. The absorption/attenuation coefficient of radiation within a tissue is used during CT reconstruction to produce a grayscale image. The physical density of tissue is proportional to the absorption/attenuation of the X-ray beam. The Hounsfield unit, also referred to as the CT unit, is then calculated based on a linear transformation of the baseline linear attenuation coefficient of the X-ray beam, where distilled water (at standard temperature and pressure) is arbitrarily defined to be zero HU and air defined as -1000 HU. The linear transformation produces a Hounsfield scale that displays as gray tones. More dense tissue, with greater X-ray beam absorption, has positive values and appears bright; less dense tissue, with less X-ray beam absorption, has negative values and appears dark.

The *Threshold* tool in Mimics was used to create a first definition of the segmentation object. This tool identifies a set of voxels which have values within a user-defined range of Hounsfield Units (or Gray Values). Therefore, the cartilages mask was filtered from 0–300 HU, which provides a good range for visualization of cartilage pixel intensities. The bones mask, instead, was filtered from 226-2839 HU (Mimics' default threshold for bones). However, due to image artifact, it is difficult to perfectly segment a region of interest with just a thresholding operation. Therefore, the threshold tool is used to create an initial mask that can be further edited using additional segmentation tools. After thresholding, it was necessary to separate the regions of interest from the various masks and clean them from image artefact. To do so, the *Region Grow* tool was used to remove any regions of the masks that were not attached directly to the regions of interest, such as floating pixels, speckles, or noise. This tool works by selecting an initial seed point within the image, and then iteratively growing a region around that seed point based on predefined criteria. Then *Split Mask* was used to separate parts of the same mask into different structures. In particular, femur and tibia were separated from the bone mask and femoral cartilage from the cartilage mask. If necessary, editing operations were performed to refine the masks and improve their fitting accuracy. These operations included *Crop Mask, Edit Mask*, *Smart Fill* and *Boolean Subtraction*.

The *Crop Mask* tool was used to select a region of interest and restrict the segmentation to that region. When cropping a mask, everything outside the region of interest will be removed from the mask. *Edit Mask* was used to draw, erase, or locally threshold a specific mask. It allows editing on individual 2D image slices or directly on the 3D preview of the mask. Advanced editing tools are *Smart Fill* and *Boolean Operations*. These tools provide additional functionality that can be helpful when fine-tuning the mask. The *Smart Fill* tool has two modes: the *global filling*, which will try to fill a user-specified number of voxels in a mask and the *manual filling* which allows local areas of a mask to be marked for filling. This tool was used to fill holes when was necessary. After segmenting all the parts, a *Boolean subtraction* was performed to prevent overlapping pixels between masks and ensure no penetrations. This was necessary to avoid issues in the Finite Element Analysis for cases where the geometries overlapped.

The whole segmentation process was performed precisely, in order to extract meaningful and consistent information from images. Then, to convert the selected masks into a 3D parts, *Calculate Part* was used. Some other refinements were performed on the 3D objects to improve the overall quality of the parts for the subsequent Finite Element Analysis. The *Smooth* tool was used to remove spikes and existing artefacts, smoothing the surfaces. Instead, to filter small

inclusions and close small holes, the *Wrap* tool was used. The final result (for the control patient) is shown in the Figure 5.
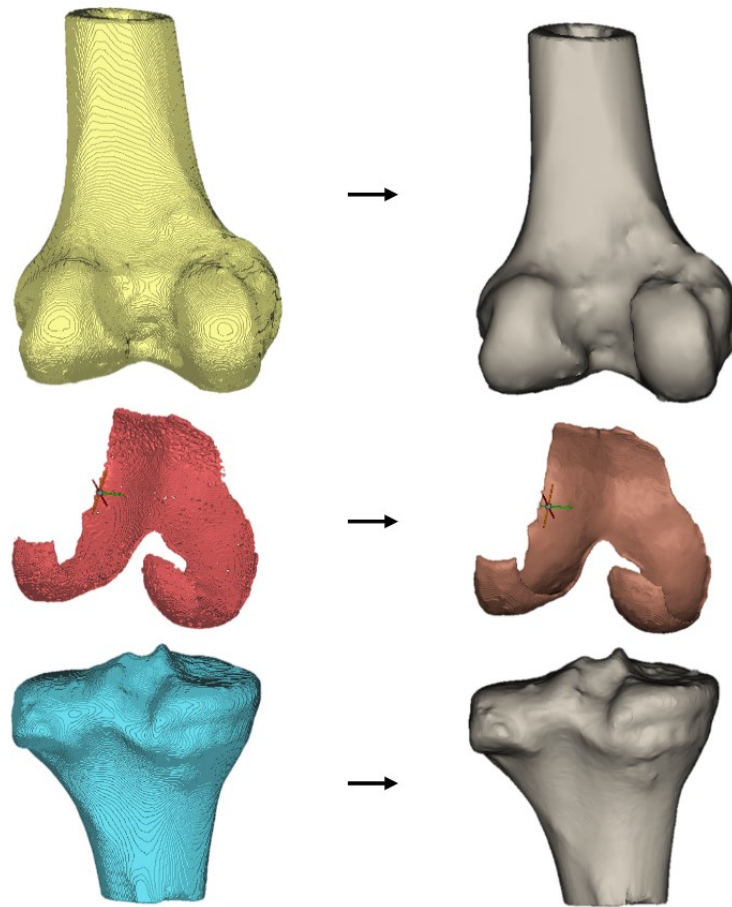

Figure 5. 3D model of the control's patient knee joint after smoothing and wrapping.

It is important to specify that throughout the segmentation process, the aforementioned tools were used with caution. The specific anatomies of the patients had to be preserved in the best possible way. This becomes even more crucial in the case of the patient with degenerative cartilage, where imperfections and small holes were present that obviously had to be preserved for the purpose of the analysis.

Mimics is able to calculate a 3D model using the segmented structures, the information on the pixel size and the distance between the image slices. This 3D object is an STL file.

STL (STereoLithography interface format or acronym for "Standard Triangulation Language") is a file format commonly used for 3D printing and computer-aided manufacturing (CAM) since is able to represent complex geometries such as anatomical parts accurately. The main feature of an STL file is that it represents a solid object by discretizing its surface into a collection of triangles. Each triangle is defined by the X, Y, and Z coordinates of its three vertices, which are repeated in the file for each triangle. Additionally, a vector is included to

define the normal direction of each triangle, which is important for calculating the surface orientation and shading of the object when it is rendered or 3D printed.

The 3D objects of the femur, tibia, and femoral cartilage of each patient were finally exported in STL format to 3-Matic modeling software to prepare the models for Finite Element Analysis.

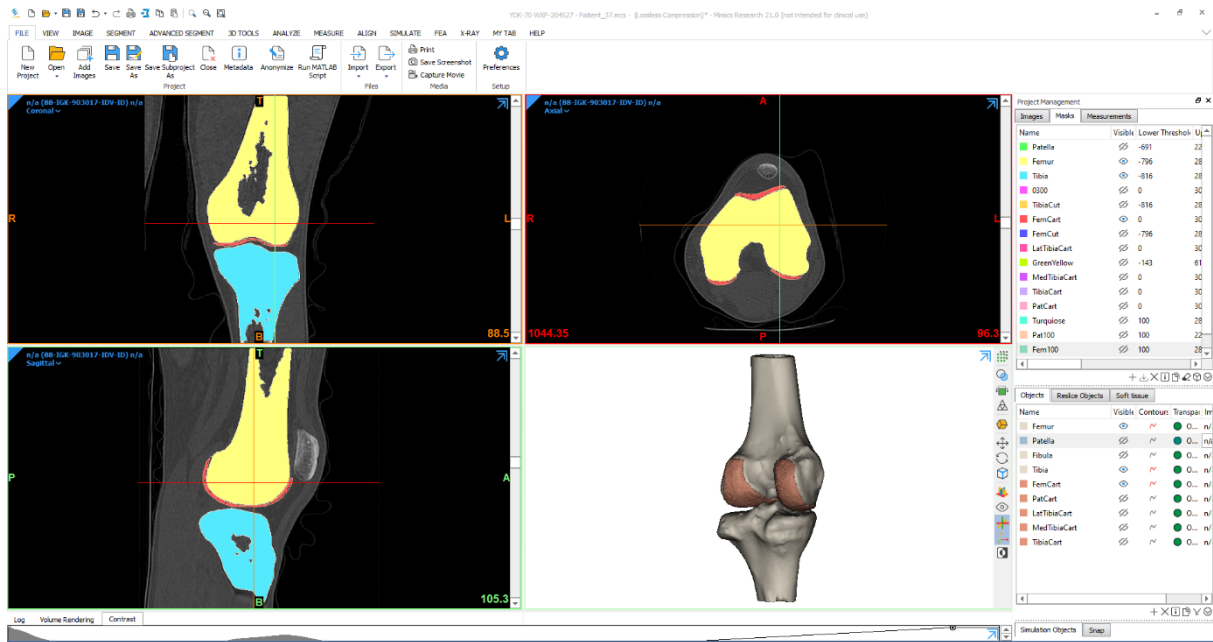Figure 6 shows the final result on Mimics.

Figure 6. 3D model of the knee after segmentation on Mimics.

3.2 3D Modeling

The .stl files from Mimics were exported into the 3D modeling software 3-matic. Here, editing operations were carried out to improve the overall quality of the models, taking care to avoid interpenetration between parts. Subsequently, each part was carefully meshed and prepared for the Finite Element Analysis. The models were then exported in .cbd file format to Ansys simulation software. The following paragraph aims to give an explanation of the workflow and tools used, together with the justification of the assumptions made.

3.2.1 Knee Joint Modeling

The 3D models of femur, tibia, and femoral cartilage were imported into 3-Matic (Materialise, Leuven, Belgium) in .stl file format. 3-Matic is a high-performing medical imaging software that allows users to easily manipulate and edit 3D models, such as repairing errors, creating textures and patterns, and adding support structures for 3D printing. Among these, its primary features are mesh editing and analysis tools which offer a variety of options to help users identify and correct errors.

In 3-matic, the geometry of each part was optimized, improving the overall quality of the objects. Local smoothing was carried out if necessary to remove undesired spikes. Figure 7 shows both models.
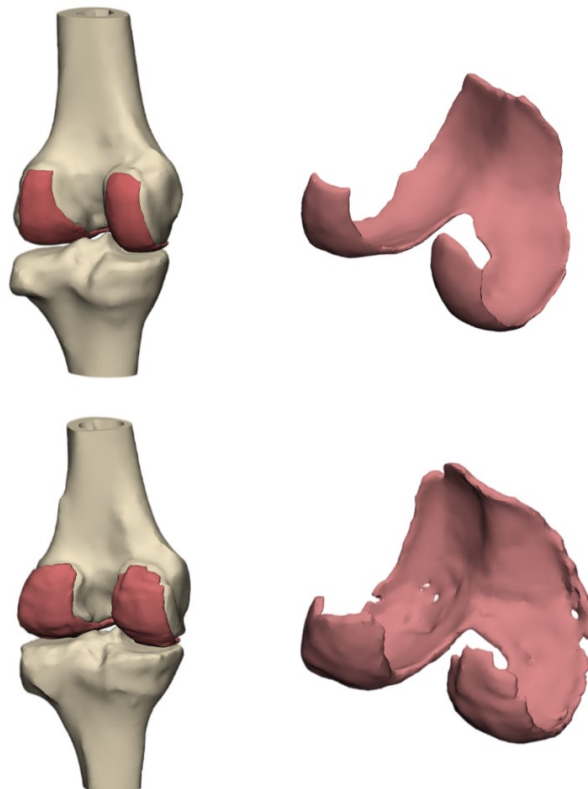
Figure 7. 3D anatomical models of control (top) and degenerative patient (bottom).

The 3D surface meshed models generated by Mimics contained a large number of triangles with high aspect ratios, so a first reduction of the number of triangles was performed. At this point, triangular surface meshes were generated on the surface layer of bones and cartilage using the *Adaptive remesh* tool. This tool allows to remesh an entity while preserving its geometry. Compared to *Uniform Remesh*, it offers finer control over the generated mesh, and can even restrict the remeshing to a small region of interest.

Since the focus of the analysis is on cartilage, the bones were meshed coarsely to reduce computational requirements, while a finer mesh was used for the femoral cartilage. Specifically, a 2D triangular mesh with a size of 4 mm was used for most of the bone surface, while a 2 mm triangular mesh was used for the cartilage. To achieve a better load distribution at the transition from bone to cartilage, the bone mesh was refined towards the contact zones with the cartilage, ultimately reaching 2 mm (Figure 8). Additionally, the areas of the cartilage with geometric singularities were finer meshed with a 1 mm mesh. This was necessary in the case of degenerative cartilage as the presence of holes in it could have caused incorrect load transmission (Figure 9).
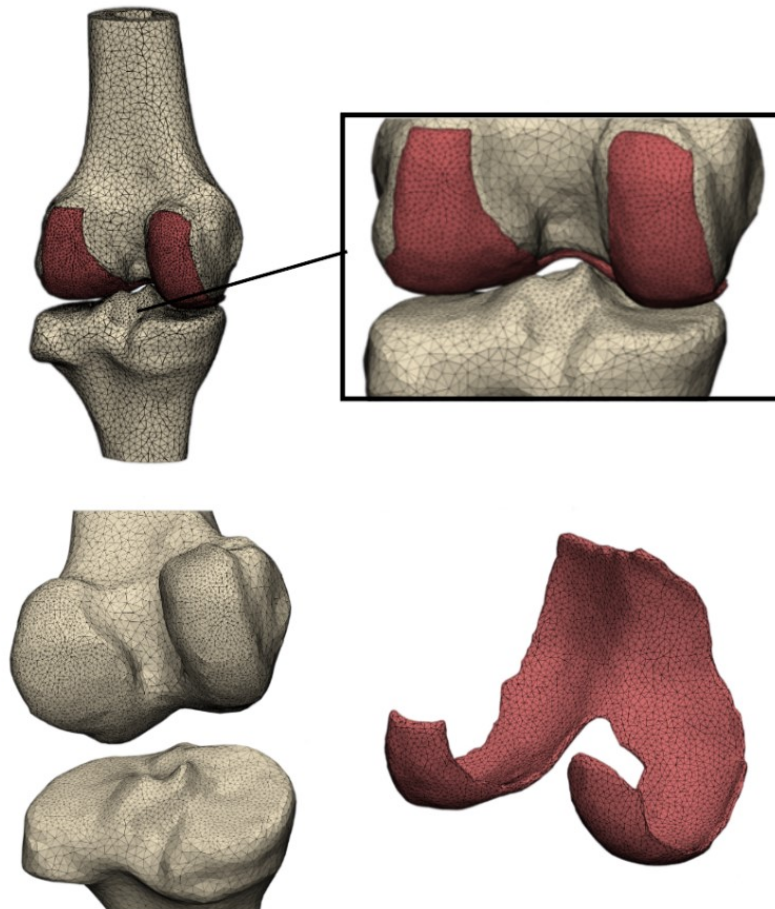
Figure 8. Triangular surface meshes were created on bones (4 mm) and cartilage (2 mm). The bone mesh was refined towards the contact zones with the cartilage, ultimately reaching 2 mm.
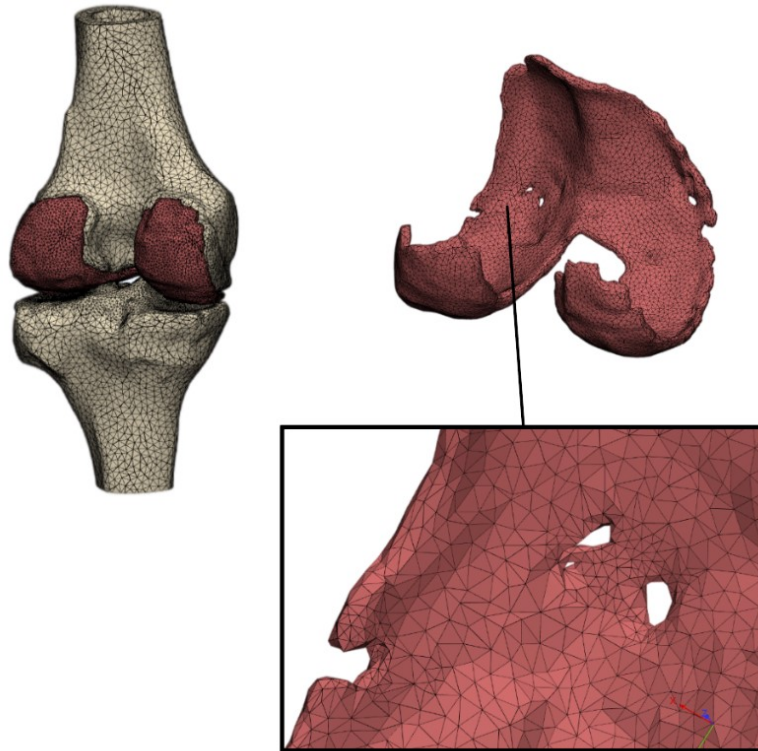
Figure 9. The areas of the cartilage with geometric singularities were finer meshed with a 1 mm mesh.

Furthermore, the knee joint geometry underwent a thorough check to ensure proper anatomical size and shape. After creating a high-quality mesh, the number of elements that made up the mesh was reduced to decrease the computational cost. The *Quality preserving reduce triangles* tool was used to reduce the mesh while preserving most of its quality.

A *Boolean operation* of subtraction was performed to ensure that there were no intersection bodies existing in the models. Surface meshes were then converted into volume meshes with the *Create volume mesh* tool to generate 3D solid models. Regarding this, it is important to specify a few things.

Linear tetrahedral elements (TET4) are widely used in FEA due to their simplicity and computational efficiency. They have been used in recent literature on contact analysis of the knee joint for their ability to represent complex and irregular geometries, such as ligaments and menisci. However, when it comes to model cartilage, they are limited in accuracy because they may overestimate stiffness and require many elements to achieve analysis convergence. This is because TET4 elements can only represent a constant strain state and lock for nearly incompressible materials and bending deformations.

Because of these issues, trilinear hexahedral elements (HEX8) have seen much wider use in joint contact analysis due to their ability to better simulate structures with a regular, box-like shape, such as bone. They are considered the gold standard for modeling cartilage due to their

accuracy and computational efficiency. However, meshing intricate and complex geometries such as femoral cartilage with only hexahedral meshes can be challenging and time-consuming.

The scenario changes when using more advanced high-order elements like quadratic hexahedral elements (HEX20). These advanced elements boast the addition of nodes not only at the vertices but also halfway along the edges, guaranteeing an accurate representation of complex curved geometries. In general, high-order elements (TET10, HEX20) are recommended to better track deformations and stresses in soft tissues such as cartilage, muscles, or ligaments as they produce smoother strain and stress estimates with fewer elements compared to their linear approximations (TET4, HEX8). Nevertheless, the issue with HEX20 elements still remains their high computational cost.

In this frame, quadratic tetrahedral elements (TET10) offer an attractive alternative for modeling articular cartilage. They maintain the advantages of tetrahedral mesh generation, such as the computational efficiency, while offering more accurate representation of curved boundaries compared to HEX8 elements, as their edges and faces can deform. Additionally, TET10 elements have a higher order of interpolation, can represent curvature and strain gradients more accurately, and have been shown to be comparable both in computational cost and accuracy to the gold standard HEX8 elements for articular contact analysis [29].

To summarize, when analysing deformation and stress distribution, a hexahedral mesh may be more advantageous than a tetrahedral mesh due to the greater stiffness of tetrahedral elements. However, for extremely complex geometries like cartilage, tetrahedral elements are more suitable. By utilizing quadratic elements, the limitations of linear elements can be overcome, and the accuracy can approach that of hexahedral elements. The volume mesh was therefore generated using quadratic tetrahedral elements (TET10) for femoral cartilage, while for the femur and tibia, as the bone components were of least focus, were used linear tetrahedral elements (TET4). TET4 is the simplest linear-interpolation tetrahedron-shaped element with 4 nodes, each having only 3 translational degrees of freedom (rotations of nodes are ignored). TET10 element is a higher order 3D element with 10 nodes. It has a quadratic displacement behaviour and suitable for modelling irregular meshes. Each node has 3 translational degrees of freedom in the nodal x, y, and z directions.

During the creation of the volume meshes, is possible to have an error message: this is due to the presence of intersecting triangles, overlapping triangles or bad edges in the model. To overcome this problem, you may have to use the *Auto Fix* tool to automatically repair the model. If the problem persists, the *Fix Wizard* tool is used instead to mark bad triangles or edges and manually delete and create the new triangles. 3-Matic, in fact, offers numerous tools for this type of problems.

To evaluate the quality of the meshes obtained, several parameters were computed such as the aspect ratio, which is the ratio between the longest and shortest sides of an element, and the Jacobian, a metric used to measure the deviation of an element from its ideal shape. The evaluation of these parameters indicated that the obtained meshes had an acceptable level of quality.

We also attempted to create a *Non-Manifold Assembly*, which allows for the combination of multiple intersecting parts into a single unit. The result contains non-manifold connections at the intersecting regions. Additionally, the original parts remain linked to the assembled part, and as long as the names of the surface sets are not altered, it is possible to restore the part to its original state using the *Split Non-manifold Assembly* tool. However, we encountered an issue with this tool as it was unable to preserve the geometry, such as the holes in the degenerative cartilage.

The final models were then exported from 3-Matic to Ansys Workbench in .cdb file format for the Finite Element Analysis. In parallel, each part was also converted in .stl file format and exported to GrabCAD Print and Objet Studio to be 3D printed. Figure 10 shows the femoral cartilages of the two patients after the meshing.

Control   **Degenerative**
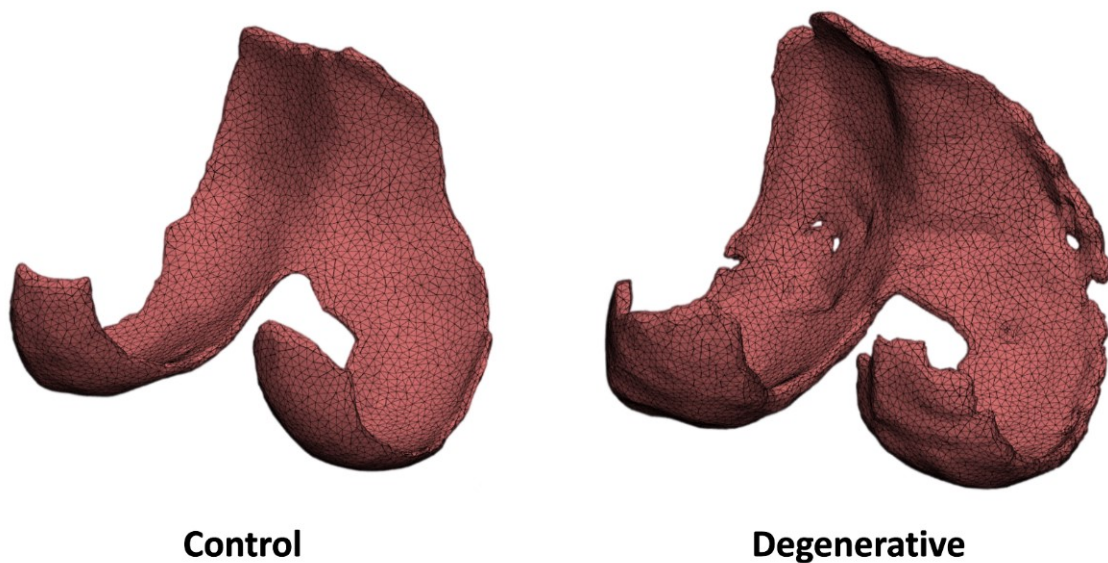
Figure 10. Femoral cartilages of the two patients after the meshing process.

3.3.2 Anatomy-specific Supports Prototyping

To accurately replicate the loads that the femoral cartilage experiences in real-life scenarios, we decided to customize the mechanical tests by inserting, in addition to the femoral cartilage, also the distal femur and the proximal tibia. Specifically, custom patient-specific supports were designed and printed, which could be adapted to fit the mechanical testing machine. We created two types of supports, one for compression tests and one for tensile tests. In both cases, our goal was to keep the testing process unaltered, meaning we would not alter the plates for compression or the pneumatic grips for tensile. Instead, we would simply insert the custom supports between the platens or grips and the printed cartilage. This would help maintain both the geometry and distribution of the loads present in the patient's knee joint. After conducting several tests directly on the machines, we concluded that the supports designed for the tensile test were the best fit for our analysis. The latter, in fact, once correctly attached to the grips, remained fixed in place without the risk of misalignment or incorrect positioning both in the preparation phase and during the test. It is crucial to ensure that a mechanical test is reproducible, which requires reducing operator-dependent errors as much as possible. The chosen supports, in fact, were designed to fit dimensionally with the size of the grips, ensuring that the inserted part fits snugly.

The 3-Matic software (Materialise, Leuven, Belgium) was used for the design of the custom supports. Starting from the segmented 3D models of each patient's femur and tibia, a cutting plane was created on both bone structures using the *Create Datum Plane* tool. The datum planes were then positioned so that the distal femur and proximal tibia were of equal length. To ensure accuracy, the planes were placed perpendicular to the axes passing through the femur and tibia, and oriented in the same direction.

Next, the femur and tibia were cut using the *Cut* tool and selecting the two datum planes as cutting entities. Using the two datum planes, two sketches were then created. In particular, a 25 x 10 mm rectangle and an 80 x 80 mm square were drawn. Finally, using the *Extrude* tool, the rectangle was extruded by 25 mm and the square by 4 mm. The choice of dimensions was made following several measurements in order to correctly adapt the supports to the jaws and ensure the correct positioning of the structures.

In particular, the 80 x 80 mm square was specifically designed to provide a surface area large enough to ensure proper distribution of compression forces. On the other end, the 25 x 10 mm rectangle was designed to ensure precise closure between the grips of the testing machine, and to ensure that the square support was properly situated on the end part of the grips.

To validate the accuracy of the created supports, we checked whether the distances between the vertices of the two extruded squares were the same.

The final models were meshed using the same parameters described in the previous paragraph and were then exported from 3-Matic to Ansys Workbench in .cdb file format for the Finite Element Analysis. In parallel, each part was also converted in .stl file format and exported to GrabCAD Print and Objet Studio to be 3D printed. Figure 11 shows the models created and meshed.
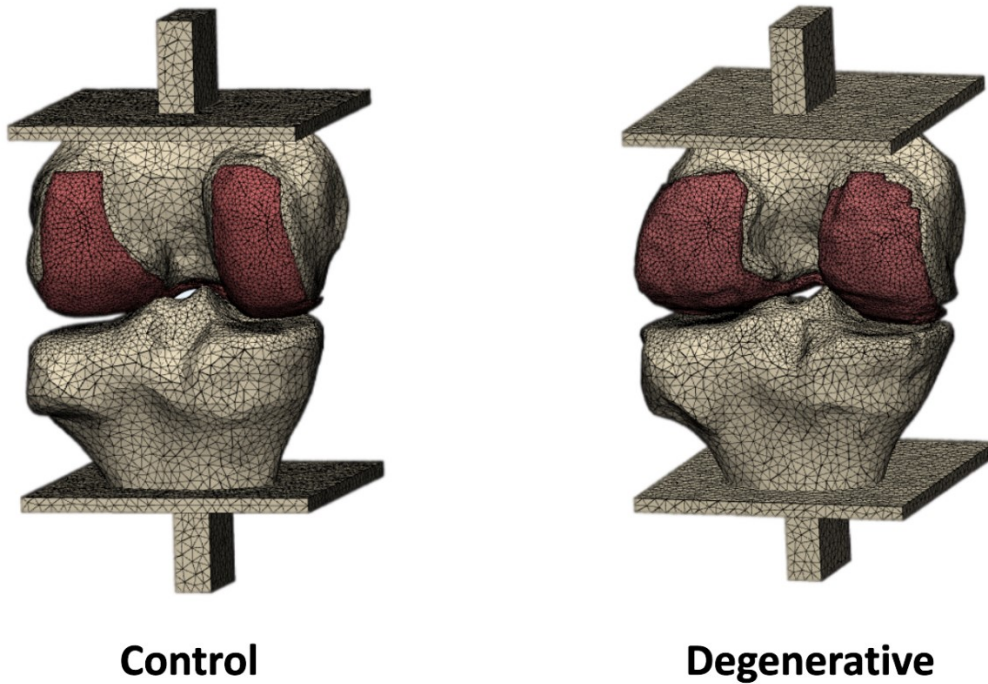

Control　　　　　**Degenerative**

Figure 11. Anatomical models with supports.

3.4 Finite Element Analysis of the Knee Joint

This chapter deals with the various finite element analyses of the knee joint that were performed during the project. A total of twelve FEM analyses were carried out. The first six were performed on two anatomical models (control and degenerative), assigning to each of them three different materials (soft, medium, literature). The remaining six analyses used the two anatomical supports (control and degenerative), always assigning to each of them the three materials (soft, medium, literature).

The analyses on the anatomical models were used to evaluate the behaviours of soft and medium materials and compare them with that of literature materials, also highlighting the differences between the control and degenerative models. The analyses on the supports, on the other hand, were used to verify that the created supports were actually able to correctly simulate the load distribution that occurs in patient-specific anatomical models, hence in reality. For actual verification and validation, the results obtained were then compared with the results of real mechanical tests carried out on models with supports.

Below is a detailed explanation of what was assigned and used for the computational simulations on ANSYS, in particular: material properties; contacts and formulation methods; boundary conditions and loads.

Workflow on ANSYS

To set up the ANSYS Workbench project, the *Metric measurement system* (kg, mm, s, °C, mA, N, mV) was selected by clicking on *Units* in the toolbar. A *Static Structural* analysis was added to the *Project Schematic* by dragging it from the *Analysis Systems* of the toolbox. An *External Model* was also added from the *Component Systems* of the toolbox and linked to the *Static Structural*. The materials were created and inserted into the *Engineering Data* section of the *Static Structural* window.

The material properties were obtained both from literature review and through experimental methods. It is worth noting that the entire workflow of the project, from 3D printing to mechanical testing, passing through computational analysis, is quite interchangeable. After printing standardized samples with the two digitally customized materials, mechanical tests were carried out to determine their tensile and compression properties. The resulting data was then processed to calculate the Young's modulus and Poisson's ratio for each material. These properties were used in ANSYS to characterize the bones and cartilages during the analyses. The behaviour of the models with these properties was then compared and validated by

analysing the same models with literature-derived properties assigned to the cartilage and bones.

Our study exclusively investigated the response of the femoral cartilage to specific loading conditions, and thus, the tibial cartilages, menisci, and ligaments were not included in the analysis. Despite the critical role that these structures play in the overall function and health of the knee joint, their exclusion allowed for a deeper and more accurate comprehension of the femoral cartilage's behaviour and potential implications for knee joint health. Consequently, this approach yielded valuable insights into the potential failure mechanisms related with the femoral cartilage. Below are explained the properties assigned to cartilage and bones.

3.4.1 Material Properties

In total, five different materials were created, which were named: *Cartilage Literature*, *Bone Literature*, *Printed Cartilage Soft*, *Printed Cartilage Medium* and *Printed Bone*. The first two were assigned the properties found in literature of cartilage and bone, respectively. The third and fourth material instead refer to the properties found experimentally after mechanical tests carried out on samples printed with *Soft* and *Medium* materials. Finally, the properties of *Printed bone* are the properties of the VeroWhite material with which the supports were printed, also found in the literature. Below are described the specific properties assigned.

Femoral Cartilage

Under dynamic loading, the mechanical response of cartilage can be modelled as an elastic isotropic material. This is because the loading time of interest corresponding to that of a fully extended leg touching the ground is much shorter than the viscoelastic time constant of cartilage, which is 1500 s. Moreover, this approach is considered appropriate due to the elastic response of cartilage during activities, such as walking or stair climbing, which involve loading frequencies greater than 1 Hz. Donzelli et al. demonstrated that this modeling technique is accurate enough to predict instantaneous cartilage response, as they found no significant changes in the cartilage contact responses shortly after loading [24].

Blankenvoort et al. modeled cartilage as an elastic isotropic material with a Young's modulus of 5 MPa and Poisson's ratio of 0.45. This choice was based on the instantaneous response of cartilage to loading, which corresponds to a Young's modulus of 5-15 MPa and a Poisson's ratio of 0.5, and the response to long-term loading, which corresponds to a Young's

modulus close to 1 MPa and a Poisson's ratio ranging from 0 to 0.4. Subsequently, many 3D FEA knee investigations have used the properties from the studies of Blankevoort et al. [24].

For the reasons just mentioned, the material *Cartilage Literature* was modeled with a linear elastic isotropic behaviour, specifying a Young's modulus of 5 MPa and a Poisson's ratio of 0,46.

The *Printed Cartilage Soft* and *Printed Cartilage Medium* materials were also modeled with a linear elastic isotropic behaviour, but with a Young's modulus of 2,4317 MPa and 7,2396 MPa and a Poisson's ratio of 0,3462 and 0,3451 respectively. These values were those found in the mechanical tests.

Femur and Tibia

Since the stiffness and density of bones are much higher compared to those of soft tissues, their influence on cartilage behaviour in many FEA studies available in the literature was minimal. For this reason, bone is often modeled as a linear isotropic elastic material, despite its well-known heterogeneous and biphasic nature, to simplify the analysis. In previous 3D FEA studies, bone structures were assumed to be rigid bodies to reduce computational costs. On the other hand, several articles in the literature have considered bones as deformable bodies. In this regard, Donahue et al. developed a 3D FE knee joint model based on CT images to investigate the effect of assuming bone as a rigid or deformable body on contact behaviour [24]. The results showed no significant difference in contact responses within the knee joint, whether bone was assumed to be a rigid or deformable body. This explains why bones are considered either as a rigid body or as a linearly elastic isotropic material in the literature. To conclude, when the interest is focused on cartilage only, the difference between cortical and trabecular bone is also negligible.

For the reasons just mentioned, the *Bone Literature* material was created assigning a linear elastic isotropic behaviour with a Young's modulus of 17000 MPa and a Poisson's ratio of 0.31. The difference between cortical and trabecular bone was not considered. The *Printed Bone* material was also modeled with a linear elastic isotropic behaviour, but with a Young's modulus of 2500 MPa and a Poisson's ratio of 0,38.

We verified that the influence on cartilage of the properties assigned to bones was minimal, by assigning the *Printed Bone* and *Bone Literature* materials to bones and evaluating the results. What we discovered was that, despite the large difference in stiffness values between the two materials, the differences in stress and strain values recorded on the femoral cartilage were of the order of 10^{-2}.

All the material properties assigned to bones and cartilage both from literature and experimental methods are shown in Table 4.

Name	Constitutive model	Young's Modulus (MPa)	Poisson's ratio
Cartilage Literature	Linear isotropic elastic	5	0.46
Bone Literature	Linear isotropic elastic	17000	0.31
Printed Cartilage (Soft)	Linear isotropic elastic	2.4317	0.3462
Printed Cartilage (Medium)	Linear isotropic elastic	7.2396	0.3451
Printed Bone	Linear isotropic elastic	2500	0.38

Table 4. Material properties assigned during the finite element analysis on ANSYS.

3.4.2 Contacts Definition, Behaviour and Formulation Method

Contact and Target Surface

When a model is imported into ANSYS, the software is able to automatically detect the contacts between the single elements of the model. However, this recognition may not always be accurate, particularly for complex geometries and different materials. Therefore, it is important to review and check the contact settings.

The *Contact* and *Target* surfaces are important considerations for modeling the interactions between different components of a structure or system in ANSYS. The choice of which surface to assign as the *Contact* surface and which surface to assign as the *Target* surface depends on the expected behaviour of the surfaces under loading. As a general rule, the *Contact* surface is the surface that is expected to move or deform under loading, while the *Target* surface is expected to remain stationary.

The *Contact* and *Target* form a contact pair. In simple terms, when two separate bodies touch each other, *Contact* and *Target* represent the two bodies. This means that the nodes on the *Contact* surface will be prevented from penetrating into the volume of the *Target* surface. Forces can be transmitted across the contact pair. To determine correctly which surface to assign as the *Contact* and *Target*, there are several characteristics to consider. For example, *Contact* detection points must not pass through the *Target* face. The *Contact* surface should be selected as the body with the finer mesh and the convex shape, while the *Target* surface should be the one with the flat or concave shape. Softer materials should be assigned to the *Contact*

surface to prevent node penetration into the *Target* surface. Additionally, if one surface is lower order, stiffer, or larger than the other, the corresponding surface should be selected as the *Target*. Contact results are only available on the *Contact* side. When *Contact* and *Target* sides are not easily distinguishable or both have coarse meshes, symmetric contact behaviour should be used.

In the analysis two contacts were defined: one between femur and femoral cartilage and the other one between tibia and femoral cartilage. Following the guidelines mentioned above, the femoral cartilage was defined as the *Contact* surface, and the bones were assigned as the *Target* surface in both cases (Figure 12). The same was done for the models with supports.
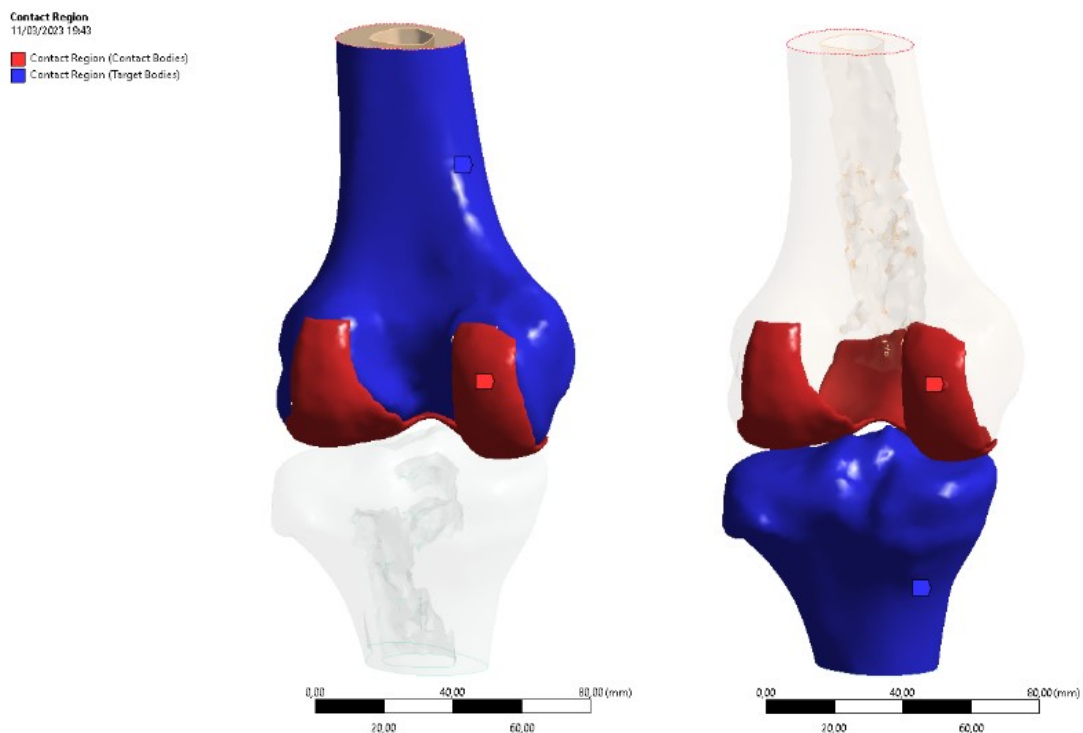
Figure 12. Contact and Target surfaces assigned.

In ANSYS, there are several contact types and behaviours that can be used to define interactions between surfaces, each corresponding to different constraint equations. The choice of contact type and behaviour depends on the specific problem being analysed.

Contact Types

In ANSYS, five types of contact definitions are available: *Bonded*, *No Separation*, *Frictionless*, *Frictional* and *Rough*.

- *Bonded*: the two bodies are tied together in such a way that they cannot slide or separate from each other since their surfaces are rigidly connected. The nodes on the *Contact* surface are prevented from penetrating into the volume of the *Target* surface. This means that the two surfaces behave as if they were glued together and move as a single unit. Compressive normal forces and tangential shear forces can be transmitted across the contact pair, but there is no relative motion between the surfaces. This setting is widely used whenever two bodies are expected to move together.

- *No Separation*: once the contact is detected, then the *Target* and *Contact* surface are tied up for the rest of the analysis. Frictionless sliding is allowed, but the nodes in contact are bonded to the *Target* surface in normal direction. The nodes on the *Contact* surface are allowed to penetrate the *Target* surface, but with a penalty applied to the penetration. This means that the contact surfaces are allowed to touch and deform into each other, but the deformation is restricted to prevent the two surfaces from separating from each other. This type of contact behaviour is useful for simulating interfaces between materials that are meant to stick together or in cases where a small amount of penetration is expected and allowed, but separation is not.

- *Frictionless*: separation and frictionless sliding are permitted between the surfaces, meaning they can slide past each other without any resistance. The contact pair can slide on the target surface in the tangential direction and also translate in the normal direction. A coefficient of friction of zero is assumed, allowing for free sliding between the surfaces. However, the model must be well-constrained when using this contact setting, and weak springs are often added to the assembly to help stabilize the model and produce a reasonable solution. Frictionless contact is commonly used when modeling situations where there is no friction or where friction can be neglected. Examples include modeling of soft tissues in biomedical simulations or when modeling impact or collision between two bodies.

- *Frictional*: the frictional contact type is used to simulate contact between two bodies that involve frictional forces. This type of contact allows for relative sliding and

separation between the surfaces. To define frictional contact in ANSYS, the user must specify a coefficient of friction, which represents the ratio of the frictional force to the normal force at the contact interface. Sliding motion between the two bodies is allowed, but the frictional force resists this movement. The coefficient of friction determines the strength of the frictional force and therefore the resistance to sliding, affecting the tangential movement between the two surfaces. This type of contact modeling is commonly used in simulations where frictional forces play a significant role, such as mechanical systems where components rub against each other, or in material simulations where sliding or slipping may occur.

- *Rough*: separation is allowed but sliding cannot occur. The contact pair cannot move in the tangential direction because nodes in contact are glued on the target surface in tangential direction. This case corresponds to an infinite friction coefficient between the contacting bodies.

The different types of contact are summarized in Table 5.

Type	Separation	Sliding
Bonded	No	No
Rough	Yes	No
No Separation	No	Yes - frictionless
Frictional	Yes	Yes – frictional
Frictionless	Yes	Yes - frictionless

Table 5. Types of contact on ANSYS.

In the knee joint, cartilage covers and adheres to the surfaces of bony structures. Between the cortical bone and the articular cartilage there is a transition zone, called the calcified zone, which is partially mineralized [6]. This layer plays an integral role in securing the cartilage to the bone, by anchoring the collagen fibrils of the deep zone to subchondral bone. As a result, the articular cartilage is bound to the bony end plate and surrounded by a set of collagen fibres. This is the reason why in computational simulations the connection between bones and cartilages is typically defined as *Bonded* [20]. Added to this is the fact that the knee is held firmly by muscles and ligaments which ensure that all surfaces are in close contact with each other, as if they are glued together.

Defining this contact as *Bonded* simplifies the analysis, reduces computational complexity, and allows for easier application of loads and boundary conditions. Although minor movements

and sliding may occur between the two surfaces, significant movements or sliding are not observed. This assumption is commonly adopted in literature and provides a reasonable approximation of the knee joint behaviour under certain loading conditions. Therefore, it is reasonable to extend this assumption to include the contact between the tibia and femoral cartilage as *Bonded* as well. While this may not perfectly capture the full range of motion and forces at play in the knee joint, it is a rational simplification given the limitations of computational modeling.

In light of what has been said so far, in the analysis the contacts between the femoral cartilage and the femur and between the femoral cartilage and tibia were both defined as *Bonded*. The same contact type was assigned to the models with supports.

Behaviour

In ANSYS, in addition to contact types, there are also different contact behaviours that can be applied to surfaces. Contact behaviours refer to how two surfaces interact when they come into contact with each other in a simulation. The four types of contact behaviours in Ansys are: *Asymmetric*, *Symmetric*, *Auto Asymmetric*, and *Program Controlled*.

- *Asymmetric*: this is the most common contact behaviour used in ANSYS. It assumes that the contact between two surfaces is not symmetric and can be described by a one-sided friction coefficient, meaning that one surface is designated to be the *Contact* side and one to be the *Target* side. The nodes on the contact surface are prevented from penetrating into the *Target* surface. The important thing to underline is that the contact results are only available on the *Contact* surface. *Asymmetric* contact behaviour can be used to simulate situations where one surface is much harder or softer than the other.

- *Symmetric*: this contact behaviour assumes that the contact between two surfaces is symmetric and can be described by a two-sided friction coefficient, meaning that each surface is both the *Target* and the *Contact*. The nodes on the *Contact* and *Target* surface are prevented from interpenetrating. This is computationally more expensive than asymmetric contact because implies the generation of two contact pairs from the same two surfaces. Assigning this type of behaviour can make the interpretation of the results and the processing of contact force very difficult, as the contact result values are an average of both the *Contact* and *Target* surfaces. This type of behaviour is useful when

both surfaces have similar mechanical properties and recommended when the *Contact* side and the *Target* side are not easily distinguished, or both have coarse meshes.

- *Auto Asymmetric*: the solver automatically creates an asymmetric contact pair. This is similar to *Asymmetric* contact behaviour but uses a two-sided friction coefficient. ANSYS automatically adjusts the friction coefficient based on the direction of the contact force, which is useful when the direction of contact changes during the simulation.

- *Program Controlled*: the solver defaults to a setting based on the body types. ANSYS can automatically detect contact surfaces, but it is important to check and adjust the settings to ensure accuracy. It is useful when you are not sure of the specific behaviour to assign or when the standard contact behaviours do not provide adequate results.

Our analysis focused on the femoral cartilage's behaviour in terms of stress and deformation. It is therefore important to clearly define which is the *Target* surface and which the *Contact*, in order to obtain specific results for the *Contact* surface of interest, which in our case is the femoral cartilage. Additionally, since femoral cartilage is significantly softer than bone, an *Asymmetric behaviour* was assigned to both contacts. The same was applied to the models with supports.

Pinball region

The *Pinball Region* is the area around a contact body which defines the searching range where the contact status is evaluated and calculations will occur. When two or more bodies are in contact, the *Pinball Region* is used to determine which nodes of the bodies are in contact and whether the contact is open or closed. It is essentially a sphere or a cylinder that surrounds the contact body and is used to detect the proximity of other bodies. Setting a *Pinball Region* can be helpful in cases where two bodies are initially too far apart for the program to detect contact by default. It is possible then to increase the *Pinball Region* as needed specifying a *Pinball Radius* large enough to ensure that contact occurs. The *Pinball Region* helps also to accelerate the contact analysis by evaluating only the nodes inside the pinball region, rather than all the nodes on the body. This reduces the computational load and speeds up the simulation. The size and shape of the *Pinball Region* can be adjusted depending on the requirements of the analysis.

As mentioned previously, the analysis did not consider the tibial cartilages and menisci, which resulted in the presence of a gap in the contact between the femoral cartilage and the

tibia. To compensate for this, a *Pinball Radius* was assigned based on precise measurements of the distance between the two bodies, thereby filling the gap. In particular, a *Pinball Radius* of 1.5 mm was defined for the control model, while for the degenerative model the *Pinball Radius* was set to 1.7 mm.

Formulation Methods

In order to enforce compatibility at the contact interface, different contact formulations are available. These formulations define the solution method used and differ in how the contact interaction is treated mathematically. In ANSYS, there are several options available for the formulation method: *Pure Penalty*, *Normal Lagrange*, *Augmented Lagrange*, *Multi-Point Constraint* and *Beam* formulations.

Numerically, a contact is enforced by following three rules:

- No penetration between the two bodies
- A proper balance between the applied and the contact forces in case of a static problem
- Conservation of momentum in case of dynamic problems

These are the most important requirements for any contact formulation that is introduced into a model in order to enforce contact between bodies and to capture the interactions accurately. In general, there are two most popular formulations that meet these criteria: Penalty formulation and Lagrange formulation.

Penalty Formulation

In Penalty formulation, the contact is treated as a stiff spring that is attached between the two bodies which resists them from penetrating (Figure 13). This resistance is modeled in the form of contact stiffness, which is derived as a function of several factors such as the material properties of the bodies, their geometries, kinematics of the bodies and various other factors. Two distinct contact stiffnesses are used for every contact, one in the normal direction and the other in the tangential direction.
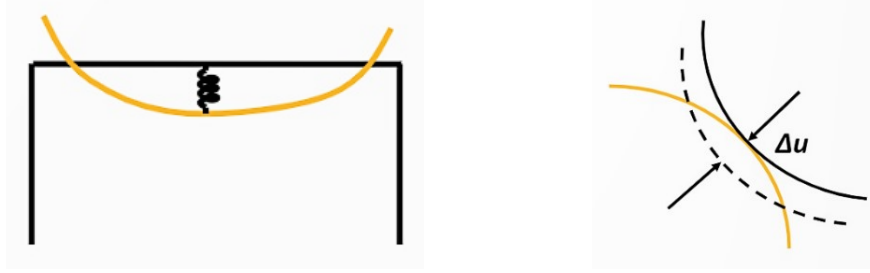
Figure 13. In the Penalty formulation the contact is treated as a stiff spring that is attached between the two bodies which resists them from penetrating.

In the penalty formulation, the two bodies can penetrate by a small amount at the beginning. Called Δu the initial penetration (Figure 10), then the contact formulation tries to restore this penetration by applying some contact force in the opposite direction. This restoring force is nothing but the contact force (F_c), that is the product of the amount of penetration (Δu) and the contact stiffness (K):

$$\{F_c\} = [K]\,\{\Delta u\}$$

So, in principle, the penalty formulation treats the contact as a stiff spring. The stiffness of this spring should be large enough to provide enough restoring force to reduce the final penetration close to zero.

This formulation can be used for calculating both the normal and tangential contact stresses, also called the normal contact pressure and the frictional stresses. Mathematically, if u_n is the contact gap, and Δu_1 and Δu_2 are the sliding distances in lateral direction, then the contact traction vector is defined by vector:

$$\{F_c\} = [P, \tau_1, \tau_2]^T$$

The normal contact pressure P is given by this equation, where K_n is the normal contact stiffness.

$$P = \begin{cases} 0 & if\ u_n \geq 0 \\ K_n u_n & if\ u_n < 0 \end{cases}$$

This equation means that if the surfaces are moving away from each other then there are no contact forces but if they are pressed into each other, then the contact forces kick it. In case of tangential contact stresses, if Δu_1 and Δu_2 are the sliding distances in the lateral directions, then the tangential contact stress (frictional stress) is given by this equation:

$$\tau_i = \begin{cases} \tau_i^{n-1} + K_t \Delta u_i & if\ \|\tau\| = \sqrt{\tau_1^2 + \tau_2^2} - \mu\,P < 0\ \ (sticking) \\ \mu\,P\,\dfrac{\Delta u_i}{\|\Delta u\|} & if\ \|\tau\| = \sqrt{\tau_1^2 + \tau_2^2} - \mu\,P = 0\ \ (sliding) \end{cases}$$

where μ is the coefficient of friction, K_t is the tangential contact stiffness and τ_1 e τ_2 are the shear stresses developed in the two lateral directions.

Lagrange Formulation

In the case of Lagrange formulation, the contact is treated as a constraint (Figure 14) which means that this formulation enforces zero penetration, unlike the Penalty formulation which allows a small amount of penetration. The Lagrange method, unlike the Penalty, does not require contact stiffness.
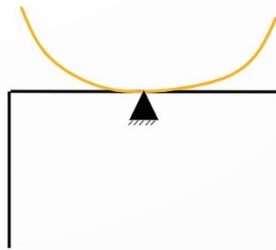

Figure 14. In the Lagrange formulation, the contact is treated as a constraint.

In order to do this, a contact traction vector (F_r) is defined to represent the total reaction force vector. In addition to this, contact gap (u_n) and sliding distances (Δu_1, Δu_2) are also solved as additional degrees of freedom. The full vector of degrees of freedom is shown here:

$$\{F_r\} = [P, \tau_1, \tau_2, u_n, \Delta u_1, \Delta u_2]^T$$

The equations of motion are then solved by imposing a constraint on contact gap and sliding distances to be zero. Due to this strong constraint, the solution results in zero penetration. While this makes results very accurate, in case there are any additional constraints imposed on the same surface, they will interfere with the contact formulation and result in over constraint.

Each method has its own pros and cons. Four factors are considered to compare these two formulations: penetration, contact stiffness, over constraint and computational time. In case of penetration, Penalty formulation allows some amount of penetration, which is not physical, whereas a Lagrange formulation does not allow penetration, which is more realistic. In terms of contact stiffness, a Penalty formulation relies on accurate calculation of contact stiffness as it is very dependent on it. But a Lagrange formulation does not use any contact stiffness, so does not depend on it. Moreover, the Lagrange formulation is prone to running into over constraint issues which is not the case with Penalty method. Also, due to the number of constraints imposed, a Lagrange formulation greatly increases the number of calculations and therefore is computationally more expensive compared to the Penalty formulation, which is relatively cheaper. The differences are summarized in Table 6.

Formulation Method	Penalty	Lagrange
Penetration	Allowed / Required	Not Allowed / zero
Contact Stiffness	Dependent	Independent
Over constraint	Never	Possible
Accuracy	Low	High
Computational Time	Cheap	More Expensive

Table 6. Differences between Penalty and Lagrange formulations.

In term of basic principle, these two are the most common forms of contact formulations that are used for capturing the interactions between bodies. There are other formulations available, some are hybrid versions of both these two versions.

Augmented Lagrange Formulation

The Augmented Lagrange formulation is a hybrid method that combines the Penalty and Lagrange methods. Like the Penalty method, the Augmented Lagrange method imposes a penalty on the bodies when they come into contact with each other. The contact is described as a stiff spring between two contacting bodies that causes them to interact. The higher the stiffness of the spring, the lower the penetration between the two parts. However, unlike the penalty method, there is an additional check on the penetration, and the formulation is augmented to enable this. In particular, the Augmented Lagrange method introduces a set of Lagrange multipliers to enforce contact constraints between the bodies. The Lagrange multipliers are iteratively adjusted during each time step to ensure that the final penetration is smaller than a predefined tolerance. The Augmented Lagrange method produces physically realistic behaviour and is less sensitive to the magnitude of contact stiffness compared to the penalty method. It also has better conditioning properties than the Lagrange method, making it more computationally efficient. This formulation is also the default in ANSYS.

A comparison of the three contact formulations is shown Table 7.

Formulation	Penetration	Convergence Difficulties	Computational Time	Accuracy
Normal Lagrange	Zero Penetration	Chattering (rapid changes in contact status)	High	High
Augmented Lagrange	Some Penetration	Most Robust	Medium	Medium
Pure Penalty	Maximum Penetration	Too Much Penetration	Low	Low

Table 7. Comparison between the formulations described.

So, based on what has been said so far, the *Augmented Lagrange* formulation was used for the contacts between the femur and femoral cartilage, and between the femoral cartilage and tibia, both for anatomical and supports models.

3.4.3 Boundary Conditions and Loads

In the analyses, flexion-extension and varus-valgus rotations were constrained for the femur in order to analyse the knee joint in full extension. To do this was inserted a *Remote Displacement* in the femur to constrain the rotations along the x-, y- and z-axis and the translation along x- and y-axis. Only the translation along z-axis was free. The tibia was constrained at the lower surface using a *Fixed Support*. A vertical compressive force of 1150 N was applied to the top surface of the femur, which matches with the force of the gait cycle for full extension position (Figure 15).

The same assumptions were applied to the models with supports. The only difference is that, in order to compare the computational tests with the real ones, specific load and displacement values were assigned to the supports for each model and material. These values were taken from the results of the mechanical tests, by taking an average.
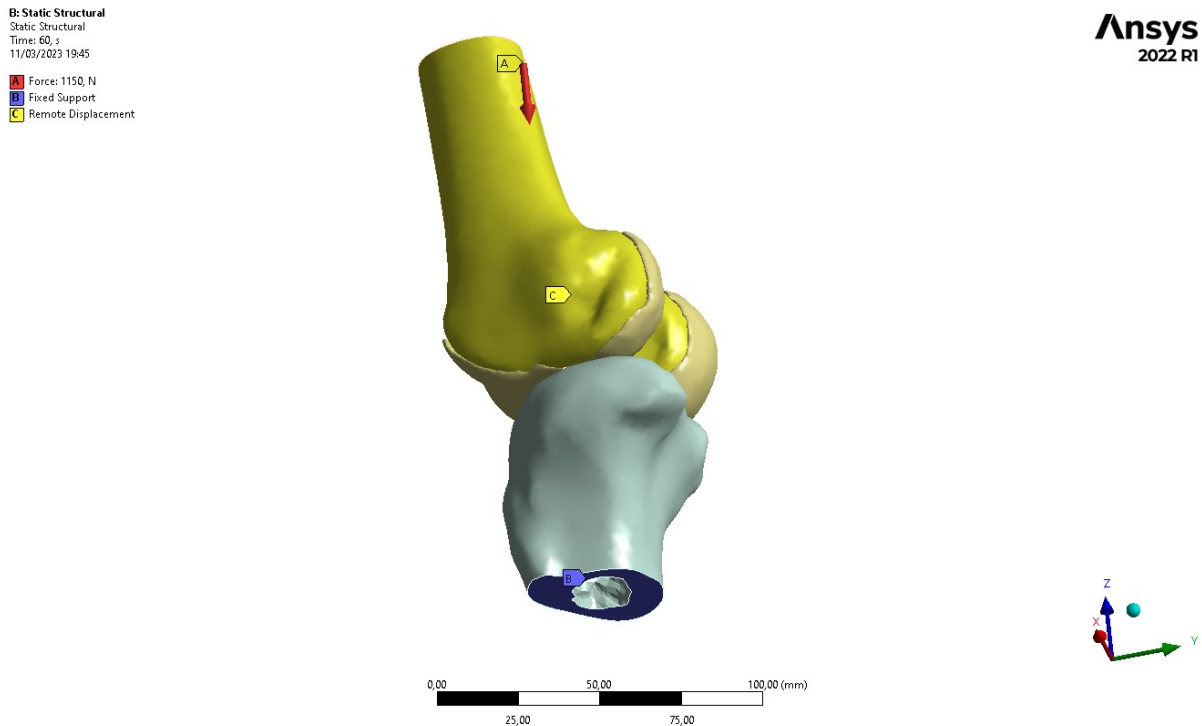
Figure 15. Boundary conditions and loads applied in the finite element analysis.

3.5 3D Printing

This chapter focuses on the 3D printing process of anatomical models, standardized samples, and anatomical supports. There is also a brief description of the two digital materials created to emulate the mechanical properties of cartilage, as well as a comprehensive overview of the mechanical properties of all the materials used throughout the printing process.

3D Printers and Printing Technology

Two 3D printers were used to print the models, both of which operate using the PolyJet technology. The first one, the Stratasys J850 Digital Anatomy Printer, was used to 3D print both standardized samples and the cartilages with two different digitally created materials. The second one, the Stratasys Objet260 Connex3, was instead used to print customized femur and tibia supports.

Before proceeding, below is a brief description of the mechanical properties of the materials used throughout the printing process.

3.5.1 Printing Materials

Agilus30Clear

Agilus30Clear is a flexible and durable rubber-like material developed by Stratasys for their PolyJet 3D printers. It is ideal for creating prototypes, models, and end-use parts that require rubber-like properties, such as soft-touch surfaces, gaskets, and living hinges. In addition to its non-medical applications, Agilus30Clear has found its use in the medical field for creating anatomical models and soft tissue mimics for surgical planning, device testing, and medical education. The material's flexibility and durability make it well-suited for simulating human tissues, such as skin, organs, and blood vessels. Medical researchers have also used Agilus30Clear to create soft, flexible implants, prosthetics and surgical guides that can be customized to a patient's specific needs. It possesses excellent elongation and tear resistance, making it ideal for creating soft, rubber-like prototypes with high accuracy and fine feature detail. Agilus30Clear has a shore hardness of 30, which makes it feel like a soft rubber material. Additionally, Agilus30Clear has good colour stability, enabling the creation of anatomical models with accurate colouration and can also be blended with other PolyJet materials to create a wide range of harnesses and colours.

BoneMatrix

BoneMatrix is a material developed by Stratasys specifically for biomedical applications. It is a blend of polymers and ceramic particles that can replicate the properties of natural bone, including strength, flexibility, and density. BoneMatrix is highly biocompatible, meaning it is well tolerated by the human body and does not cause adverse reactions, making it suitable also for in vivo implantation. Because of its unique properties, BoneMatrix is an ideal material for producing anatomical models, surgical guides, and implants that require high precision and accuracy in both design and performance. It is a tough and flexible material that can maintain its shape and can be sterilized using standard sterilization methods such as gamma irradiation, ethylene oxide gas, and autoclaving. Musculoskeletal models printed with BoneMatrix can replicate bone density characteristics and behave like native bone when force is applied, such as during discectomy, drilling, reaming, or sawing. Studies have shown that screw pull-out force during screw insertion in BoneMatrix 3D models matches that found in the cortex of a cadaver bone, demonstrating that the model accurately replicates the cortex thickness and haptic response of the natural bone. Additionally, the mechanical disc compression, displacement, and elasticity values for BoneMatrix 3D models corresponded to those found in cadaver lumbar spines. BoneMatrix can also be combined with other materials to recreate tissue such as fibrotic tissue, cartilage, and ligaments.

VeroWhite

VeroWhite is a rigid, opaque white material developed by Stratasys for use in its 3D printing systems. It is a type of PolyJet photopolymer resin that is cured by UV light. The material is known for its ability to produce smooth, high-resolution models with excellent detail and accuracy. VeroWhite is widely used in a range of industries, including medical and dental, where it is often used to create surgical guides, dental models, and anatomical models for educational and research purposes. Its rigid properties make it an excellent choice for applications requiring high strength and stiffness, and its opaque nature makes it ideal for simulating human bone or other opaque materials. Additionally, VeroWhite is bio-compatible and can be sterilized using gamma radiation or ethylene oxide. It has a high strength-to-weight ratio, making it an excellent option for producing lightweight and durable parts.

GelMatrix

GelMatrim is a 3D printing material developed by Stratasys that is known for its unique mechanical properties. It is a soft, flexible material that exhibits high elongation and good tear resistance, making it ideal for creating complex, intricate shapes that require flexibility and durability. With a Shore A hardness rating of 00-30, GelMatrix is one of the softest materials available for 3D printing, which makes it an excellent choice for simulating soft tissue in medical applications. It can be used to create anatomical models and medical devices that closely mimic the feel and flexibility of real human tissue. In addition to its flexibility, GelMatrix is also biocompatible, which means it is safe for use in the human body. This makes it an ideal material for creating implants, prosthetics, and other medical devices that require close interaction with biological tissue.

SUP706

Stratasys SUP706 is a support material used in 3D printing to create complex geometries and high-quality prints. One of the key benefits of SUP706 is its water-solubility, which allows for easy and efficient removal of support structures without damaging the printed parts. This makes it ideal for creating intricate or delicate parts that would be difficult or impossible to remove with traditional support materials. SUP706 is also known for its compatibility with a wide range of build materials, including ABS, PC, Nylon, and more. This makes it a versatile choice for a variety of 3D printing applications, from functional prototypes to end-use parts.

3.5.2 Digital Anatomy Materials

The purpose of this study is to create a material that can accurately replicate the mechanical properties of human femoral cartilage. To achieve this goal, the Digital Anatomy Creator (Stratasys, Rehovot, Israel) software was used. Starting from the different materials available on the J850 Digital Anatomy Printer (Stratasys, Rehovot, Israel), this software allows to create new customized materials with the desired mechanical properties and geometry in each print slice by combining different materials together.

In particular, we worked in collaboration with a medical application engineer at Stratasys who provided us the materials as .adm file format. Using the Digital Anatomy Creator software, two custom materials, namely *Soft Cartilage* and *Moderately Stiff Cartilage*, were created with different stiffness levels. These custom materials were created by blending three existing materials on the Digital Anatomy Printer, BoneMatrix, GelMatrix and Agilus30Clear, in

different proportions. In particular, the *Soft Cartilage* material is a combination of Agilus30Clear, BoneMatrix, and GelMatrix in different percentages, 70%, 15%, and 15% respectively. On the other hand, the *Moderately Stiff Cartilage* material is composed of 75% Agilus30Clear and the remaining 25% BoneMatrix.

The reason for creating two different mixtures of materials to replicate a single anatomical structure was due to the fact that cartilage can vary among individuals based on several factors, such as age, health, and lifestyle. By doing this, we aimed to mimic the mechanical properties of femoral cartilage more accurately, which can differ significantly from person to person.

3.5.3 3D Printing Softwares

To obtain meaningful and comparable results, multiple pieces of the same models were 3D printed. In particular: for the characterization of digital custom materials through mechanical tests, ten cylindrical standardized samples were printed for the compression test, five assigning the *Soft Cartilage* material and five with the *Moderately Stiff Cartilage* material. Another ten dog-bone samples were printed for the tensile test, five with the *Soft* and five with the *Moderately Stiff* material.

For the patient-specific test, a total of twenty cartilages were printed. Ten for the control model, including five *Soft* and five *Moderately Stiff*, and ten for the degenerative model, five *Soft* and five *Moderately Stiff*.

Standardized samples for compression and tensile tests, as well as femoral cartilages, were printed using the J850 Digital Anatomy Printer (Stratasys, Rehovot, Israel). The .stl files of the models were exported from 3-Matic to be loaded on the GrabCAD Print software.

GrabCAD Print

GrabCAD Print is a straightforward and intuitive software that simplifies the preparation, scheduling, monitoring, and management of 3D printing jobs. It is compatible with many 3D printers and supports various 3D file formats. The software has an intuitive interface that allows users to drag and drop 3D models into the print queue and preview the print job before sending it to the printer. It also includes an automatic support generation tool that helps users to generate the necessary supports for their 3D models, improving print quality and reducing the risk of printing failures. The software automatically repairs damaged files before sending them to the printer. Advanced print settings allow users to optimize print quality and speed by adjusting parameters such as resolution, infill density, and layer height. A material manager is also

available, allowing users to manage their 3D printing materials, track usage, inventory, and reordering, and add custom-designed materials. GrabCAD Print natively reads and understands CAD files, including those created from segmented DICOM data sets and modeling software, eliminating the need to convert them to STL files. For medical purposes, GrabCAD Print has a unique voxel-based engine that eliminates the need to redesign micro-structures for each new pathology, offering predictable performances with each anatomy choice. It also has a comprehensive library of human anatomy pre-sets that reduce the need to design internal structures. The pre-set anatomy menu offers more than one hundred options, including bones, blood vessels, and hearts, which allows users to print accurate, lifelike models by simply choosing the desired anatomy. Users can also add custom-designed materials for further customization.

For our purpose, the .stl files of the models were loaded into GrabCAD Print software. Once the models were positioned on the virtual tray to optimize printing times, it was checked if the files were damaged and needed repair (Figure 16). The next step was the assignment of materials. Specifically, *Soft Cartilage* and *Moderately Stiff Cartilage* materials were designed and provided by a Stratasys engineer in .adm file format, which were then uploaded to the software using the Digital Anatomy Creator tool. Once completed this step, the surface finish for the pieces was chosen, opting for either Matte or Glossy. These two finishes refer to the surface texture or appearance of a 3D printed object. A *Matte* finish has a non-shiny, dull appearance with a rough texture, and tends to scatter light, making it less reflective. On the other hand, a *Glossy* finish has a smooth, shiny appearance with a reflective surface that reflects light evenly. A *Matte* finish was assigned to each piece, from cartilages to standardized samples. Printing supports were then generated automatically by the software. After careful review and control of printing parameters, all the pieces were printed simultaneously for a more efficient printing job in terms of time and material consumption (Figure 17-19).

Once completed this step, the customized femur and tibia supports were printed using the Objet260 Connex3 (Stratasys, Rehovot, Israel). The .stl files of the models were exported from 3-Matic to be loaded on the Objet Studio software.
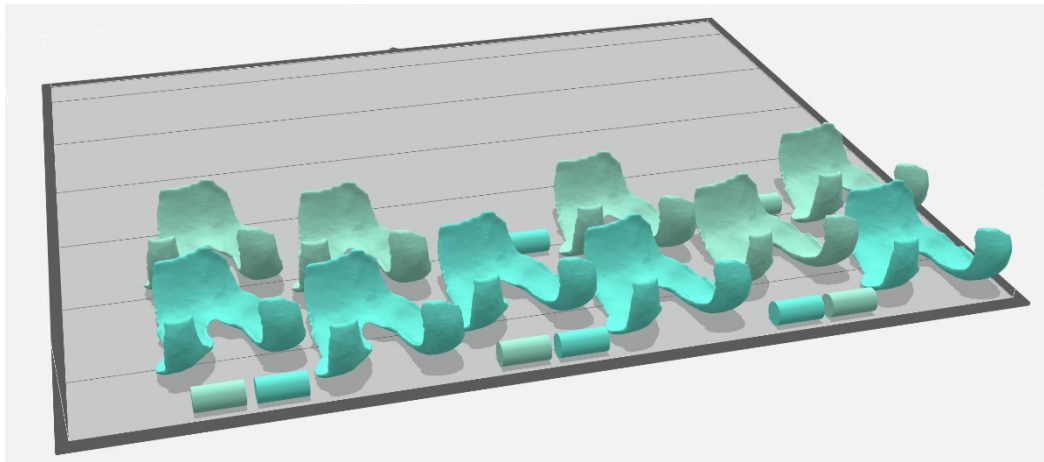
Figure 16. Femoral cartilages and standardized samples on the virtual tray of GrabCAD Print.
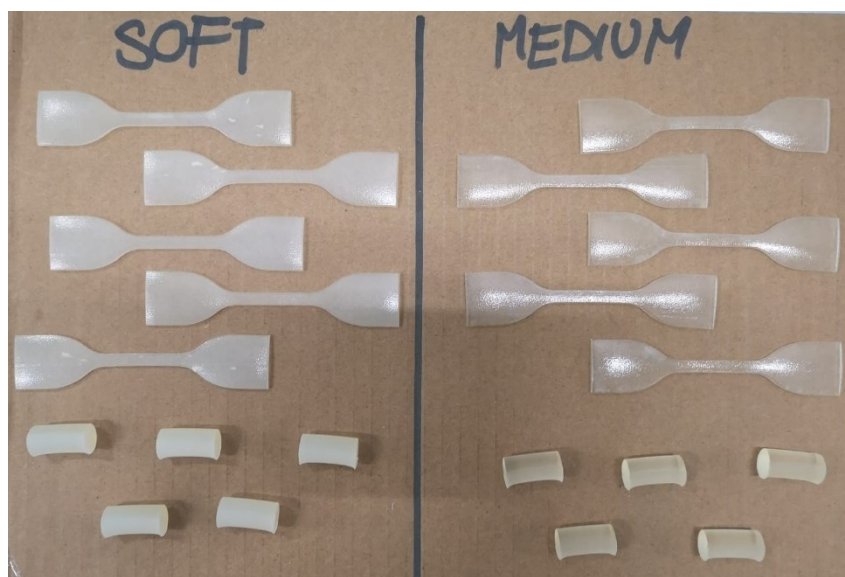

Figure 17. Standardized samples printed with *Soft* and *Medium* materials.

Figure 18. Femoral cartilages of control model after printing and cleaning.

Figure 19. Femoral cartilages of degenerative model after printing and cleaning.

Objet Studio

Objet Studio is another application for preparing print jobs on Stratasys 3D printing systems, specifically suited in our case for the Objet260 Connex3. The interface is divided into two main screens: on the Studio screen, source files are prepared for production on the printer. The Manager screen displays the queue and status of all jobs sent to the 3D printer. Compared to GrabCAD Print, this is an older software and does not allow for the design of digital anatomy materials. This is the reason why it has been used to handle the printing queue for the anatomical supports printed with Objet260 Connex3. Each support was printed with the VeroWhite and with a *Matte* finish, prioritizing the uniformity of the printed surface (Figure 20).

After the printing process, all pieces went through a cleaning process to remove the support material (Figure 21). Each part was then carefully inspected and measured. This was especially important for the standardized samples as there are strict protocols to follow regarding the dimensions of the sample to be used in mechanical testing. Samples that were found to be non-compliant due to inaccuracies were reprinted. At this point, some mechanical tests were performed.
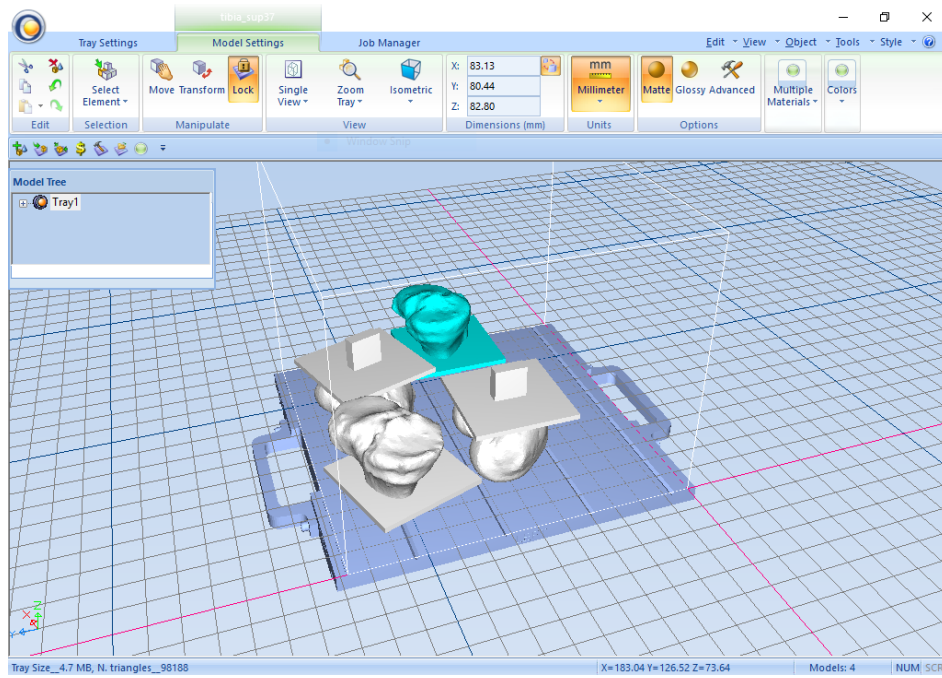
Figure 20. Supports on the virtual tray of Objet Studio software.

Figure 21. Supports after printing and cleaning.

3.6 Mechanical Tests

To characterize the mechanical properties of the two custom materials, compression and tensile mechanical tests were performed. In particular, ASTM D695 protocol was followed for the compression test and the corresponding ASTM D638 protocol for the tensile test. These protocols have rigid standard technical specifications regarding the dimensions of the specimens that must be subjected to the tests. The standardized samples were therefore printed, with the two different materials, using specific .stl files for each of the two tests. In particular, the ASTM D695 protocol requires cylindrical samples for compression, while the D638 protocol requires dog-bone shaped specimens.

All mechanical tests were carried out at the Tæknisetur (Technological Institute of Iceland, Reykjavik). The Two-Column MTS Insight® Electromechanical 10kN standard length (MTS Systems Corporation, Minnesota, United States) testing machine was used. Tensile and compression tests were carried out using specific cylindrical and dog bone samples for each test. For the anatomical models, however, compression tests were carried out with a preload of 700 N. The TestWorks 4 software was used to control all the tests and export the final results. Each model and sample were measured using a calliper before and after each trial.

MTS Insight 10

This testing machine is designed for use in materials testing, including tension, compression, flexure, and shear testing. The machine is electromechanical, meaning that it uses an electric motor to apply force to the specimen being tested. It has a maximum load capacity of 10 kN, which is equivalent to approximately 1 metric ton of force. The standard length of the machine refers to the distance between the two columns that support the load frame, which is 595 mm. The MTS Insight Electromechanical 10 kN testing machine has a range of features and capabilities that make it suitable for a variety of applications. For example, it has a closed-loop servo control system that ensures accurate and repeatable test results, as well as a variety of test modes and data acquisition options. The machine is also equipped with a variety of safety features, including emergency stop buttons, overload protection, and interlocks to prevent accidental operation. Additionally, it can be operated using MTS software or other third-party software, allowing for greater flexibility and ease of use. It is used for medium force testing of components, biomaterials, plastics, metals, elastomers, paper products, adhesives, and foam specimens in a wide range of sizes.

TestWorks 4

TestWorks 4 is a comprehensive and innovative Windows-based software program designed to help engineers and technicians develop and execute test programs for electronic and mechanical systems by adapting to the way users work. It includes a range of tools and features that streamline the test development process and make it easier to create complex test programs. These tools include a graphical user interface (GUI) that provides an intuitive and easy-to-use environment for test development, as well as a powerful scripting engine that allows users to create custom test sequences and test procedures. The software can be configured to handle demanding requirements while maintaining a user-friendly interface. Standard test types, such as peel, tear, sheer, tensile, compression, and flex tests, are included in the TestWorks 4 package. Additionally, TestWorks 4 includes hardware drivers and interfaces that enable communication with a wide range of test instruments and systems, supporting various communication protocols such as GPIB, VXI, PXI, and USB. The software also features a powerful data acquisition and analysis module that enables real-time capture and analysis of test data, supporting multiple data formats such as waveform, time-domain, frequency-domain, and statistical data. TestWorks 4 includes intuitive menus and controls for test set-up, execution, and report generation.

3.6.1 Compression Test

The ASTM D695 Compression Test is a standard test method used to determine the compressive properties of rigid plastics, composites, and reinforced plastics. The test is typically conducted on a universal testing machine and involves applying a compressive force to a cylindrical or rectangular sample of the material until it fractures or deforms, while measuring the amount of force applied. During the test, a sample is placed between two parallel compression platens of a testing machine (Figure 22) and a compressive load is applied at a specified rate until the sample fractures or reaches a predetermined deformation. The force and deformation data obtained from the test are used to determine the material's mechanical properties, such as its compressive strength, modulus of elasticity, yield strength, and ultimate strength. Several compression tests were conducted on cylindrical standardized samples printed with different materials. Specifically, ten compression tests were performed on ten different samples, with five printed using the *Soft Cartilage* material and the other five using the *Moderately Stiff Cartilage* material. Since some samples did not meet the dimensional requirements dictated by the ASTM D695 protocol, they were reprinted. All samples were measured before and after each test.

Figure 22. Compression test on standardized samples.

3.6.2 Tensile Test

The ASTM D638 Tensile Test is a standard test method used to determine the tensile properties of plastic materials. This test is used to measure the force required to stretch a plastic sample to its breaking point and to determine the deformation characteristics of the material. During the test, a standardized specimen is clamped onto a testing machine at either end and subjected to a controlled, uniaxial tensile force until it breaks (Figure 23). The amount of force required to break the specimen, as well as the deformation characteristics of the material, are measured and used to calculate various tensile properties of the material, including its ultimate tensile strength, yield strength, elongation at break, and modulus of elasticity. Several tensile tests were conducted on dog-bone standardized samples printed with different materials. Specifically, ten compression tests were performed on ten different samples, with five printed using the *Soft Cartilage* material and the other five using the *Moderately Stiff Cartilage* material. All samples were measured before and after each test.

Figure 23. Tensile test on standardized samples.

3.6.3 Patient-specific Test Setup

The ultimate goal of our study is to assess the mechanical behaviour of the entire femoral cartilage under real loading conditions. In a mechanical test, this translates into simulating the load distribution that occurs in the human knee joint to investigate how the cartilage behaves and analyse which areas of the cartilage are most susceptible to stress and deformation. The best way to do this is to include the patient's specific anatomy in the mechanical test. Therefore, we customized a mechanical test by using a 3D-printed patient-specific anatomical model. Specifically, the printed models of the patient's femur and tibia were modified by adding custom-designed supports for the test, in order to simulate the force distribution that occurs in reality. Since cartilage is mainly subjected to compressive loads, we deemed reasonable to modify the supports to better fit the compression plates, in order to carry out a compression test (Figure 24). Supports were designed to fit dimensionally above the plates. However, a problem arose when attempting to make this test repeatable: despite the correct dimensions of the supports, the compression plates are round in shape. This was a problem because once the supports were attached, they were not completely fixed and could rotate. Therefore, even if the two supports were placed in the correct position, they could have shifted during the test under the action of the load.

Figure 24. Anatomical supports modified for the patient-specific compression test.

We thus decided to consider an alternative solution.

The most commonly used biomechanical tests to evaluate the behaviour of biomaterials and tissues are compression and tensile tests. In general, a compression test involves compressing a sample between two compression plates. On the other hand, a tensile test involves pulling a sample clamped between two grips. Both tests are performed using the same universal testing machine since the tensile or compression of the samples is translated into a simple movement, upwards for tensile or downwards for compression, of a bar interposed perpendicular to the two columns of the machine. What differentiates the two tests is the use of grips and plates specifically designed for each of the two tests.

Ideally, based on what has been said, it might be possible to use the grips of the tensile test to perform a compression test, but there are some important factors to consider. Firstly, the grips may not be designed to exert a compression force effectively. Adaptations or modifications may be necessary to allow for the application of a compression force in a uniform and controlled manner. Secondly, the compression test typically requires a flat loading surface to ensure a uniform distribution of force on the surface of the sample being tested. The grips of the tensile test may not be able to provide a sufficiently flat loading surface for precise compression testing. Therefore, using the pneumatic grips of the tensile test to perform a compression test has its limitations. The advantages of using grips for a compression test are: they allow the correct positioning of the supports; they allows the proper fixation so the supports cannot move during the test; they ensure the repeatability of the test. However, the disadvantages are that they are not designed to effectively exert a compressive force because

they would require a sufficiently flat loading surface. Additionally, they cannot withstand excessively high loads as this would risk compromising their functioning and even causing them to break. By designing appropriate custom supports, these limitations can be overcome (Figure 25). The supports we have designed provide a vertical surface of the same size as the grips. In this way, correct positioning and fixation were guaranteed throughout the test. An additional wider horizontal surface was added that rested on the end of the grips to ensure a sufficiently flat and wide surface for proper and efficient load distribution. Finally, in a knee joint compression test, the loads applied are not high enough to compromise the functioning of the grips. All of these considerations seemed reasonable to us in order to carry out a compression test using the pneumatic grips.

Therefore, the test is a revisitation of the tensile test as were used the pneumatic grips, but to apply a compressive load. Once the supports were attached, the femoral cartilage was placed between the two parts.

Figure 25. Anatomical supports utilized for the patient-specific test.

Patient-Specific Mechanical Test

For the patient-specific mechanical test, specific protocols were not followed as the test required customization through specific supports. The addition of these supports allowed for the application of compressive force to the cartilage in a manner similar to what occurs in reality. In fact, the supports preserved the patient-specific geometry of the femur and tibia bones, simulating the same distribution of real loads.

Specifically designed femoral and tibial supports were attached to the pneumatic grips, with the femur support above and tibia support below, taking care to position and secure them correctly (Figure 26). The femoral cartilage printed with the two custom materials was then placed between the two supports. Since cartilage positioning is operator-dependent and prone to errors, it was necessary to make the test repeatable by minimizing misalignments. To achieve this, we deemed reasonable to apply a preload of 700 N, corresponding to one time the body weight. The cartilage was thus already in direct contact with the femur and tibia supports and no longer susceptible to minimal position changes. The choice of 700 N was also driven by the need to subject the cartilage to a specific load to eliminate operator-dependent errors, while also exposing it to a sufficiently wide range of loads to analyse its behaviour.

Figure 26. Patient-specific anatomical test setup.

4 RESULTS

All the data obtained from both mechanical tests and computational analyses were then saved and uploaded on Matlab software for the post-processing phase. The most significant results are shown in the following paragraphs and will be discussed in detail in the next chapter.

Results of the Mechanical Tests on Standardized Samples

The results of the mechanical tests conducted on standardized samples were recorded in .txt file format and imported into Matlab software for post-processing. Using this software, stress-strain graphs were generated for each specimen for the two materials under consideration. Starting from these graphs, the values of Young's modulus and Poisson's ratio were determined for both the *Soft* and *Medium* materials. These values were then employed in the finite element analysis performed on ANSYS to characterize the material properties of the cartilages.

Here are reported the graphs depicting the relationship between stress and strain of *Soft* and *Medium* materials, both for the tensile and compression test, in order to provide a comprehensive overview of the behaviour of the materials.
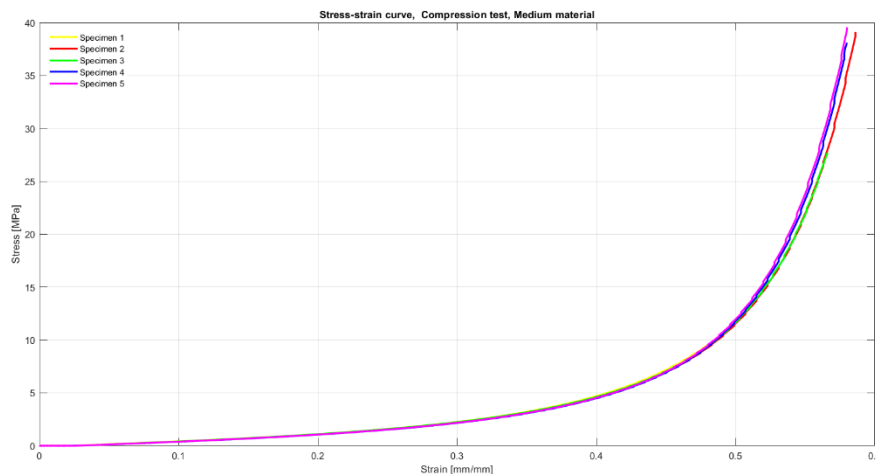
Figure 27. Stress-strain curve, compression test, *Medium* material.
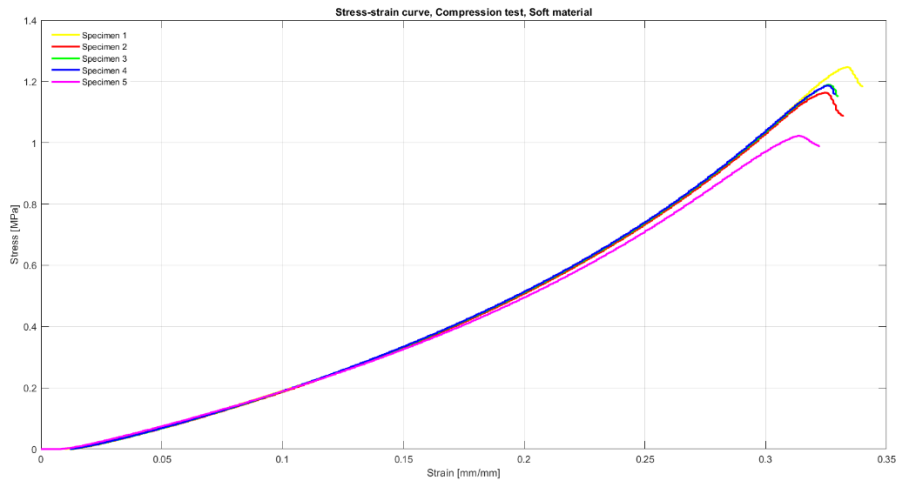
Figure 28. Stress-strain curve, compression test, *Soft* material.
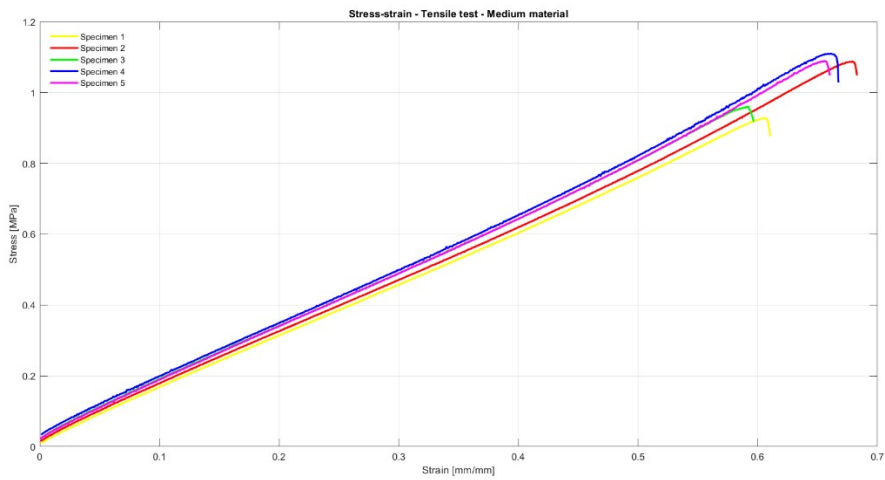
Figure 29. Stress-strain curve, tensile test, *Medium* material.
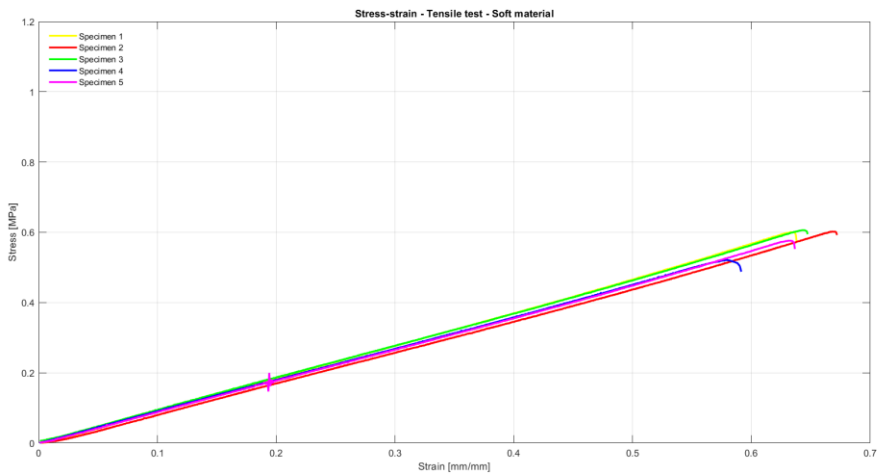
Figure 30. Stress-strain curve, compression test, *Soft* material.

Calculation of Young's Modulus and Poisson's ratio

As previously mentioned, from these graphs, the values of Young's modulus and Poisson's ratio of the two materials under examination were extrapolated and calculated according to the instructions outlined in the ASTM D695 and ASTM D638 protocols, respectively. The specific calculations and assumptions made have been discussed in another work [38]. Below are the values found.

	Compression	**Tensile**
***Medium* material**	**7.2396**	**1.8377**
***Soft* material**	**2.4317**	**0.8784**
Native tissue	**5**	**N/A**

Table 7. Young's modulus of the different materials (MPa).

	Poisson's ratio
***Medium* material**	**0.34**
***Soft* material**	**0.3462**
Native tissue	**0.46**

Table 8. Poisson's ratio of the different materials.

Results of FEM Analyses on Anatomic Models

After completed the computational analysis on ANSYS, the models of the knee joint were mainly analysed for the equivalent von Mises stress and equivalent von Mises strain. The von Mises stress is a measure of the equivalent or effective stress in a material, which considers both the normal stresses and the shear stresses that act on the material. Similarly, the von Mises strain is a measure of the equivalent or effective strain in a material, which takes into account both the normal strains and the shear strains that act on the material.

Initially, the analyses were carried out by assigning the *Soft* and *Medium* materials to the femoral cartilages and using the *Printed Bone* material for the bones. Subsequently, to compare and validate the obtained results, a further analysis was conducted by using literature values of cartilage and bone materials. The stress and strain values recorded on the femoral cartilages were exported in .txt file format and imported into Matlab to create stress-strain graphs for the *Soft*, *Medium*, and literature materials.

The following graphs are the results of simulations on ANSYS of a compression test on the anatomical models of two patients, control and degenerative, with the knee fully extended. To do this was inserted a *Remote Displacement* in the femur to constrain the rotations along the x-, y- and z-axis and the translation along x- and y-axis. Only the translation along z-axis was free. The tibia was constrained at the lower surface using a *Fixed Support*. A vertical compressive force of 1150 N was applied to the top surface of the femur, which matches with the force of the gait cycle for full extension position.
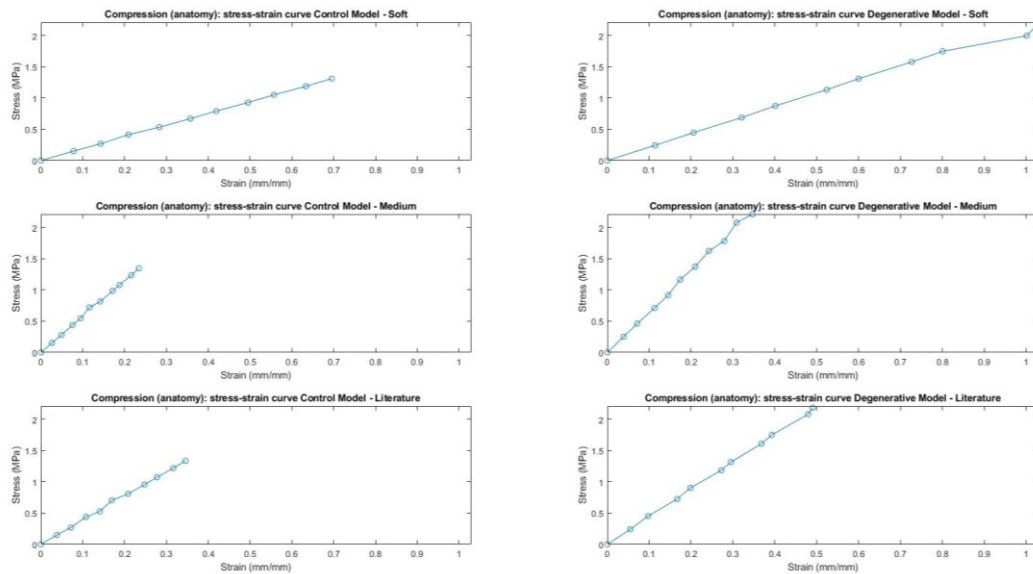
Figure 31. The three graphs on the left show the results of the analyses on the control model, assigning, from top to bottom, the *Soft*, *Medium*, and *Literature* materials, respectively. The graphs on the right, instead, refer to the degenerative model, again assigning, from top to bottom, the *Soft*, *Medium*, and *Literature* materials, respectively.
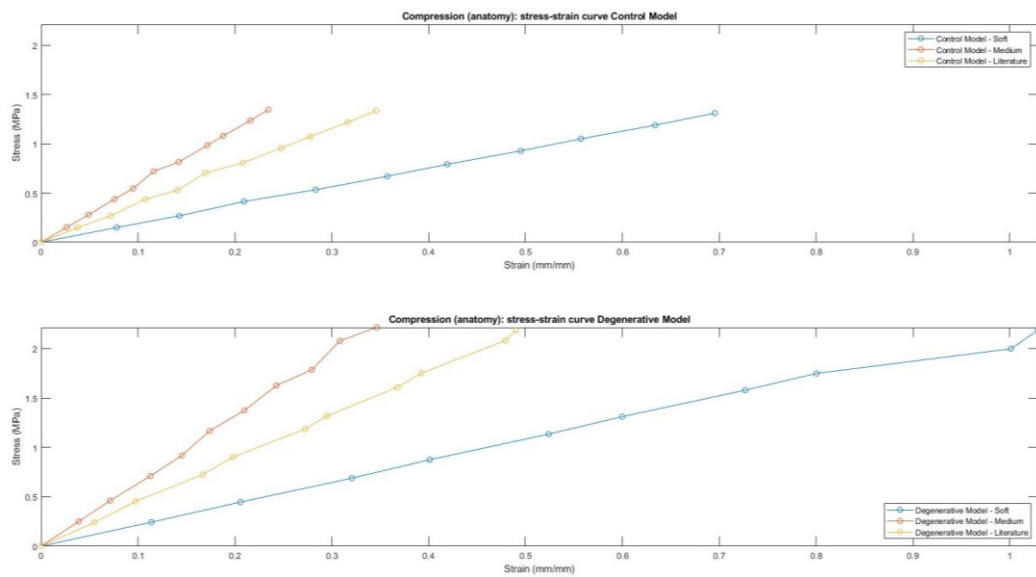
Figure 32. Stress-strain curves of the control patient, at the top, and the degenerative patient, at the bottom. The results of tests performed on the same model but with different materials were plotted. The orange curves refer to the *Medium* material, the yellow curves to the materials taken from literature, and the blue curves to the *Soft* material.
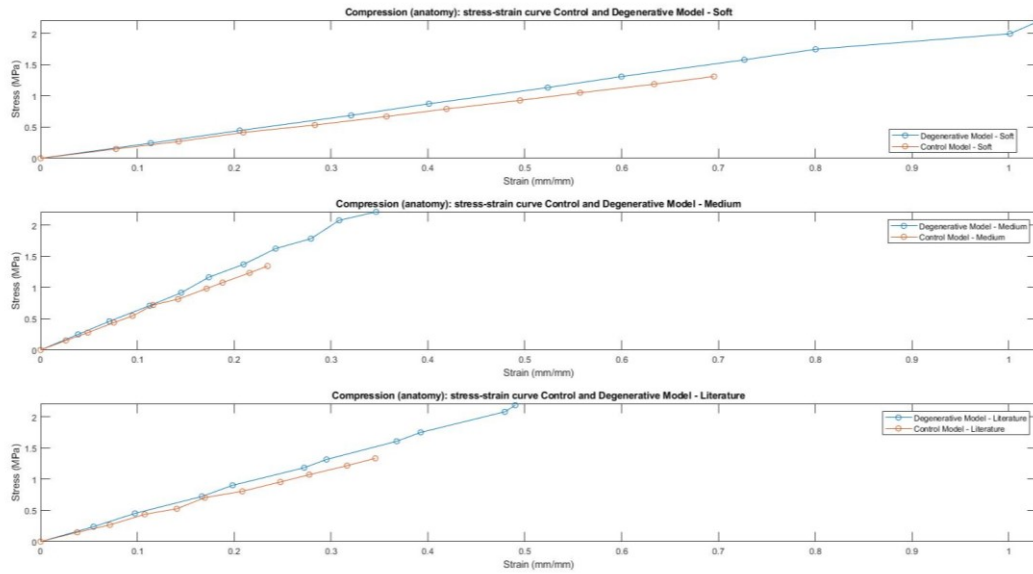
Figure 33. The three stress-strain graphs refer to the three different materials. For each material, the results of the control model (orange curve) and the degenerative model (blue curve) were plotted together.
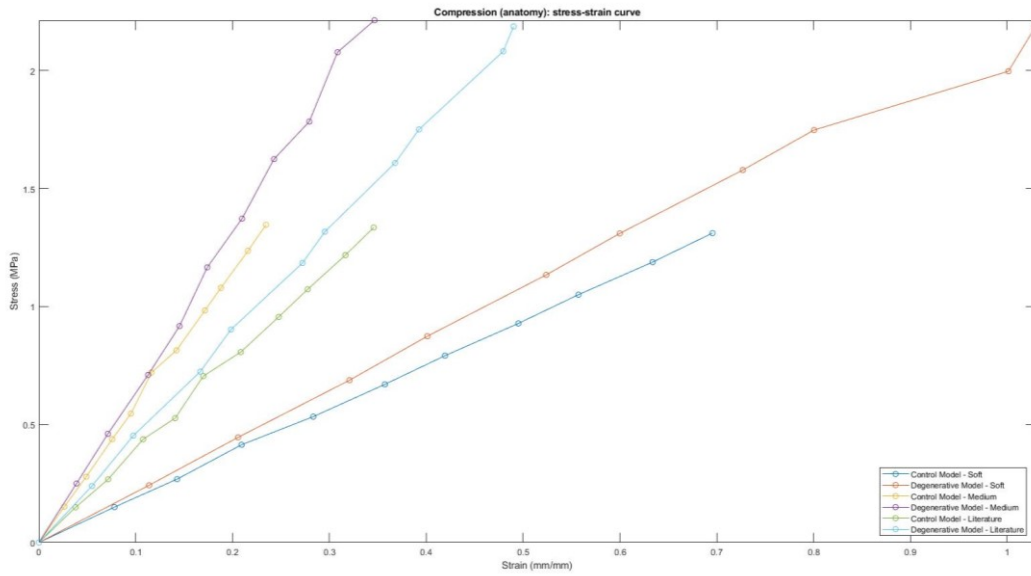
Figure 34. Stress-strain graph in which the results of all tests were plotted. Starting from the top, the purple curve represents the result of the test performed on the degenerative patient using the *Medium* material; the yellow curve refers to the control model with Soft material; the blue and green curves represent the behaviour of the Literature material in the degenerative and control models, respectively. Finally, the orange and blue curves are the results of the tests on the degenerative and control patients, respectively, both using the *Soft* material.

The following images represent the distribution of strain on femoral cartilages normalized on the values of the literature material (here are not reported the stress distributions).
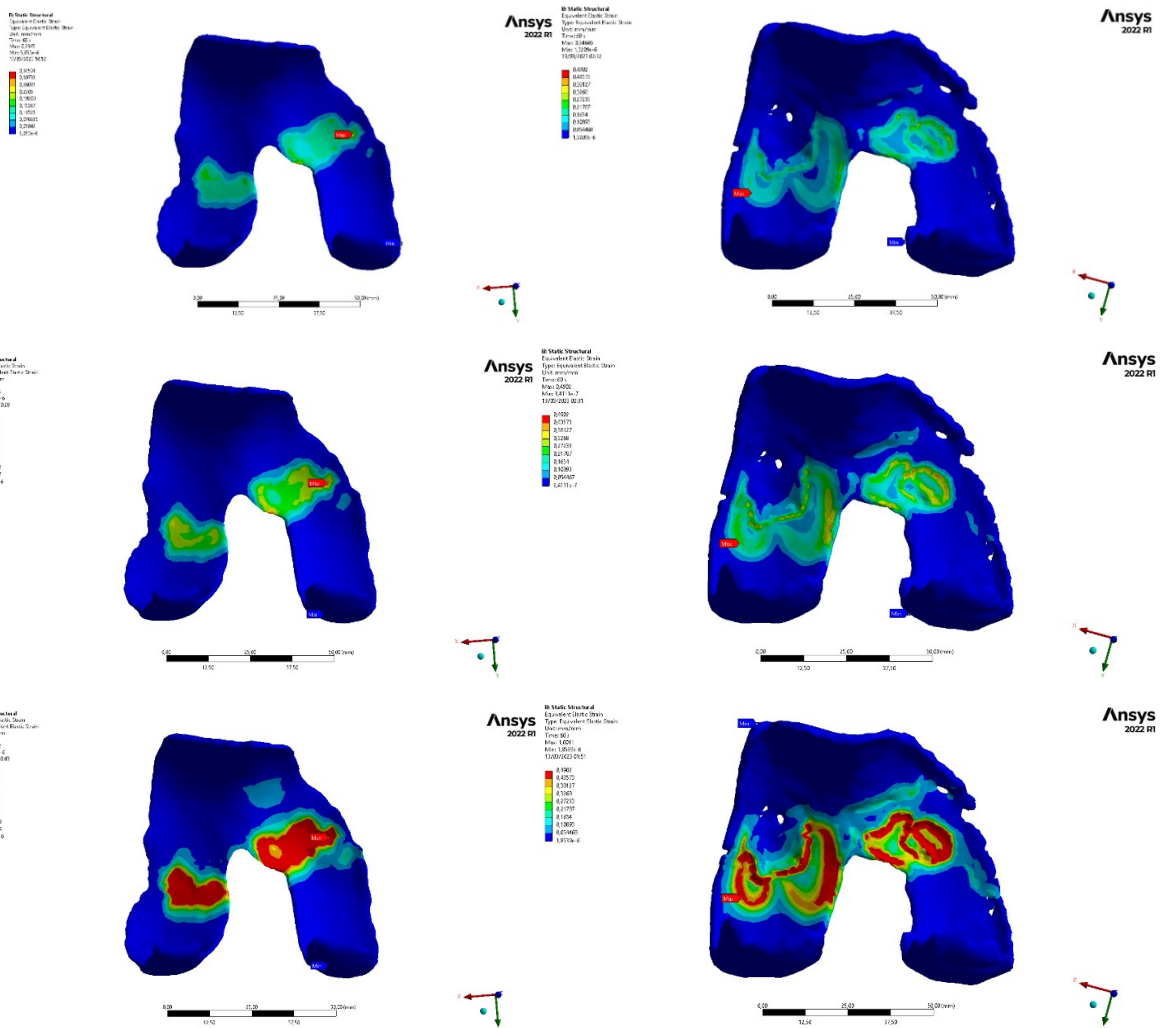
Figure 35. Strain distribution on control (left) and degenerative (right) femoral cartilages normalized with the values obtained from the literature material to better visualize the differences.

Results of FEM Analyses on Anatomical Support Models

Subsequently, computational analyses were conducted on the anatomical supports, assigning again the *Soft*, *Medium*, and *Literature* materials. The results of these analyses were first compared with those from analyses on the anatomical models, then validated with those from mechanical testing on the anatomical supports.

For the first comparison, the same boundary conditions and loads described previously were maintained. These tests aimed to verify whether the created supports were able to accurately replicate the load distribution in anatomical models of patients, and hence in reality. Similar to the previous tests, the results were evaluated and compared in terms of equivalent von Mises stress and equivalent von Mises strain. The stress and strain values were imported into Matlab to generate graphs.

These results are presented specifically in another work, but the Figure 36 and the Figure 37 have been inserted to give an idea of the behaviours and strain distributions obtained from the analyses with or without supports.

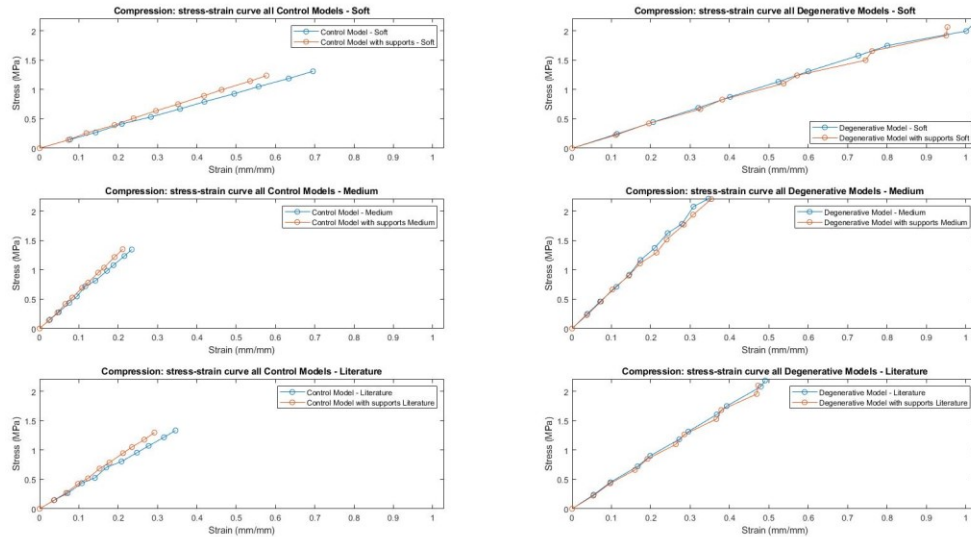The results of the second comparison are described in the next paragraph.

Figure 36. The three graphs on the left show the results of the analyses on the control model, both for the analyses on the anatomical model and supports models. There were assigned, from top to bottom, the *Soft*, *Medium*, and *Literature* materials, respectively. The graphs on the right, instead, refer to the degenerative model, again assigning, from top to bottom, the *Soft*, *Medium*, and *Literature* materials, respectively.
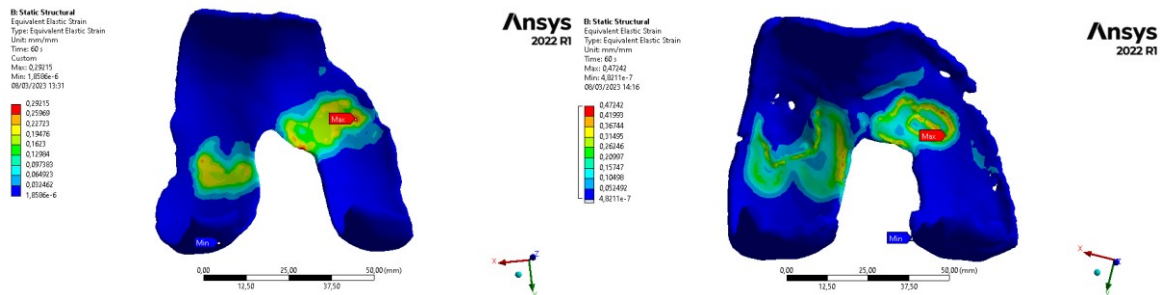
Figure 37. Strain distributions on control (left) and degenerative (right) femoral cartilages obtained from the analysis with the support models.

Results of FEM Analyses and Mechanical Tests on Anatomical Supports Models

In order to validate the computational analyses with the mechanical tests, specific load and displacement values were assigned to the supports for each model and material. These values were taken from the results of the mechanical tests, by taking an average. The results that appeared to be the most reasonable to use were the values of force and displacement. In mechanical tests, force values are calculated by sensors in terms of the reactive force that the load cell perceives when it comes into contact with the sample. As for displacement, the result is given by how much the bar moves from the starting point. To make the results as comparable as possible, a probe for the reactive force was placed on the fixed support in the computational analysis to evaluate the force, while a deformation probe was placed along the z-axis on the horizontal support to evaluate displacement. The force-displacement relation was chosen as it allows for an intuitive understanding of the test's trend and thus it leads to a direct comparison with the computational results for the final model validation.

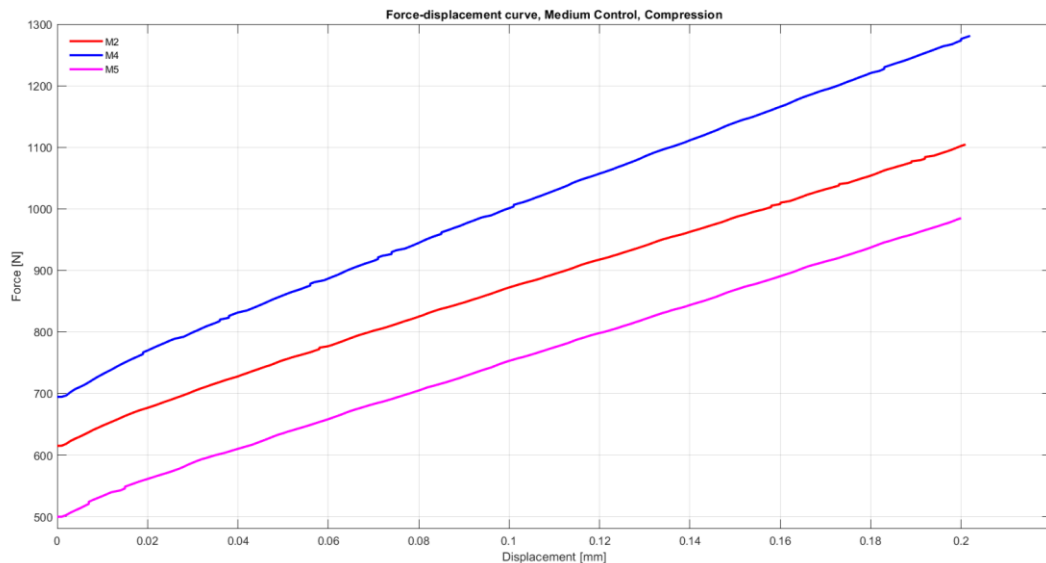The following graphs represent the force-displacement curves extracted from the mechanical tests.

Figure 38. Force-displacement curve obtained from a compression test of the control model printed with *Medium* material.
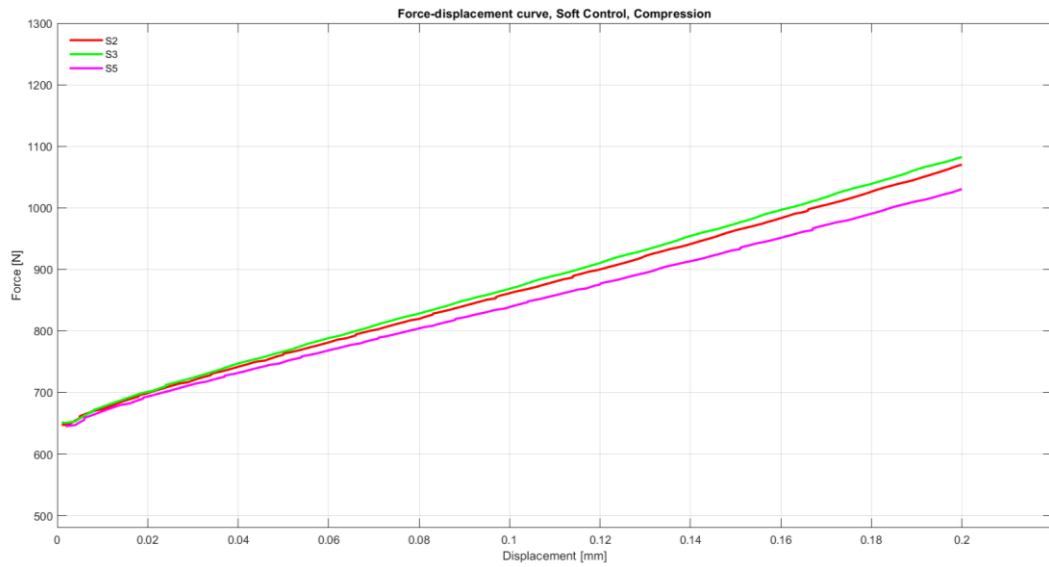
Figure 39. Force-displacement curve obtained from a compression test of the control model printed with *Soft* material.
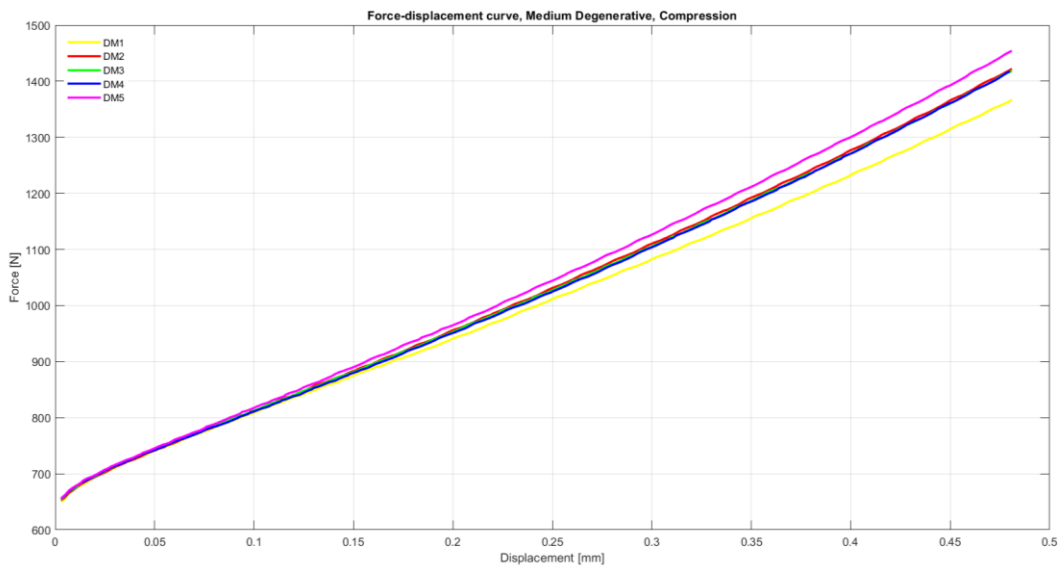

Figure 40. Force-displacement curve obtained from a compression test of the degenerative model printed with *Medium* material.
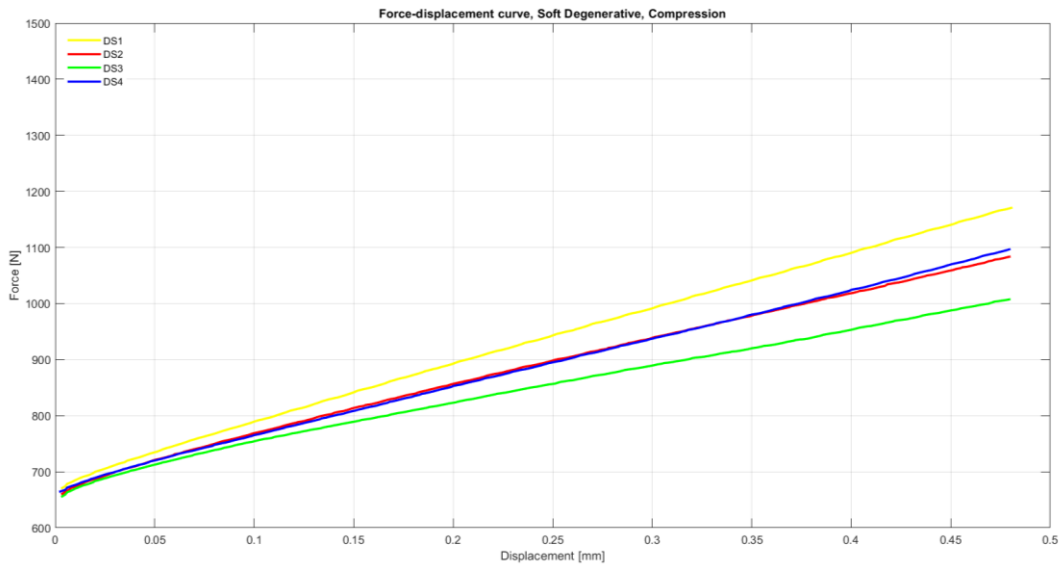
Figure 41. Force-displacement curve obtained from a compression test of the degenerative model printed with *Soft* material.

The following graphs represent instead the force-displacement curves extracted from the computational analyses.
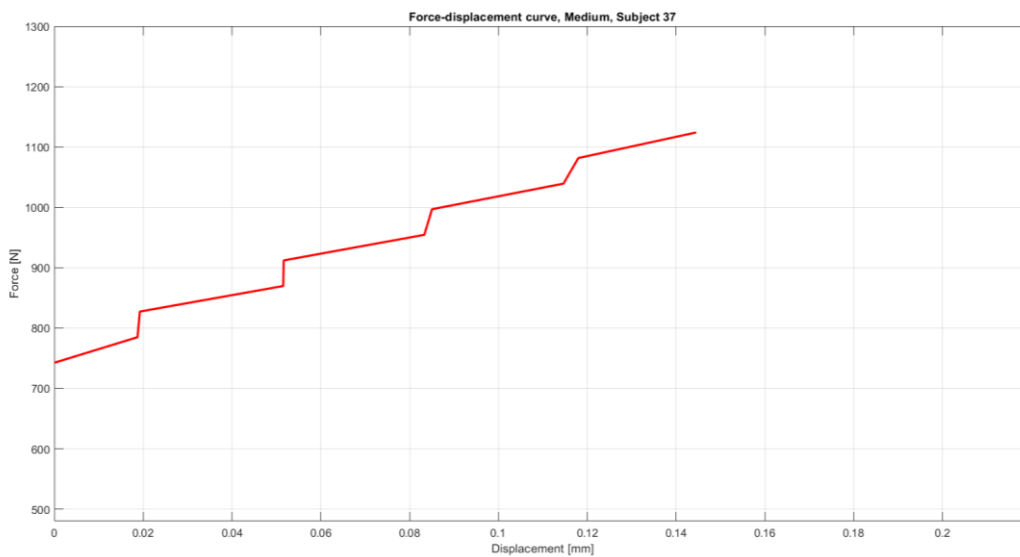

Figure 42. Force-displacement curve obtained from the computational analysis of the control model printed with *Medium* material.
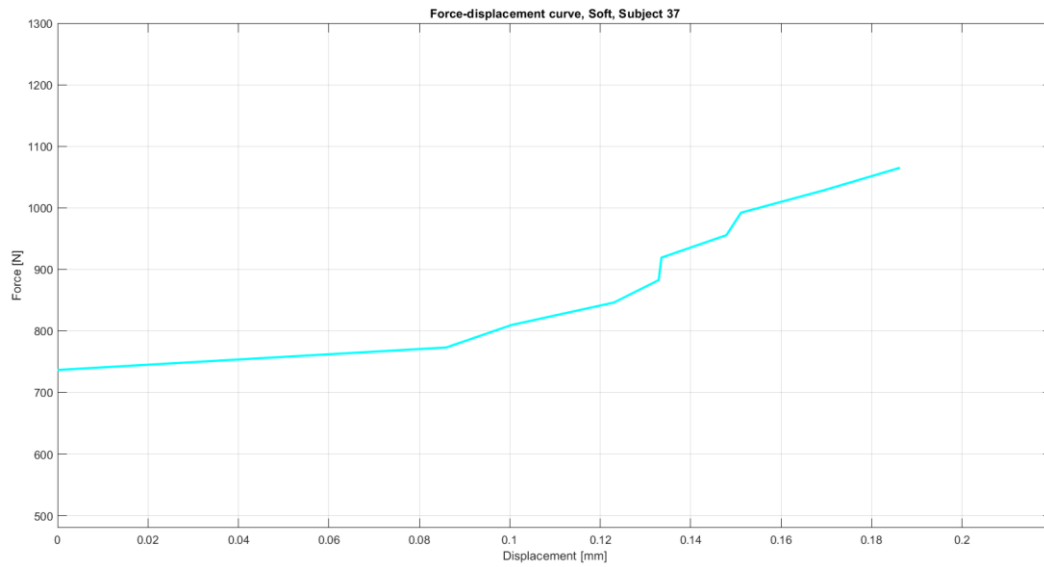
Figure 43. Force-displacement curve obtained from the computational analysis of the control model printed with *Soft* material.
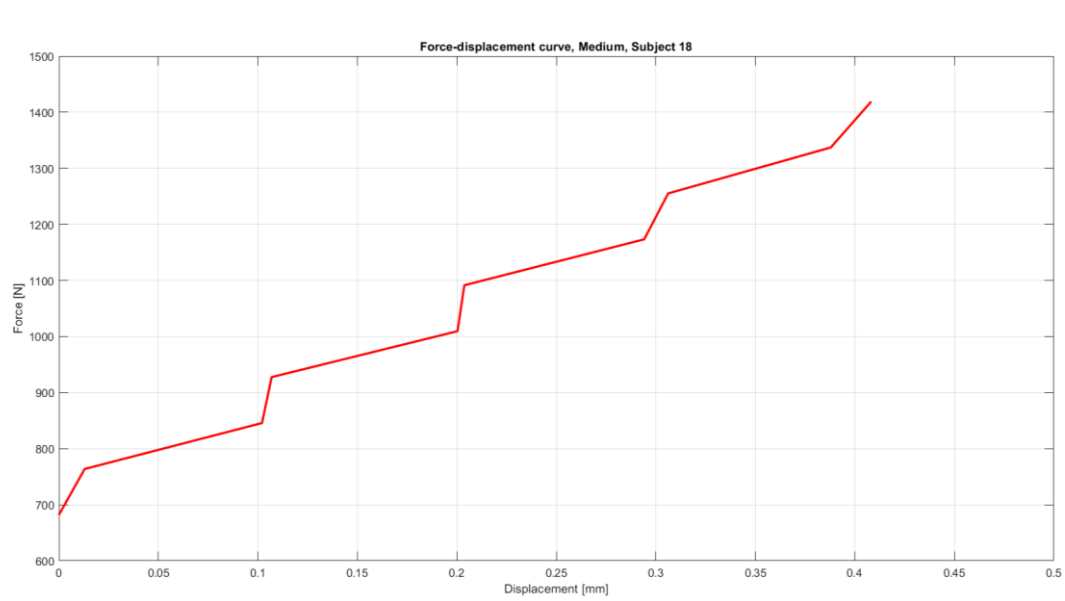

Figure 44. Force-displacement curve obtained from the computational analysis of the degenerative model printed with *Medium* material.
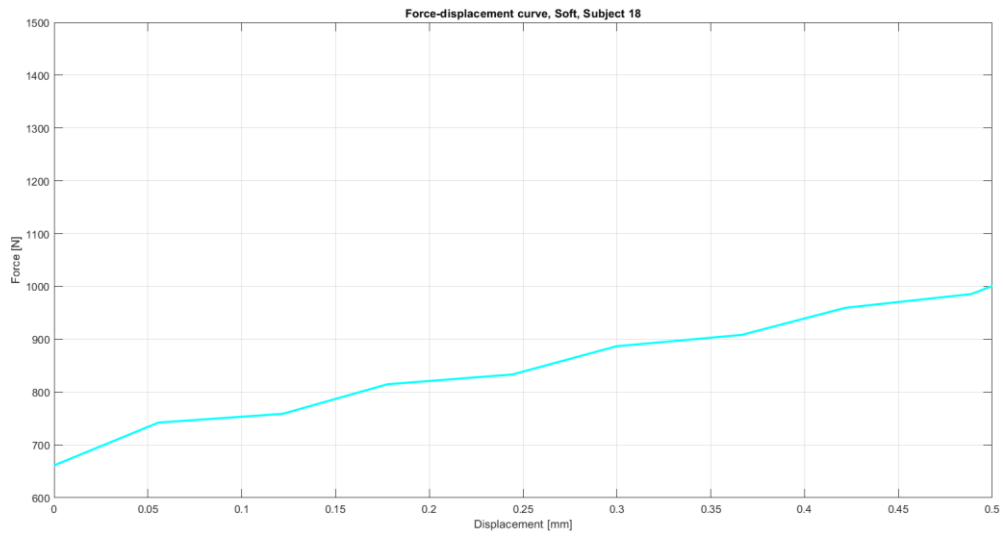
Figure 45. Force-displacement curve obtained from the computational analysis of the degenerative model printed with *Soft* material.

5 DISCUSSION

FEM Analysis Results on Anatomical Models

When looking at Figure 31, it's challenging to provide a precise interpretation of the behaviour of *Soft* and *Medium* materials in comparison to the literature material. However, it's evident that the curves display a relatively linear trend, and the slope of the curves in different models assigned with the same material is quite similar. The sole variation lies in the diverse stress and strain values reached. This implies that computational models are accurate enough to discriminate between the behaviour of different materials, as the slope of the curves remains consistent even with varying geometries. However, these geometries lead to different stress and strain values reached in the two models. In Figure 32, it's much clearer how the behaviour of the literature material is positioned between that of the *Soft* and *Medium* materials. This is a significant result as it suggests that the two created materials closely approximate the behaviour of human femoral cartilage, with some differences related to geometry. Figure 33 confirms what was said for Figure 31, namely that the graphs of different models printed with the same material have a very similar slope. Here, the differences dictated by the different geometries of the two patients can be appreciated more clearly, although they are not so pronounced. Finally, Figure 34 confirms what has been said so far. It can also be observed that, for small deformations and stresses, the behaviours of the materials are linear and very similar. The differences dictated by geometry become increasingly pronounced as the stresses and deformations increase.

As for the values of stress and strain reached (Figure 35), there are few comparable studies in the literature. In fact, there is significant variability among the values themselves, which makes comparisons difficult. This variability is mainly due to the different applications for which the FE analysis is employed. Depending on the application, the computational analysis is tailored to better suit the intended purpose, which results in varying geometries, the inclusion or exclusion of certain anatomical structures, specific load variations, and the extraction and evaluation of different results. Our analysis is preliminary and simplified, so it is not appropriate to evaluate the results solely in terms of pure stress and strain values. This is also quite logical considering that some anatomical structures present in the knee, such as menisci and ligaments, were not considered in our analysis, as they were not the focus of our study. These structures, however, play a crucial role in the absorption and distribution of knee loads. Furthermore, even if stress and strain values were compared, they would not be comparable to real values.

FEM Analysis Results on Anatomical Models with Supports

The FEM analyses carried out on the models with supports were used to verify that the created supports were actually able to simulate the correct distribution of loads in the knee. This translates into verifying that the areas of concentration and distribution of stresses and strains on the femoral cartilage were the same as those found in the analyses with the anatomical models. This was not obvious as the use of supports modified the surfaces on which the load was applied and on which the fixed support was inserted. However, the results obtained confirmed that this modification did not have an influence on the analysis results. Firstly, the behaviour of the materials in the stress-strain graphs remained very similar (Figure 36). Then, the distributions of stresses and strains on the cartilages remained almost unchanged, thus confirming that the introduction of the supports did not influence the correct transmission of forces (Figure 37).

FEM Analysis and Mechanical Testing Results on Models with Supports

To validate the FEM analyses performed on models with supports, the results obtained were compared with those derived from mechanical tests carried out on the printed supports. For the comparison, the force-displacement relationship was chosen as it allows for an intuitive understanding of the test trend and thus leads to a direct comparison with computational results for the final validation of the model. Before comparing computational curves with the ones from mechanical tests, is worth to point out that the FEA results are evaluated with far less data. This leads to less linear curves and thus that's why the focus is mostly for the average trend and max values.

For the control subject, it is straightforward to notice that the computational force-displacement curves do not match properly the ones from mechanical tests. Both soft and medium curves have similar trends (this is more true for the medium material) but they do not reach the same max forces and displacements. On the other hand, degenerative subject results show a very close match between the two approaches. The computational cures do not only exhibit the same trend as the ones from mechanical testing, but they also have just slightly lower maximum values for both stress and strains. This applies to the medium and the soft material as well.

The results obtained confirm that the imposed force and displacement values are similar. The differences are not so relevant and are mostly dictated by operator-dependent errors during the positioning of the cartilage before the mechanical tests.

Qualitative Validation

The confirmation of what have been said so far also derives from the visual evaluation of the femoral cartilages immediately after the mechanical tests. These pictures serve as a qualitative comparison between the zone subjected to major strains on the cartilage surface. On the left of each picture, the printed cartilages after their respective mechanical tests. On the right side, the corresponding cartilage from the computational analysis.
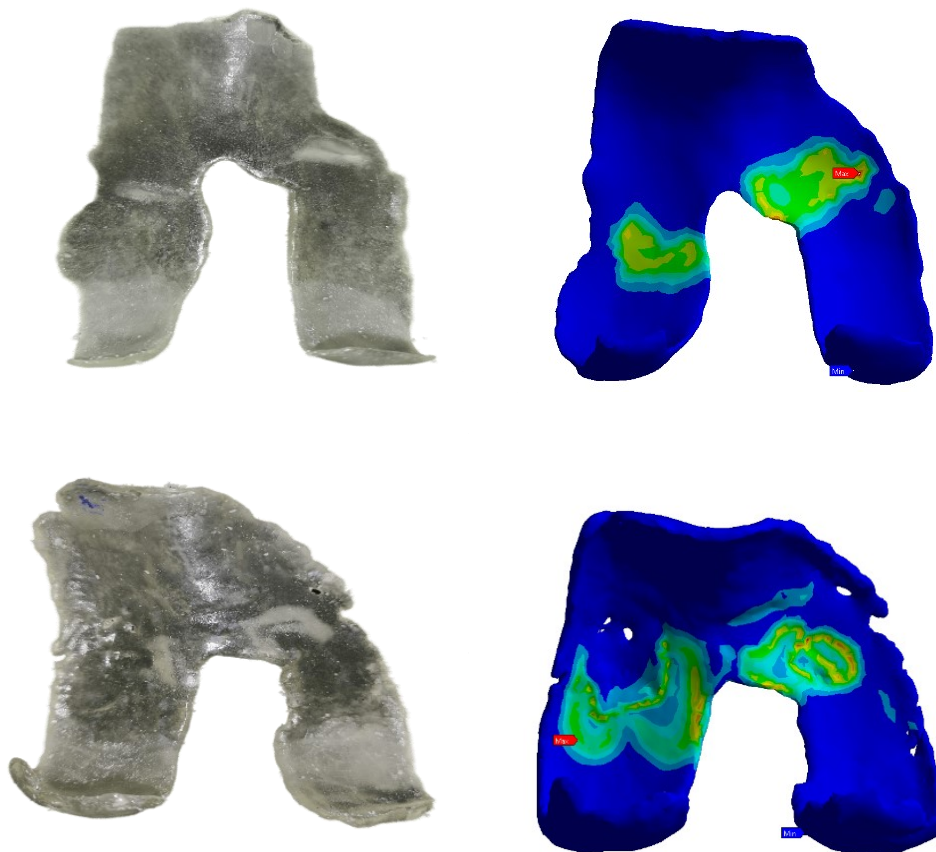

Figure 46. Qualitative comparison between the strain distributions between the femoral cartilages after the mechanical and computational tests.

6 CONCLUSION AND FUTURE DIRECTIONS

Summary

Two 3D models of the human knee were generated using magnetic resonance imaging and CT scans from two patients, one with normal cartilage and the other with degenerative cartilage. These models were then modified and printed using digitally synthesized materials. Specifically, two distinct materials were created to emulate the mechanical properties of native femoral cartilage and address the variances in cartilage composition and behaviour linked to factors such as age, health, and lifestyle. Subsequently, these models underwent a custom mechanical test that mimicked the loading conditions and distributions that take place in a human knee. Alongside the mechanical assessments, finite element analyses were conducted on both the anatomical models and the modified models with supports, to verify the results obtained from the physical tests and compare with the mechanical properties of cartilage documented in scientific literature. The outcome revealed that the produced materials closely matched the behaviour observed in previous research, with only slight variations due to patient-specific geometries. Moreover, the created supports were able to simulate a real loading scenario while preserving the original geometry and distribution of forces.

Conclusions

This study represents a first step towards the development of new methodologies and concepts for evaluating the condition of cartilage and preventing complications such as osteoarthritis. Predicting the progression of these complications and their impact on anatomical structures of interest is a challenging and costly issue in terms of both time and resources. Identifying new criteria for predicting the degeneration status of knee cartilage can help improve patients' quality of life by allowing timely treatment and care to reduce severe consequences and painful conditions. Finding new patient-specific, timely, and low-cost methods may be the solution.

This work can be considered a preliminary study on the use of 3D printing and finite element analysis to study and evaluate cartilage behaviour in order to diagnose and resolve potential problems associated with it. This approach enables the planning and improvement of treatments that are specific to each patient based on their individual needs.

Future Directions

Being a preliminary analysis, this study aims at several future objectives, some of which are still ongoing. First of all, it is necessary to expand the workflow used by introducing other patients, including those from the traumatic group, to identify behavioural differences and to make patients with the same age range, gender, etc. more comparable. The next step is to find a balance between model optimization and the easy reproducibility of the entire process. The 3D models can be improved by using more precise finite elements, such as HEX20, by inserting missing anatomical parts (menisci, ligaments, and tibial cartilages), but also by assigning more specific material properties. However, care must be taken not to make the process too specific and difficult to replicate. Another future direction is to use the Digital Anatomy Creator software to create new materials to be tested. In particular, since femoral cartilage is structured in multiple layers, diversifying the compositions of materials in the various layers instead of having a single one would make the model more precise. Another improvement can be made in the setup of mechanical tests, by introducing strain gauges to obtain more precise and reliable results of the deformations that occur in the tested model. Moreover, the extrapolation and evaluation of other parameters in addition to those already considered, perhaps more specific to the study of osteoarthritis, such as the thickness and density of cartilage, can be included. In conclusion, it would be interesting to create patient-specific anatomical models to be inserted into a database for applications related to study, training, and surgical planning, even for other anatomical parts. The entire workflow used, in fact, can be used for other applications outside of the knee.

7 REFERENCES

[1] Drake, R.L., Vogl, W., Mitchell, A.W.M., & Gray, H. (2015). Gray's Anatomy for Students (3rd ed.). Churchill Livingstone/Elsevier.

[2] Netter, F.H. (2014). Atlas of Human Anatomy (6th ed.). Elsevier Limited.

[3] Ethier, C.R., & Simmons, C.A. (2007). Introductory Biomechanics: From Cells to Organisms. Cambridge University Press.

[4] Fox, A.J.S., Bedi, A., & Rodeo, S.A. (2009). The basic science of articular cartilage: structure, composition, and function. Sports Health, 1(6), 461-468. doi: 10.1177/1941738109350438.

[5] Yang, X., Konstantin, I.M., Zhe, C., Christopher, T.C., David, K., & Farid, B. (2016). Introduction to Cartilage, Biophysics and Biochemistry of Cartilage by NMR and MRI, Yang Xia, Konstantin Momot.

[6] http://web.mit.edu/cortiz/www/3.052/3.052CourseReader/27_BiomechanicsofCartilage.pdf

[7] Mow, V., Kuei, S.C., Lai, W.M., & Armstrong, C.G. (1980). Biphasic Creep and Stress Relaxation of Articular Cartilage in Compression: Theory and Experiments. Journal of Biomechanical Engineering, 102, 73-84.

[8] S., N., A., D., & Carlos, J. (2012). Mechanical Behavior of Articular Cartilage. InTech. doi: 10.5772/48323.

[9] Global Burden of Disease Collaborative Network. (2020). Global Burden of Disease Study 2019 (GBD 2019) Results. Institute for Health Metrics and Evaluation (IHME). http://ghdx.healthdata.org/gbd-results-tool.

[10] Hunter, D.J., & Bierma-Zeinstra, S. (2019). Osteoarthritis. The Lancet, 393(10182), 1745-1759.

[11] Paz, A., Orozco, G.A., Korhonen, R.K., García, J.J., & Mononen, M.E. (2021). Expediting Finite Element Analyses for Subject-Specific Studies of Knee Osteoarthritis: A Literature Review. Applied Sciences, 11(23), 11440. doi:10.3390/app112311440

[12] Grässel, S., & Muschter, D. (2020). Recent advances in the treatment of osteoarthritis. F1000Research, 9(F1000 Faculty Rev-325). doi:10.12688/f1000research.22115.1.

[13] Ciliberti, F.K., Guerrini, L., Gunnarsson, A.E., et al. (2022). CT- and MRI-Based 3D Reconstruction of Knee Joint to Assess Cartilage and Bone. Diagnostics, 12(2), 279. doi:10.3390/diagnostics12020279.

[14]   Roemer, F.W., Demehri, S., Omoumi, P., Link, T.M., Kijowski, R., Saarakkala, S., Crema, M.D., & Guermazi, A. (2020). State of the Art: Imaging of Osteoarthritis—Revisited 2020. Radiology, 296, 5-21.

[15]   https://www.sciencedirect.com/topics/engineering/medical-image-segmentation

[16]   Suetens, P., Bellon, E., Vandermeulen, D., et al. (1993). Image segmentation: methods and applications in diagnostic radiology and nuclear medicine. European Journal of Radiology,

[17]   http://restoreproject.eu/

[18]   https://restore-project.ru.is/

[19]   Welch-Phillips, A. (n.d.). What is finite element analysis?

[20]   Yang, Z. (n.d.). Finite element analysis for biomedical engineering applications.

[21]   Pfeiffer, F. M. (2013). The use of finite element analysis to enhance research and clinical practice in orthopedics. Current Reviews in Musculoskeletal Medicine, 6(1), 56-61. https://doi.org/10.1007/s12178-012-9146-8

[22]   Srirekha, A., & Bashetty, K. (2013). Infinite to finite: An overview of finite element analysis. Journal of Indian Prosthodontic Society, 13(1), 7-13. https://doi.org/10.1007/s13191-013-0214-4

[23]   Magomedov, A., Khaliev, M., & Elmurzaev, I. (2017). Application of finite element analysis in medicine. Journal of Physics: Conference Series, 803, 012080. https://doi.org/10.1088/1742-6596/803/1/012080

[24]   Zahra Trad, Abdelwahed Barkaoui, Moez Chafra, João Manuel R.S. Tavares; FEM Analysis of the Human Knee Joint, Springer, 2018

[25]   Kazemi, M., Dabiri, Y., & Li, L. P. (2013). Recent advances in computational mechanics of the human knee joint. Computational and Mathematical Methods in Medicine, 2013, 718423. https://doi.org/10.1155/2013/718423

[26]   Sathasivam, S., & Sivakumar, S. S. (2016). Finite element modeling of the human knee joint for biomechanical analysis. BONES linear elastic, 9(2), 1-7. http://eprints.covenantuniversity.edu.ng/7303/

[27]   Cooper, R. J., Wilcox, R. K., & Jones, A. C. (2013). Finite element models of the tibiofemoral joint: A review of validation approaches and modelling challenges. Journal of Biomechanics, 46(15), 2539-2546. https://doi.org/10.1016/j.jbiomech.2013.08.004

[28]   Daniela, T., Marius, C., & Nicolae, T. D. (2014). Modeling and finite element analysis of the human knee joint affected by osteoarthritis. In Proceedings of the International Conference on Applied and Computational Mathematics (pp. 157-162). Springer. https://doi.org/10.1007/978-3-319-04849-9_17

[29]   Maas, S. A., Ellis, B. J., Rawlins, D. S., & Weiss, J. A. (2016). Finite element simulation of articular contact mechanics with quadratic tetrahedral elements. Journal of Biomechanics, 49(5), 659-667. https://doi.org/10.1016/j.jbiomech.2016.01.024

[30]   Devaraf, A. K., Adhikari, R., Acharya, K. K. V., et al. (2016). Finite element analysis of a human knee joint. In NAFEMS India Regional Conference (pp. 1-8).

[31]   Salmi, M. (2021). Additive Manufacturing Processes in Medical Applications. Materials (Basel), 14(1), 191. https://doi.org/10.3390/ma14010191

[32]   Tuomi, J., Paloheimo, K., Björkstrand, R., Salmi, M., Paloheimo, M., & Mäkitie, A. A. (2010). Medical applications of rapid prototyping— From applications to classification. In Innovative Developments in Design and Manufacturing—Advanced Research in Virtual and Rapid Prototyping (pp. 701–704). CRC Press.

[33]   Ghomi, M. (n.d.). Future of additive manufacturing in healthcare.

[34]   Chen, W. J., Chen, Y. X., & Chen, H. H. (2019). Application of 3D printing knee joint disease model based on MRI reconstruction technology in orthopaedics teaching. China Modern Medicine, 25, 159-61.

[35]   Sun, B., Ma, Q., Wang, X., Liu, J., & Rejab, M. R. M. (2019). Additive manufacturing in medical applications: A brief review. Rapid Prototyping Journal, 25(1), 174-181. https://doi.org/10.1108/RPJ-03-2017-0045

[36]   DenOtter, T. D., & Schubert, J. (2023, March 6). Hounsfield Unit. In StatPearls [Internet]. Treasure Island (FL): StatPearls Publishing. PMID: 31613501.

[37]   Ciliberti, F. K., Guerrini, L., Gunnarsson, A. E., Recenti, M., Jacob, D., Cangiano, V., Tesfahunegn, Y. A., Islind, A. S., Tortorella, F., Tsirilaki, M., Jónsson, H. Jr., Gargiulo, P., & Aubonnet, R. (2022). CT- and MRI-Based 3D Reconstruction of Knee Joint to Assess Cartilage and Bone. Diagnostics, 12(2), 279. https://doi.org/10.3390/diagnostics12020279

[38]   Dolino, G., Master's Thesis